

Model Building and Phenomenology in Supersymmetry

Dissertation

zur

Erlangung des Doktorgrades (Dr. rer. nat.)

der

Mathematisch-Naturwissenschaftlichen Fakultät

der

Rheinischen Friedrich-Wilhelms-Universität Bonn

vorgelegt von

JONG SOO KIM

aus Bonn

Bonn 2008

Angefertigt mit Genehmigung der Mathematisch-Naturwissenschaftlichen Fakultät
der Universität Bonn

Referent: Prof. Herbert K. Dreiner

Korreferent: Prof. Manuel Drees

Tag der Promotion: 1 Juli 2008

Diese Dissertation ist auf dem Hochschulschriftenserver der ULB Bonn

http://hss.ulb.uni-bonn.de/diss_online elektronisch publiziert.

Erscheinungsjahr: 2008

Contents

1	Introduction	5
1.1	Global supersymmetry	6
1.2	MSSM, proton–hexality and baryon–triality model	9
1.2.1	Supersymmetric Standard Model	9
1.2.2	MSSM, proton–hexality and baryon–triality	10
1.2.3	Mass eigenstates	11
1.3	mSUGRA	14
2	Supersymmetric Jarlskog invariants: the neutrino sector	18
2.1	Introduction	18
2.1.1	CP violation in the Standard Model	18
2.1.2	Jarlskog invariant in the Standard Model	19
2.1.3	Generalization	20
2.2	SM with 3 right-handed neutrinos	20
2.2.1	High-energy theory	22
2.2.2	Low-energy theory	26
2.2.3	Degenerate case	28
2.3	MSSM with 3 right-handed neutrinos	29
2.3.1	SUSY CP phases and CP-odd invariants	31
2.3.2	Low energy theory	35
2.4	Observables and CP-odd invariants	35
2.5	Conclusion	37
3	A simple baryon triality model for neutrino masses	38
3.1	Introduction	38
3.2	Simple B_3 -model	40
3.3	Other ansätze	44
3.4	B_3 neutrino masses	46
3.5	Neutrino masses from the simple B_3 -model	48
3.6	Numerical evaluation of the neutrino masses	49
3.6.1	General outline	49
3.6.2	Discussion of the results	51
3.7	Bounds on the products of the parameters of the simple B_3 -model	54

3.8	Collider tests	55
3.8.1	Stau LSP decays	56
3.9	Conclusions and outlook	58
4	Electroweak contributions to squark pair production at the LHC	59
4.1	Introduction	59
4.2	General formula	62
4.3	$qq' \rightarrow \tilde{q}\tilde{q}'$	63
4.3.1	$u_i u_j \rightarrow \tilde{u}_{i\alpha} \tilde{u}_{j\beta}$	64
4.3.2	$d_i d_j \rightarrow \tilde{d}_{i\alpha} \tilde{d}_{j\beta}$	65
4.3.3	$u_i d_j \rightarrow \tilde{u}_{i\alpha} \tilde{d}_{j\beta}$	65
4.3.4	$u_i d_j \rightarrow \tilde{d}_{i\alpha} \tilde{u}_{j\beta}, \quad i \neq j$	66
4.4	$q\bar{q}' \rightarrow \tilde{q}\tilde{q}$	67
4.4.1	$u_i \bar{u}_j \rightarrow \tilde{u}_{i\alpha} \tilde{u}_{j\beta}$	68
4.4.2	$u_i \bar{u}_i \rightarrow \tilde{q}_{j\alpha} \tilde{q}_{j\alpha}, \quad i \neq j$	69
4.4.3	$u_i \bar{u}_j \rightarrow \tilde{d}_{i\alpha} \tilde{d}_{j\beta}$	69
4.4.4	$d_i \bar{d}_j \rightarrow \tilde{q}\tilde{q}$	70
4.4.5	$d_i \bar{u}_j \rightarrow \tilde{d}_{i\alpha} \tilde{u}_{j\beta}$	70
4.4.6	$d_i \bar{u}_i \rightarrow \tilde{d}_{j\alpha} \tilde{u}_{j\beta}, \quad i \neq j$	71
4.5	Numerical results	72
4.5.1	Preliminary remarks	72
4.5.2	Results	73
4.5.3	Discussion	73
4.6	Experimental signals	83
4.7	Summary and conclusions	83
5	Summary	86
A	Independent CP-odd invariants	88
B	Couplings	91
B.0.1	Neutralino and Gluino Couplings	91
B.0.2	Chargino Couplings	92
B.0.3	Gauge Boson Couplings	92

Chapter 1

Introduction

The Standard Model (SM) has some shortcomings, though it is very successful [1]. The neutrino experiments [73] yield the first experimental evidence, that the SM is incomplete. It is not possible to generate Dirac neutrino masses, since there are no right-handed neutrinos. One could construct a Majorana mass term for the left-handed neutrinos, but this term is not SU(2) gauge-invariant and in addition the Majorana mass term breaks lepton-number. Non-perturbative mechanism like weak instanton effects cannot generate neutrino masses either, since $B - L$ is still conserved [137], where B and L denotes baryon- and lepton-number. In the presence of gravity, any global symmetry is violated [2]. Thus the effective low-energy SM Lagrangian should contain non-renormalizable baryon- and lepton-number violating terms. A possible non-renormalizable mass term for the left-handed neutrinos would be $\Psi_L \phi \Psi_L \phi / M_{\text{Pl}}$, where Ψ_L is the left-handed lepton field and ϕ is the Higgs doublet. The resulting neutrino mass is m_W^2 / M_{Pl} , where m_W is the electroweak mass scale and M_{Pl} is the Planck scale. However, the resulting neutrino mass is too small [137]. Thus the SM must be extended, in order to incorporate massive neutrinos.

Introducing gravity leads to a hierarchy problem [3]. The ratio of 2 mass scales $m_W / M_{\text{Pl}} \approx 10^{-17}$ is very small. The squared mass of the Higgs boson receives quadratically divergent radiative corrections. The cut-off scale would be M_{Pl} . Extreme fine-tuning is required [4] to obtain a Higgs mass of the order of the electroweak scale. Fine-tuning can be avoided, if one introduces boson-fermion pairs with identical couplings and masses. The resulting radiative contributions to the Higgs boson will then cancel. Thus supersymmetry stabilizes the electroweak scale [5].

The supersymmetric extension of the SM Lagrangian contains baryon and lepton-number violating operators [31, 157]. These operators trigger proton decay [31] and there are strict bounds on the baryon- and lepton-number violating couplings due to experimental bounds on the proton lifetime [6]. These operators can be forbidden by introducing the discrete symmetry R-parity [33] as done in the minimal supersymmetric SM (MSSM). Since the MSSM is a low-energy effective theory, one can generate neutrino masses via the seesaw mechanism [80]. It requires the introduction of right-handed neutrinos with a new large mass scale M_R , which is typically below the grand unified theory (GUT) scale.

Since no supersymmetric partners of the SM particles have been observed [7], supersymme-

try must be broken. In order to maintain the stability of the electroweak scale, the breaking terms must be soft [29], i. e., no new quadratically divergences must be introduced. The explicit soft-breaking terms introduce many new parameters [8], which can be complex and thus are possible sources of CP violation. The Yukawa couplings and the soft breaking terms with flavor indices contain flavor dependent CP phases. It is interesting to classify all flavor-dependent CP phases in terms of basis independent quantities [55, 48]. In the SM, the only flavor-dependent CP phase can be written in term of a Jarlskog invariant [41]. In the framework of the MSSM with right-handed neutrino superfields, we formulated basis-independent necessary and sufficient conditions for CP conservation. Our results [48] are presented in Chapter 2.

Within supersymmetry, one can impose the discrete symmetry baryon triality instead of R-parity. In the baryon triality conserving model [64, 85], renormalizable lepton-number violating operators are allowed. Neutrino masses are generated via tree-level mixing with the neutralinos as well as via radiative corrections [89]. However, the lepton-number violating Yukawa couplings introduces 36 new parameters in the superpotential. In a simple ansatz [71], the number of free parameters is reduced to 6. We fit these parameters, in order to solve the solar and atmospheric neutrino anomalies in terms of neutrino oscillations [74]. The resulting couplings are consistent with the stringent low-energy bounds. In the MSSM, the lightest supersymmetric particle (LSP) is stable, and is a candidate for dark matter [9]. In baryon triality models the LSP can decay, and thus the LSP is not required to be a neutral color singlet [31]. The resulting large hadron collider (LHC) signals for a stau LSP scenario are investigated [156]. The results of our work [72] are given in Chapter 3.

The LHC will start in 2008. If low-energy supersymmetry is realized in nature, one expects to discover supersymmetry at the LHC [144]. Squark production has a large cross section $\mathcal{O}(\alpha_s^2)$ and it is expected that ten thousands of squarks will be produced [19]. We calculated the complete electroweak leading order contribution to squark pair production. Since in many cases, QCD diagrams and EW diagrams interfere constructively, the total cross section is enhanced. In typical supersymmetric scenarios, the electroweak contributions to the QCD prediction amount to 10% to 20% for the production of two SU(2) doublet squarks. Our calculations and the discussion of the results were published in [159] and are given in Chapter 4.

In the following, a brief summary to global supersymmetry is given in Sec. 1.1. In Sec. 1.2 the MSSM, the proton-hexality and baryon-triality conserving model and our notation are introduced. In Sec. 1.3, some comments on minimal supergravity (mSUGRA) are given. There are several textbooks [10, 11, 12, 13, 14, 19, 20] and review articles [15, 16, 17, 18] about supersymmetry and supergravity. The notation and content of the first and third section closely follows the textbook [10].

1.1 Global supersymmetry

Supersymmetry is a global symmetry of the Lagrangian. Each bosonic particle has a fermionic partner. Thus the bosonic generators of the Poincare group are supplemented by Weyl spinor

generators Q_α , where $\alpha = 1, 2$. The algebra is given by [10, 21, 22]

$$\{Q_\alpha, Q_\beta\} = 0, \quad \{\bar{Q}_{\dot{\alpha}}, \bar{Q}_{\dot{\beta}}\} = 0, \quad \{Q_\alpha, \bar{Q}_{\dot{\beta}}\} = 2\sigma_{\alpha\dot{\beta}}^\mu P_\mu, \quad (1.1)$$

$$[P^\mu, Q_\alpha] = 0, \quad [M^{\mu\nu}, Q_\alpha] = -i(\sigma^{\mu\nu})_\alpha^\beta Q_\beta, \quad (1.2)$$

where $\bar{Q}_{\dot{\alpha}} = Q_\alpha^*$, P_μ is the generator of translations, $M^{\mu\nu}$ is the generator of rotations and $\sigma^{\mu\nu} = \frac{1}{4}(\sigma^\mu \bar{\sigma}^\nu - \sigma^\nu \bar{\sigma}^\mu)$. $\sigma^\mu = (I_2, \vec{\sigma})$ and $\bar{\sigma}^\mu = (I_2, -\vec{\sigma})$, where $\vec{\sigma}$ are the 3 Pauli matrices. A consequence of the last anti-commutator relation in Eq. (1.1) is, that in a supersymmetric theory the energy of any state, which is not the vacuum, is positive definite. Another consequence is that every representation has an equal number of bosonic and fermionic states with the same mass.

The commutator of P_μ and Q_α is zero and the spinor generator does not commute with the spin operator. As a result, irreducible representations are obtained, with equal masses, but different spins. The most important representations of the supersymmetry algebra are given in the following [10].

The chiral supermultiplet contains a Majorana spinor and a complex scalar field. It is used to describe matter fields like quarks, leptons and Higgs bosons and their corresponding supersymmetric partners, squarks, sleptons and higgsinos, respectively.

The vector supermultiplet consists of a vector field and its partner, a Majorana partner. The vector supermultiplet describes the gauge bosons and the fermionic partners, namely the gauginos, e. g. gluinos, photinos, zinos and winos.

The gravity supermultiplet consists of helicity $\pm 3/2$ particle and the supersymmetric partner with helicity ± 2 . It constitutes a graviton and the gravitino.

In order to construct supersymmetric Lagrangians, the superfield formalism [23, 24] is very useful. A general superfield $S(x, \theta, \bar{\theta})$ is a function of the space-time coordinates x and of the anti-commuting Grassmann variables θ_α and $\bar{\theta}_{\dot{\beta}}$. A general expansion of the superfield in a power series in θ and $\bar{\theta}$ is finite. The coefficients of the expansion are quantum fields. A general superfield is reducible. Requiring certain constraints on the superfields, irreducible representations can be obtained. Two important irreducible superfields are the chiral and vector superfield.

A chiral superfield Φ is obtained from a general superfield by requiring that a covariant fermionic derivative, acting on the general superfield, vanishes. It contains a Weyl spinor ψ , a complex scalar ϕ and an auxiliary scalar field F . Renormalizable supersymmetric Lagrangians are constructed by products of chiral superfields. It is convenient to write the supersymmetric Lagrangian as

$$\mathcal{L} = [\Phi^\dagger \Phi]_D + ([W(\Phi)]_F + h.c.). \quad (1.3)$$

with the superpotential [10],

$$W(\Phi) = \frac{1}{2}m\Phi\Phi + \frac{1}{3}\lambda\Phi\Phi\Phi, \quad (1.4)$$

where m and λ are real constants. The superpotential only contains powers of Φ up to the third order, since renormalizability is required. The subscript F and D in Eq. (1.3) denotes

the coefficient of $\theta\theta$ and $\bar{\theta}\bar{\theta}\theta\theta$ of the expansion, respectively. These terms are called F- and D-term. The F- and D-terms transform as a total divergence under supersymmetry and thus can be used for constructing invariant Lagrangians. The D-term of the product $\Phi^\dagger\Phi$ yields the kinetic energy terms of the scalar field ϕ and the Weyl field ψ . The F-term of $\Phi\Phi\Phi$ gives the Yukawa interaction. The scalar field F is an auxiliary field, necessary to formulate off-shell supersymmetric field theories. The Lagrangian does not contain any derivatives of the auxiliary field F and is removed by its equation of motion. From the D-term of $\Phi^\dagger\Phi$, one obtains the tree level effective potential,

$$V = F^\dagger F, \quad (1.5)$$

where $F^\dagger = -\frac{\partial W(\phi)}{\partial \phi}$. $W(\phi)$ is the superpotential, where each Φ is replaced by ϕ .

A vector superfield is obtained from a general superfield $V(x, \theta, \bar{\theta})$ by requiring following reality condition [26],

$$V(x, \theta, \bar{\theta}) = V(x, \theta, \bar{\theta})^\dagger. \quad (1.6)$$

A general vector superfield contains a vector field and its supersymmetric Majorana partner. In addition, it includes 4 auxiliary scalar fields and an auxiliary Weyl spinor field. If the vector superfield is used in the framework of abelian gauge field theory, one can use the unitary gauge freedom, namely the Wess-Zumino gauge [25], to remove all auxiliary fields, except one scalar field, the D-field.

A field strength superfield and the coupling of the gauge field with matter fields are necessary ingredients, in order to construct a supersymmetric gauge field theory. The field strength superfield W_α is obtained by taking several covariant derivatives of the vector superfield V . The F-term of $W^\alpha W_\alpha$ contains the kinetic energy terms of the gauge field and the corresponding gaugino. The coupling of the chiral matter fields to the gauge fields in a gauge-invariant way is obtained by taking the D-term contribution of

$$\Phi^\dagger \exp[2gV]\Phi, \quad (1.7)$$

where g is a $U(1)$ coupling. The auxiliary field $D = -g\phi^\dagger\phi$ contributes to the tree-level scalar potential $V = DD$. The generalization of the abelian case to the non-abelian case can be found in the literature [10, 11, 12, 13, 14, 19, 20].

In unbroken supersymmetry, the fields in the same supermultiplet are degenerate in mass. Since no supersymmetric partners of SM particles have been found, supersymmetry must be broken. Supersymmetry can be spontaneously broken, if the vacuum state is not annihilated by a supersymmetry generator. Thus the vacuum state has positive energy. This can be achieved by a non-vanishing vacuum expectation value (vev) of the F- [27] or the D-auxiliary field [28]. By breaking supersymmetry spontaneously, a massless Goldstone fermion, the Goldstino, arises. It is the supersymmetric partner of the F- or D-term, which obtained a vev.

In low energy-supersymmetry, the mass splitting between the fermions and the corresponding scalars can be parametrized by introducing explicit soft supersymmetric breaking terms, which do not introduce new divergencies [29, 30].

$$\tilde{M}_1 \text{Re } \phi^2 + \tilde{M}_2 \text{Im } \phi^2 + c(\phi^3 + h.c.) + \tilde{M}_3(\lambda^a \lambda^a + \bar{\lambda}^a \bar{\lambda}^a) + \tilde{M}_4(\lambda' \lambda' + \bar{\lambda}' \bar{\lambda}'), \quad (1.8)$$

where $\phi^2 \equiv d_{ij}\phi_i\phi_j$ and $\phi^3 \equiv d_{ijk}\phi_i\phi_j\phi_k$. ϕ^2 and ϕ^3 are group invariant combinations. The terms proportional to \tilde{M}_1 and \tilde{M}_2 describe the mass splittings between the scalar fields ϕ_i and the fermion fields ψ_i . The index i denotes the various chiral superfields. The complex scalar ϕ_i has 2 distinct real scalar fields, so the real part and the imaginary part have different masses. The term proportional to c describes new trilinear interactions of scalar fields and the last 2 terms parameterize the mass splittings of the gauginos.

1.2 MSSM, proton–hexality and baryon–trinality model

1.2.1 Supersymmetric Standard Model

Gauge Multiplets					
Superfield	Boson Fields	Fermionic Partners	$SU(3)_C$	$SU(2)_L$	$U(1)_Y$
\hat{G}	g	\tilde{g}	8	1	0
\hat{V}	W^a	\tilde{W}^a	1	3	0
\hat{V}'	B	\tilde{B}	1	1	0

Matter Multiplets					
Superfield	Boson Fields	Fermionic Partners	$SU(3)_C$	$SU(2)_L$	$U(1)_Y$
\hat{L}	$\tilde{L}^j = (\tilde{\nu}, \tilde{l})_L$	$(\nu, l)_L$	1	2	-1
\hat{E}	$\tilde{E} = \tilde{e}_R^*$	e_R^\dagger	1	1	2
\hat{Q}	$\tilde{Q}^j = (\tilde{u}_L, \tilde{d}_L)_L$	$(u, d)_L$	3	2	$\frac{1}{3}$
\hat{U}	$\tilde{U} = \tilde{u}_R^*$	u_R^\dagger	3^*	1	$-\frac{4}{3}$
\hat{D}	$\tilde{D} = \tilde{d}_R^*$	d_R^\dagger	3^*	1	$\frac{2}{3}$
$\hat{H}_1 = \hat{H}_d$	H_1^i	$(\tilde{H}_1^0, \tilde{H}_1^-)_L$	1	2	-1
$\hat{H}_2 = \hat{H}_u$	H_2^i	$(\tilde{H}_2^+, \tilde{H}_2^0)_L$	1	2	1

Table 1.1: Minimal particle spectrum of the supersymmetric Standard Model [32].

A supersymmetric extension of the SM is obtained by introducing supersymmetric partners of the SM particles. In the SM, the conditions for anomaly cancellation [32],

$$\text{Tr } T_3^2 Y = \text{Tr } Y^3 = 0, \quad (1.9)$$

are automatically satisfied. T_3 and Y are isospin and hypercharge. In the supersymmetric SM, the supersymmetric partner of the Higgs doublet contributes to the anomaly. E. g., inclusion of the supersymmetric partners to the SM matter content yields $\text{Tr } Y^3 = 2$. By including an additional $SU(2)$ doublet Higgs with hypercharge -1 , the gauge anomaly cancellation is again satisfied. The minimal particle spectrum of the supersymmetric SM is given in Table 1.1 [32].

The most general renormalizable superpotential of the supersymmetric SM is given by [36, 157]

$$W = h_{ij}^e \hat{L}_i \hat{H}_d \hat{E}_j + h_{ij}^d \hat{Q}_i \hat{H}_d \hat{D}_j + h_{ij}^u \hat{Q}_i \hat{H}_u \hat{U}_j + \mu \hat{H}_d \hat{H}_u \\ + \lambda_{ijk} \hat{L}_i \hat{L}_j \hat{E}_k + \lambda'_{ijk} \hat{L}_i \hat{Q}_j \hat{D}_k + \lambda''_{ijk} \hat{U}_i \hat{U}_j \hat{D}_k + \kappa_i \hat{L}_i \hat{H}_u, \quad (1.10)$$

where h_{ij}^e , h_{ij}^d , h_{ij}^u are the charged lepton, down-type quark and up-type quark Yukawa couplings, respectively. i, j, k are generation indices. μ is the Higgs superfield mass parameter. The Yukawa couplings λ_{ijk} , λ'_{ijk} and the dimensionful constant κ_i violate lepton number and λ''_{ijk} violates baryon number. The superfields \hat{L}_i , \hat{E}_i , \hat{Q}_i , \hat{D}_i and \hat{U}_i are the left-handed lepton, right-handed lepton, left-handed quark, right-handed down-type and right-handed up-type quark superfield, respectively. \hat{H}_d and \hat{H}_u are the SU(2) doublet Higgs superfields with hypercharges -1 and $+1$, respectively.

In exact supersymmetry, particles and their supersymmetric partners have degenerate masses. Since supersymmetry must be broken, soft breaking terms are added.

$$\Delta V_{\text{s.b.}} = M_{ij}^{q_L^2} \tilde{q}_{Li} \tilde{q}_{Lj}^* + M_{ij}^{u_R^2} \tilde{u}_{Ri} \tilde{u}_{Rj}^* + M_{ij}^{d_R^2} \tilde{d}_{Ri} \tilde{d}_{Rj}^* \\ + M_{ij}^{l^2} \tilde{l}_i \tilde{l}_j^* + M_{ij}^{e^2} \tilde{e}_i \tilde{e}_j^* \\ + m_1^2 |H_1|^2 + m_2^2 |H_2|^2 \\ + \left(H_2 A_{ij}^u \tilde{q}_i \tilde{u}_j^* + H_1 A_{ij}^d \tilde{q}_i \tilde{d}_j^* + H_1 A_{ij}^e \tilde{l}_i \tilde{e}_j^* + B\mu H_1 H_2 + \text{h.c.} \right) \\ - \frac{1}{2} M_1 \tilde{B} \tilde{B} - \frac{1}{2} M_2 \tilde{W}^a \tilde{W}^a - \frac{1}{2} M_3 \tilde{g} \tilde{g} \\ + A_{ijk} \tilde{l}_i \tilde{l}_j \tilde{e}_k^* + A'_{ijk} \tilde{l}_i \tilde{q}_j \tilde{d}_k^* + A''_{ijk} \tilde{u}_i \tilde{d}_j \tilde{d}_k^* + B_i \mu H_2 \tilde{l}_i + \tilde{m}_{di}^2 H_1^\dagger \tilde{l}_i + \text{h.c.} \quad (1.11)$$

The hermitian matrices $M_{ij}^{q_L^2}$, $M_{ij}^{u_R^2}$, $M_{ij}^{d_R^2}$, $M_{ij}^{l^2}$, $M_{ij}^{e^2}$ denote the soft scalar masses of the squarks and sleptons, m_1^2 and m_2^2 are the soft-terms of the 2 Higgs fields, A_{ij}^u , A_{ij}^d and A_{ij}^e are the trilinear soft breaking terms corresponding to the Yukawa couplings in the superpotential. $B\mu$ is the soft breaking term for the Higgs mass parameter. M_1 , M_2 and M_3 are the gaugino masses and the remaining soft breaking terms correspond to the lepton- and baryon-number violating terms in the superpotential. Without including the soft-breaking terms, the electroweak gauge group cannot be spontaneously broken [32].

1.2.2 MSSM, proton-hexality and baryon-triality

In the SM, baryon and lepton number are accidental global symmetries. In the supersymmetric SM, both symmetries are broken and the trilinear couplings λ' and λ'' can lead to rapid proton decay [31]. Thus stringent bounds on the trilinear couplings λ' and λ'' can be derived.

$$\lambda'_{11k} \lambda''_{11k} \leq 2 \cdot 10^{-27}, \quad (1.12)$$

where the mass of the down-type squark is assumed to be $m_{\tilde{d}} = 100$ GeV. Setting either λ' or λ'' equal to zero is the most natural explanation.

In the minimal supersymmetric SM (MSSM), a discrete \mathcal{Z}_2 symmetry is imposed, namely R-parity [33],

$$R_p = (-1)^{2S+3B+L}, \quad (1.13)$$

where S , B and L are spin, baryon number and lepton number. Imposing R-parity, all renormalizable lepton number and baryon number violating operators are forbidden. In Eq. (1.10), the couplings κ , λ , λ' and λ'' are zero. However, the supersymmetric Standard Model is an effective low energy theory and thus there are non-renormalizable operators, which can lead to rapid proton decay and which are allowed by R-parity.

In Ref. [158, 85] it is argued that all low energy discrete symmetries should be gauge symmetries, since quantum gravity effects violate all non-gauge symmetries. In addition, all gauge symmetries must be anomaly-free. Since the discrete symmetries should be a remnant of a broken gauge symmetry, the discrete gauge symmetry should obey certain anomaly conditions. In Ref. [85], the authors present a general classification of discrete \mathcal{Z}_N ($N = 2, 3$) symmetries. They find 2 discrete \mathcal{Z}_N ($N = 2, 3$) symmetries, which are anomaly-free with the light matter content. These are R-parity, a \mathcal{Z}_2 symmetry, and baryon-triality, a \mathcal{Z}_3 symmetry. In baryon triality models, dimension-5 or lower baryon number violating operators are forbidden, but lepton number violation is still possible. Thus the superpotential of the baryon triality model is given by Eq. (1.10) with $\lambda'' = 0$. Since R-parity does not forbid the dangerous dimension-5 operators, leading to proton decay, they favor baryon triality. In Ref. [64], the authors classify all \mathcal{Z}_N symmetries and find another discrete symmetry, proton-hexality. Proton-hexality is a \mathcal{Z}_6 symmetry and conserves lepton number and baryon number and forbids dimension-5 operators leading to proton decay. Thus proton-hexality and the MSSM have the same renormalizable superpotential. But it is difficult to embed proton-hexality in a grand unified theory (GUT), since the quarks and leptons are treated differently.

1.2.3 Mass eigenstates

In this section, the mass eigenstates of the MSSM (proton-hexality model) is discussed. After electroweak symmetry breaking, fields with the same color, charge and spin will mix. The mass spectrum of the baryon triality model differs from the MSSM, since lepton number is not conserved. The neutral Higgs bosons and the sneutrinos mix as well as the charged Higgs bosons and the sleptons. There is also mixing between the charginos and the charged leptons. Details can be found in Ref. [89, 83]. The mixing between neutralinos and neutrinos will be discussed in Chapter 3. This subsection closely follows Ref. [20, 32].

Gluinos

Since SU(3) is unbroken and the gluino \tilde{g} is the only color octet fermion, it cannot mix with other states. The mass is given by the soft breaking term M_3 . If M_3 is negative, the gluino field is multiplied with a factor of $-i$, which leaves the kinetic energy term unchanged [20].

Neutralinos

The weak neutral eigenstates, the higgsinos H_1^0, H_2^0 , the bino \tilde{B} and wino \tilde{W}^0 , mix. Before electroweak symmetry breaking, the masses of the bino and wino are the soft breaking terms M_1 and M_2 , respectively. When the Higgs fields acquire a vev, off-diagonal entries are generated in the 4×4 matrix in the weak basis [20],

$$Y_{\tilde{\chi}^0} = \begin{pmatrix} M_1 & 0 & -m_Z c_\beta s_W & m_Z s_\beta s_W \\ 0 & M_2 & m_Z c_\beta c_W & -m_Z s_\beta c_W \\ -m_Z c_\beta s_W & m_Z c_\beta c_W & 0 & -\mu \\ m_Z s_\beta s_W & -m_Z s_\beta c_W & -\mu & 0 \end{pmatrix}, \quad (1.14)$$

where $s_\beta = \sin \beta$, $c_\beta = \cos \beta$, $s_W = \sin \theta_W$ and $c_W = \cos \theta_W$. $M_{\tilde{\chi}^0}$ is a complex symmetric matrix and can be diagonalized by a unitary matrix Z .

$$M_{\tilde{\chi}^0} = Z^* Y_{\tilde{\chi}^0} Z^{-1}. \quad (1.15)$$

After diagonalization of the mass matrix, the 4 eigenstates $\tilde{\chi}_1^0, \tilde{\chi}_2^0, \tilde{\chi}_3^0$ and $\tilde{\chi}_4^0$ are called neutralinos. The masses are $m_{\tilde{\chi}_1^0} < m_{\tilde{\chi}_2^0} < m_{\tilde{\chi}_3^0} < m_{\tilde{\chi}_4^0}$. The mixing matrix elements Z_{ij} appear in the Feynman rules of the neutralino [32]. The sign of the mass eigenvalue corresponds to the CP quantum number. If one considers the case, where the terms proportional to m_Z are very small, then the mass eigenvalues are given by M_1, M_2 and $|\mu|$. In mSUGRA, the lightest neutralino is binolike, the second neutralino eigenstate is winolike with masses proportional to $m_{\tilde{\chi}_1^0} = M_1$ and $m_{\tilde{\chi}_2^0} = M_2$, respectively. The last 2 eigenstates are higgsinolike each having masses proportional to $m_{\tilde{\chi}_3^0} = m_{\tilde{\chi}_4^0} = |\mu|$ [20].

Assuming that the lightest neutralino is the lightest supersymmetric particle, it cannot further decay in the MSSM and is a candidate for non-baryonic dark matter [9].

Charginos

The charged higgsinos and charged winos can mix and the corresponding mass eigenstates are called charginos. Before electroweak symmetry breaking, the charged down- and up-type higgsinos mix via the μ -term. Below the electroweak scale, the charged gauginos mix with the charged higgsinos and the mass matrix is given by [20]

$$X = \begin{pmatrix} M_2 & \sqrt{2} m_W \sin \beta \\ \sqrt{2} m_W \cos \beta & \mu \end{pmatrix}. \quad (1.16)$$

Since X is an arbitrary complex matrix, 2 unitary matrices U and V are necessary to diagonalize the chargino mass matrix,

$$M_{\tilde{\chi}^\pm}^2 = V X^\dagger X V^{-1} = U^* X X^\dagger (U^*)^{-1}. \quad (1.17)$$

Since X is diagonalized by $U^* X V^{-1}$, the eigenvalues of $X X^\dagger$ or $X^\dagger X$ are not the squares of the eigenvalues of X [20]. The mass eigenstates $\tilde{\chi}_1^\pm$ and $\tilde{\chi}_2^\pm$ are called charginos. The eigenvalues are ordered $m_{\tilde{\chi}_1^\pm} < m_{\tilde{\chi}_2^\pm}$.

If the off-diagonal entries are neglected, the mass eigenvalues are $m_{\tilde{\chi}_1^\pm} = M_2$ and $m_{\tilde{\chi}_2^\pm} = |\mu|$, assuming $M_2 < |\mu|$. Then following relations between the neutralino and chargino eigenstates hold in many mSUGRA scenarios [20],

$$m_{\tilde{\chi}_1^\pm} = m_{\tilde{\chi}_2^0}, \quad m_{\tilde{\chi}_2^\pm} = m_{\tilde{\chi}_3^0} = m_{\tilde{\chi}_4^0}. \quad (1.18)$$

Squarks

There are 2 squark flavors for each generation, \tilde{u} and \tilde{d} . And for both flavors, there exist a SU(2) doublet and a SU(2) singlet squark, so that for 1 generation, there are 4 different squarks $\tilde{u}_L, \tilde{u}_R, \tilde{d}_L$ and \tilde{d}_R . In general, the down- or up-type squarks have generational mixing, but due to strong constrains in flavor changing neutral currents [69], family mixing is neglected. The mass matrix of the top squark is given by [20]

$$M_{\tilde{t}}^2 = \begin{pmatrix} M^{tL^2} + m_t^2 + \Delta_{\tilde{u}_L} & m_t(A^t - \mu \cot \beta) \\ m_t(A^t - \mu \cot \beta) & M^{uR^2} + m_t^2 + \Delta_{\tilde{t}_R} \end{pmatrix}, \quad (1.19)$$

where $\Delta_{\tilde{u}_L} = (1/2 - 2/3 \sin^2 \theta_W)m_Z^2 \cos 2\beta$ and $\Delta_{\tilde{u}_R} = -2/3 \sin^2 \theta_W m_Z^2 \cos 2\beta$. Left- and right mixing is only important for the stop sector. The lighter stop can be significantly lighter than the other squark mass eigenstates. Thus the lighter stop mass eigenstate can be much lighter than all the other squarks [20].

The sbottom mass matrix is [20]

$$M_{\tilde{b}}^2 = \begin{pmatrix} M^{bL^2} + m_b^2 + \Delta_{\tilde{d}_L} & m_b(A^b - \mu \tan \beta) \\ m_b(A^b - \mu \tan \beta) & M^{bR^2} + m_b^2 + \Delta_{\tilde{d}_R} \end{pmatrix}, \quad (1.20)$$

where $\Delta_{\tilde{d}_L} = (-1/2 + 1/3 \sin^2 \theta_W)m_Z^2 \cos 2\beta$ and $\Delta_{\tilde{d}_R} = 1/3 \sin^2 \theta_W m_Z^2 \cos 2\beta$. Left- and right-mixing is important for the sbottom sector, if $\tan \beta \gg 1$. Mixing can be neglected for the first 2 generations of down-type squarks [20, 32].

Sleptons

The mass matrix of the scalar taus is [20]

$$M_{\tilde{\tau}}^2 = \begin{pmatrix} M^{\tau L^2} + m_\tau^2 + \Delta_{\tilde{l}_L} & m_\tau(A^\tau - \mu \tan \beta) \\ m_\tau(A^\tau - \mu \tan \beta) & M^{\tau R^2} + m_\tau^2 + \Delta_{\tilde{l}_R} \end{pmatrix}, \quad (1.21)$$

where $\Delta_{\tilde{\tau}_L} = (-1/2 + \sin^2 \theta_W)m_Z^2 \cos 2\beta$ and $\Delta_{\tilde{\tau}_R} = 1/3 \sin^2 \theta_W m_Z^2 \cos 2\beta$. Again mixing must be considered, if $\tan \beta \gg 1$. The stau can be significantly lighter than the sfermions of the first 2 generations. In many mSUGRA scenarios, the squark masses are larger than the slepton masses, so that the neutralinos and charginos mainly decay into taus and staus [20].

Higgs sector

The 2 SU(2) doublet Higgs fields have 8 real degrees of freedom. 3 of these are Goldstone bosons, which are absorbed by the W^\pm and Z gauge bosons. The remaining 5 degrees of freedom are physical. The tree-level Higgs potential conserves CP, so that the CP-even and CP-odd states do not mix.

The mass of the CP-odd neutral Higgs boson is [32]

$$m_A^2 = \frac{(B\mu)^2}{\sin\beta \cos\beta}. \quad (1.22)$$

The charged Higgs mass is given by [32]

$$m_{H^\pm}^2 = m_W^2 + m_A^2. \quad (1.23)$$

The mass matrix of the 2 neutral CP-even Higgs-bosons is given in the H_1 - H_2 basis [32],

$$M^2 = \begin{pmatrix} m_{A^0}^2 s_\beta^2 + m_Z^2 c_\beta^2 & -(m_{A^0}^2 + m_Z^2) s_\beta c_\beta \\ -(m_{A^0}^2 + m_Z^2) s_\beta c_\beta & m_{A^0}^2 c_\beta^2 + m_Z^2 s_\beta^2 \end{pmatrix}. \quad (1.24)$$

Diagonalization of the 2×2 mass matrix yields the mass eigenvalues [32],

$$m_{H^0, h^0}^2 = \frac{1}{2} \left(m_{A^0}^2 + m_Z^2 \pm \sqrt{(m_{A^0}^2 + m_Z^2)^2 - 4m_Z^2 m_{A^0}^2 \cos^2 2\beta} \right), \quad (1.25)$$

where $m_{h^0} \leq m_{H^0}$. From the tree-level masses, following inequalities can be obtained [32],

$$m_{h^0} \leq m_{A^0}, \quad (1.26)$$

$$m_{h^0} \leq m |\cos 2\beta| \leq m_Z, \quad m \equiv \min(m_Z, m_{A^0}), \quad (1.27)$$

$$m_{H^0} \geq m_Z, \quad (1.28)$$

$$m_{H^\pm} \geq m_W. \quad (1.29)$$

These relations will be modified by radiative corrections [32].

1.3 mSUGRA

The supergravity supermultiplet consists of a spin-2 graviton and a spin-3/2 gravitino. In the pure supergravity case, i. e. without couplings to matter fields, the locally supersymmetric action is the sum of the Einstein action and the Rarita-Schwinger equation. The Rarita-Schwinger equation yields the kinetic energy term of the gravitino [37].

Pure supergravity should be coupled to the matter fields, i. e. to the chiral and vector superfields. The general supergravity Lagrangian depends only on the Kähler potential [38]. The Kähler potential is a function of scalar fields, being members of chiral superfields. The

renormalizability of the Lagrangian is not required in the presence of gravity. Thus the superpotential is not constrained by the requirement, that the polynomial in the superfield Φ must be up to the third power. In addition, the kinetic energy terms of the chiral and vector supermultiplets need not to be of the "minimal form".

Supersymmetry will be broken, if an auxiliary field F of a chiral superfield or a D field of a vector multiplet gets a non-vanishing vev. In global supersymmetry, a massless fermion, the goldstino, is generated, if supersymmetry is broken. Since in supergravity, supersymmetry is a local symmetry, the resulting goldstino gives mass to the gravitino. In typical supergravity models, the mass of the gravitino is given by [10, 32],

$$m_{3/2} \approx \frac{M_S^2}{M_P}, \quad (1.30)$$

where M_S is the scale of supersymmetry breaking and M_P is the Planck scale. Thus one requires $M_S \approx 10^{10}$ GeV.

In hidden-sector supersymmetry breaking, supersymmetry is broken in a gauge-singlet sector, which is coupled to the matter fields of the observable sector via gravitational interaction. Thus supersymmetry breaking is transferred through gravitation [34]. In the following, minimal kinetic energy terms for the chiral superfields are assumed. The low-energy limit is obtained by taking $m_P \rightarrow \infty$, whereas $m_{3/2}$ is constant. In this limit omitting the D term contribution, the scalar potential is given by [10]

$$V = \left| \frac{\partial \hat{W}}{\partial y_r} \right|^2 + m_{3/2}^2 |y_r|^2 + A m_{3/2} (\hat{W} + \hat{W}^*), \quad (1.31)$$

where A is a complex number and \tilde{W} is the superpotential, which is trilinear in the chiral superfields. The first term in Eq. (1.31) is the F-term as in the global supersymmetry. The other 2 terms break supersymmetry. The low-energy Lagrangian, involving the fermions, is the same as for unbroken global supersymmetry with superpotential \tilde{W} . Thus $m_{3/2}$ is the mass splitting between fermions and bosons.

In order to obtain supersymmetry breaking in the vector supermultiplet, the kinetic energy term of the gauge field strength superfield must be non-minimal. This provides a mass splitting between the gauginos and the corresponding gauge bosons. The gauginos acquire a mass of $m_{1/2} \approx m_{3/2}$.

In mSUGRA [34], it is assumed, that the soft breaking parameters are universal and flavor diagonal at the unification or Planck scale. The following boundary conditions are assumed for the flavor and Higgs sector,

$$M_{ij}^{qL^2} = M_{ij}^{uR^2} = M_{ij}^{dR^2} = M_{ij}^{l^2} = M_{ij}^{e^2} = m_0^2 \delta_{ij}, \quad (1.32)$$

$$m_1^2 = m_2^2 = m_0^2, \quad (1.33)$$

$$A_{ij}^u = A_{ij}^d = A_{ij}^e = A_0 \delta_{ij}. \quad (1.34)$$

The squared scalar masses and the A-terms are flavor diagonal and universal [20, 8]. In the gaugino sector, the following assumptions are made [20, 8],

$$\sqrt{\frac{5}{3}}g_1 = g_2 = g_3 = g, \quad (1.35)$$

$$M_1 = M_2 = M_3 = m_{1/2}. \quad (1.36)$$

In addition, it is assumed that the the gaugino masses, μ and m_{12}^2 are real [8]. mSUGRA can be parametrized with 5 parameters. These are m_0 , $m_{1/2}$, A_0 , $\tan\beta$ and $\text{sgn}(\mu)$. The latter 2 parameters are obtained by replacing m_{12}^2 and μ^2 by v^2 and $\tan\beta$, where the sign of μ is not fixed [8]. This is a great reduction of free parameters. In the MSSM, if one introduces soft breaking terms, there are more than 100 free parameters [8].

In order to obtain the mass spectrum at the weak scale, one must apply the renormalization group equations (RGE's) of the MSSM [35]. For the masses of the gauginos, the following relation can be derived from the 1-loop RGE's [20],

$$\frac{M_i(Q)}{\alpha_i(Q)} = \frac{m_{1/2}}{\alpha_i(m_P)}, \quad (i = 1, 2, 3) \quad (1.37)$$

where $\alpha_i = \frac{g_i^2}{4\pi}$ are the gauge couplings and Q is some scale. From Eq. (1.37) and $Q = m_Z$, it follows

$$M_3(m_Z) : M_2(m_Z) : M_1(m_Z) \approx 7 : 2 : 1. \quad (1.38)$$

Thus the gluino is heavier than the electroweak gauginos.

The 1-loop RGE's of the scalar particles are given by ¹ [20],

$$\frac{dm_2^2}{dt} = \left(\frac{3X_t}{4\pi} - 6\alpha_2 M_2^2 - \frac{6}{5}\alpha_1 M_1^2 \right) / 4\pi, \quad (1.39)$$

$$\frac{dM^{tL^2}}{dt} = \left(\frac{X_t}{4\pi} - \frac{32}{3}\alpha_3 M_3^2 - 6\alpha_2 M_2^2 - \frac{2}{15}\alpha_1 M_1^2 \right) / 4\pi, \quad (1.40)$$

$$\frac{dM^{tR^2}}{dt} = \left(\frac{2X_t}{4\pi} - \frac{32}{3}\alpha_3 M_3^2 - \frac{32}{15}\alpha_1 M_1^2 \right) / 4\pi, \quad (1.41)$$

$$\frac{dm_1^2}{dt} = \left(-6\alpha_2 M_2^2 - \frac{6}{5}\alpha_1 M_1^2 \right) / 4\pi, \quad (1.42)$$

where $X_t = 2|y_t|^2(m_2^2 + M^{tL^2} + M^{tR^2} + A_0^2)$ is positive. The running of the scalar masses is determined by 2 effects [20], namely by the Yukawa couplings and the gaugino loop contributions. The gaugino contributions increase the scalar masses while decreasing the scale. On the other hand, the Yukawa couplings decrease the masses of the scalar particles by decreasing the scale Q . The main contribution in the Yukawa sector arises from the top Yukawa coupling. In the following, only the contribution of the top Yukawa coupling is taken into account. The

¹For the sake of simplicity, only the top Yukawa coupling is taken into account.

down-type Higgs does not directly couple to the top quark and thus does not receive a contribution from the top quark loop. Decreasing the scale Q yields that m_1^2 gets bigger. It is possible that the running of the up-type Higgs is such that decreasing the scale can trigger radiative electroweak symmetry breaking, since m_2^2 can be negative. The running of a mass spectrum from the high to the weak scale is given in Fig. 1.1

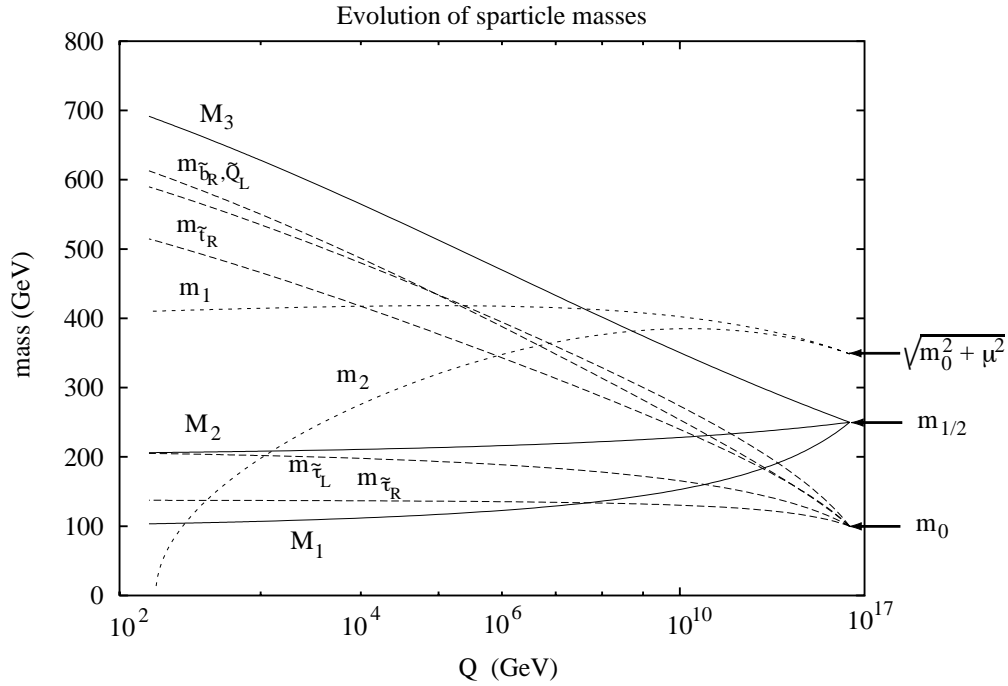


Figure 1.1: The running of scalar masses and the masses of the gauginos are shown. The figure is taken from Ref. [35]

Chapter 2

Supersymmetric Jarlskog invariants: the neutrino sector

2.1 Introduction

2.1.1 CP violation in the Standard Model

In the Yukawa sector, there are 3 arbitrary complex matrices, which are parametrized by 27 moduli and 27 phases. If the Yukawa couplings are zero, the Standard Model is invariant under the global flavor symmetry [39]

$$U_L \times U_{e_R} \times U_Q \times U_{u_R} \times U_{d_R}. \quad (2.1)$$

The number of physical CP phases can be deduced by following parameter counting [39]

$$N_{Y_{phys}} = N_Y - N_G + N_{G'}, \quad (2.2)$$

where N_Y is the number of parameters in the Yukawa couplings, N_G the number of parameters in the global symmetry, $N_{G'}$ the number of parameters after the Yukawa couplings break G to G' and $N_{Y_{phys}}$ the number of physical parameters. The formula can be understood as follows [39], if one considers the Higgs mechanism. A group G is broken to the subgroup G' by the Higgs field ϕ through its vacuum expectation value. The number of physical Higgs degrees of freedom is then given by

$$N_{\phi_{phys}} = N_\phi - N_{Goldstone} \quad (2.3)$$

N_ϕ is the number of degrees of freedom of the Higgs field ϕ and $N_{Goldstone}$ is the number of the Goldstone bosons. $N_{Goldstone}$ is given by $N_G - N_{G'}$, i. e. the number of broken generators of G .

A 3×3 unitary matrix can be parametrized by 6 phases [39]. Thus $6 \times 5 = 30$ phases can be removed by the unitary symmetry in Eq. (2.1). But the Standard Model has 4 global symmetries, namely baryon number and 3 lepton flavor numbers, which are also included in Eq. (2.1) [8], so that only 26 phases can be removed. One ends up with 1 CP phase $9 \times 3 - 30 + 4 = 1$.

In the charged quark currents, there is generally generation mixing of the quark mass eigenstates, which is described by the Cabibbo-Kobayashi-Maskawa (CKM) matrix V [1]. The unitary 3×3 matrix V is described by 9 numbers. Since an orthogonal matrix is described by 3 angles, the remaining 6 numbers are phases. But not all of them are physical, since it is possible to absorb a phase of V into the quark fields,

$$q_L \rightarrow \exp[i\alpha(q_L)]q_L, \quad (2.4)$$

where q_L is a left-handed quark field. 1 phase from either a row or a column of V can be removed. A common phase transformation of all q_L does not change V so that only $6 - 1 = 5$ phases are removed. Thus 1 physical phase remains in the CKM matrix being responsible for CP violation in the Standard Model. A common parametrization of the CKM matrix is given by the Kobayashi–Maskawa parametrization [40],

$$V = \begin{pmatrix} C_1 & -S_1 C_3 & -S_1 S_3 \\ S_1 C_2 & C_1 C_2 C_3 - S_2 S_3 \exp[i\delta] & C_1 C_2 S_3 + S_2 C_3 \exp[i\delta] \\ S_1 S_2 & C_1 S_2 C_3 + C_2 S_3 \exp[i\delta] & C_1 S_2 S_3 - C_2 C_3 \exp[i\delta] \end{pmatrix}, \quad (2.5)$$

where $S_i = \sin[\theta_i]$, $C_i = \cos[\theta_i]$ with the mixing angle θ_i and δ is the CP phase.

2.1.2 Jarlskog invariant in the Standard Model

The only CP-odd quantity of the Standard Model can be described in a weak basis invariant way [41],

$$J = \text{Im}(\text{Det}[Y^u Y^{u\dagger}, Y^d Y^{d\dagger}]). \quad (2.6)$$

J is called the Jarlskog invariant. It is invariant under quark basis transformations. CP violation is absent in the Standard Model if and only if the Jarlskog invariant is vanishing. This can be seen by expressing J in terms of the quark masses and the mixing matrix

$$J = (m_t^2 - m_u^2)(m_t^2 - m_c^2)(m_c^2 - m_u^2) (m_b^2 - m_d^2)(m_b^2 - m_s^2)(m_s^2 - m_d^2) \text{Im}(V_{11} V_{22} V_{12}^* V_{21}^*). \quad (2.7)$$

$\text{Im}[V_{11} V_{12} V_{12}^* V_{21}^*]$ is an invariant quartet of the CKM-mixing matrix. One can write the imaginary part as a function of angles and the CP phase δ . In the Kobayashi-Maskawa parametrization,

$$\text{Im}(V_{11} V_{22} V_{12}^* V_{21}^*) = \sin^2 \theta_1 \sin \theta_2 \sin \theta_3 \cos \theta_1 \cos \theta_2 \cos \theta_3 \sin \delta. \quad (2.8)$$

The expression vanishes for

$$\theta_i = 0, \quad \theta_i = \pi/2, \quad \delta = 0, \quad \delta = \pi. \quad (2.9)$$

J can also vanish, if 2 down-type or 2 up-type quarks are mass degenerate. In calculations for CP-odd quantities of the Standard Model, the CP-odd observables are related to the invariant quartet $\text{Im}(V_{11} V_{22} V_{12}^* V_{21}^*)$.

2.1.3 Generalization

The Jarlskog invariant of the Standard Model was generalized to extensions of the Standard Model, e.g. for more than 3 generations or extended Higgs sector [52, 42, 43, 53, 50, 54]. In Ref. [49, 51], the weak basis invariants in the Standard Model extended with right handed neutrinos are discussed. Jarlskog invariants for the MSSM were constructed in Ref. [55, 56]. We extended the notion of Jarlskog invariants to a supersymmetric model with 3 right-handed chiral neutrino superfields in [48]. The result of our paper is presented in the following sections.

In what follows, first the CP phases and invariants in the SM with 3 right-handed neutrinos are studied. We differ from previous work in implementing the concise techniques of [55]. Within this formalism, then the SUSY generalization is constructed, the Minimal Supersymmetric Standard Model (MSSM) with 3 right-chiral neutrino superfields, and examples of possible applications are given.

2.2 SM with 3 right-handed neutrinos

The neutrino anomalies can be explained by massive neutrinos. By extending the Standard Model with 3 heavy right-handed neutrinos, the masses of the light neutrinos are generated via seesaw mechanism [80]. In this framework, the relevant Lagrangian is given by

$$\Delta\mathcal{L} = Y_{ij}^e \bar{l}_i e_j H + Y_{ij}^\nu \bar{l}_i \nu_j \tilde{H} + \frac{1}{2} M_{ij} \bar{\nu}_i^c \nu_j + \text{h.c.},$$

where l , e , ν and H denote the left-handed charged lepton doublet, the right-handed charged lepton singlet, the right-handed neutrino singlet and the Higgs doublet, respectively. \tilde{H} is given by $i\tau_2 H^*$, where τ_2 is the second Pauli matrix. Y_{ij}^e is the charged lepton Yukawa matrix, Y_{ij}^ν is the Yukawa matrix for the neutrinos and M_{ij} is the complex symmetric Majorana mass matrix for the right-handed neutrinos. i, j are the generation indices and the superscript c denotes charge conjugation.

The kinetic energy terms of the leptons have the form

$$\mathcal{L}_{\text{kin}} = \bar{l} \not{D} l + \bar{e} \not{D} e + \bar{\nu} \not{D} \nu. \tag{2.10}$$

and are invariant under the following unitary flavor symmetry,

$$U(3)_l \times U(3)_e \times U(3)_\nu. \tag{2.11}$$

The lepton fields transform under the unitary basis transformation as

$$l \rightarrow U_l^\dagger l, \tag{2.12}$$

$$e \rightarrow U_e^\dagger e, \tag{2.13}$$

$$\nu \rightarrow U_\nu^\dagger \nu. \tag{2.14}$$

The corresponding Yukawa couplings and Majorana mass matrix transform as

$$Y^e \rightarrow U_l^\dagger Y^e U_e, \quad (2.15)$$

$$Y^\nu \rightarrow U_l^\dagger Y^\nu U_\nu, \quad (2.16)$$

$$M \rightarrow U_\nu^T M U_\nu. \quad (2.17)$$

The transformed Yukawa couplings and the Majorana mass term are equivalent to the original ones, i. e. they represent the same physics.

CP transformation on the fields is equivalent with complex conjugation of the Yukawa couplings and the Majorana mass matrix [57],

$$Y^e, Y^\nu, M \rightarrow Y^{e*}, Y^{\nu*}, M^*, \quad (2.18)$$

for an appropriate phase convention.

In seesaw models, the mass scale M_R of the Majorana mass term is below the GUT scale, in order to explain the tininess of the neutrino masses at low energies. 3 neutrinos are very light and the corresponding dimension-5 operator involves only left-handed neutrinos, since the right-handed neutrinos decouples from theory. The effective mass matrix is given by

$$m_{\text{eff}} = Y^\nu M^{-1} Y^{\nu T} \tilde{H}^2, \quad (2.19)$$

which results in neutrino masses upon the electroweak scale. Now the remaining flavor symmetry is given by

$$U(3)_l \times U(3)_e \quad (2.20)$$

with the transformation law

$$\begin{aligned} Y^e &\rightarrow U_l^\dagger Y^e U_e, \\ m_{\text{eff}} &\rightarrow U_l^\dagger m_{\text{eff}} U_l^*. \end{aligned} \quad (2.21)$$

The number of physical phases can be obtained with Eq. (2.2). The Yukawa couplings Y^e and Y^ν are arbitrary complex matrices and have $9 + 9 = 18$ phases. The complex symmetric Majorana mass matrix M has additional 6 phases, so that there are 24 phases. But not all phases are physical as seen in the last section. Each unitary matrix is parametrized by 6 phases, so that from the 24 phases in the Yukawa couplings and the Majorana mass matrix, 18 can be removed by the unitary symmetry (2.11)¹.

For the low-energy limit, Y^e and m_{eff} contain $9 + 6 = 15$ phases, 12 phases can be removed by the unitary symmetry and one ends up with 3 physical phases. The other 3 phases of the heavy neutrino sector cannot be observed at low energies. However, these can be relevant to CP violation at high energies, e. g. leptogenesis [66].

¹If the Majorana mass matrix were absent, only 17 phases could be removed since a phase transformation proportional to the unit matrix leaves Y^e and Y^ν intact, which corresponds to a conserved lepton number.

2.2.1 High-energy theory

CP Phases

The physical CP phases in the non-degenerate case are identified in a specific basis assuming a general form of Y^e , Y^ν and M . Taking advantage of the unitary symmetry in Eqs. (2.15)-(2.17), Y^ν can be diagonalized by a biunitary transformation,

$$Y^\nu \rightarrow U_l^\dagger Y^\nu U_\nu = \text{real diagonal}. \quad (2.22)$$

This basis is defined only up to a diagonal phase transformation

$$\tilde{U}_l = \tilde{U}_\nu = \text{diag}(\exp[i\alpha_1], \exp[i\alpha_2], \exp[i\alpha_3]). \quad (2.23)$$

In this specific basis, $U_l^\dagger Y^e$ can be written as

$$U_l^\dagger Y^e = H U, \quad (2.24)$$

where H is Hermitian and U is unitary. This can be done for any matrix and is known as the "radial coordinates decomposition". One can choose now,

$$U_e = U^\dagger. \quad (2.25)$$

Then there is no symmetry left, in order to bring M into a specific form.

The discussion shows, that one can start from the beginning with the following parameterization of the matrices.

$$\begin{aligned} Y^\nu &= \text{real diagonal} , \\ Y^e &= \text{Hermitian} , \\ M &= \text{symmetric} , \end{aligned} \quad (2.26)$$

where the last equation is satisfied in any basis². This basis is defined only up to a diagonal phase transformation

$$\tilde{U}_l = \tilde{U}_e = \tilde{U}_\nu = \text{diag}(\exp[i\alpha_1], \exp[i\alpha_2], \exp[i\alpha_3]). \quad (2.27)$$

Under this residual symmetry, Y^e and M transform as

$$Y_{ij}^e \rightarrow Y_{ij}^e \exp[i(\alpha_j - \alpha_i)], \quad (2.28)$$

$$M_{ij} \rightarrow M_{ij} \exp[i(\alpha_i + \alpha_j)]. \quad (2.29)$$

The physical phases must be invariant under the residual phase symmetry. In the special case that the Majorana mass term is zero, the only CP phase is given by³

$$\phi_0 = \arg[Y_{12}^e Y_{23}^e Y_{13}^{e*}]. \quad (2.30)$$

²This is not the only choice. Another basis is given, where Y^e and M are diagonal and Y^ν is arbitrary.

³The hermicity of Y^e has been used, $Y_{31}^e = Y_{13}^{e*}$.

This must be clearly the Dirac CP phase. Now, the general case ($M \neq 0$) is considered. Now there are 5 additional phases. 3 rephasing invariant phases can be constructed out of the matrix M ,

$$\phi_1 = \arg[M_{11}M_{22}M_{12}^{*2}], \quad (2.31)$$

$$\phi_2 = \arg[M_{22}M_{33}M_{23}^{*2}], \quad (2.32)$$

$$\phi_3 = \arg[M_{11}M_{33}M_{13}^{*2}], \quad (2.33)$$

while the remaining 2 involve Y^e as well,

$$\phi_4 = \arg[Y_{13}^e M_{13} M_{33}^*], \quad (2.34)$$

$$\phi_5 = \arg[Y_{23}^e M_{22} M_{23}^*]. \quad (2.35)$$

One can see, that the physical phases are indeed independent by considering the independent matrix elements. The choice of the phases is not unique. One can construct a different physical phase, e. g. the phase ϕ_4 can be replaced by ϕ'_4

$$\phi_4 = \arg[Y_{13}^e M_{13} M_{33}^*] \leftrightarrow \phi'_4 = \arg[Y_{12}^e M_{12} M_{22}^*], \quad (2.36)$$

but it can be written in terms of the phases in Eqs. (2.30)-(2.35).

The necessary and sufficient conditions for CP conservation are given by

$$\phi_i = 0 \quad (2.37)$$

for $i = 0, \dots, 5$, and the phases are understood mod π . If these conditions are satisfied, the flavor objects in Eq. (2.26) can be made real by choosing appropriate α_i . Then no CP violation is possible. Conversely, CP conservation implies that the flavour matrices are real in some basis. Then, the CP conserving Y^e, Y^ν and M are generated by phase redefinitions (2.27) leaving $\phi_i = 0$ intact.

It is clear, that the physical phases in Eqs. (2.30)-(2.35) are basis-dependent objects, which are invariant under the residual phase symmetry in Eq. (2.27). If one chooses a basis, where Y^e and M is diagonal and Y^ν is arbitrary, then the physical phases have a different form.

CP violating invariants

In the last subsection, the physical CP phases were given in the specific basis (2.26). The residual phase symmetry was used, in order to study the resulting CP phases. In this subsection, the CP-odd quantities are constructed in a basis independent way. Afterwards, in the specific basis of Eqs. (2.26), the weak basis independent invariants and the CP-phases in Eqs. (2.30)-(2.35) are related.

Now the corresponding weak basis invariants are constructed. Again, it might be useful to consider a simple example.

In the case that $M = 0$, there can be only 1 CP-violating invariant I . Of course, many other invariants can be constructed, but they will be only a function of I . Hermitian objects

are constructed, which only transform under one of the unitary symmetries in Eq. (2.11). From the Yukawa couplings Y^e and Y^ν , the following Hermitian objects are built,

$$A = Y^{\nu\dagger}Y^\nu, \quad B = Y^{\nu\dagger}Y^eY^{e\dagger}Y^\nu, \quad (2.38)$$

where A and B are Hermitian. Both transforming under the following unitary symmetry,

$$A, B \rightarrow U_\nu^\dagger A, B U_\nu \quad (2.39)$$

The trace of a product of the matrices A and B is invariant under the unitary flavor transformations U_l , U_e and U_ν . In order to construct weak basis invariants, which are CP-odd, the invariant must change sign under CP transformation. CP transformation on the fields is equivalent to complex conjugation of the matrices. Complex conjugation on the Yukawa couplings is equivalent to transposition of A and B , since A, B are Hermitian. The simplest non-vanishing CP-odd observable is then given by,

$$I = \text{Im Tr} [A, B]^3. \quad (2.40)$$

The trace of $[A, B]$ is vanishing. The trace of $[A, B]^2$ is non-vanishing, however, it does not change sign under CP transformation. Thus the invariant (2.40) is indeed the simplest possible choice⁴.

Now, the general case ($M \neq 0$) is considered. The following Hermitian matrices can be constructed

$$A \equiv Y^{\nu\dagger}Y^\nu, \quad (2.41)$$

$$B \equiv Y^{\nu\dagger}Y^eY^{e\dagger}Y^\nu, \quad (2.42)$$

$$C \equiv M^*M, \quad (2.43)$$

$$D \equiv M^*(Y^{\nu\dagger}Y^\nu)^*M. \quad (2.44)$$

In general, they are not diagonalizable simultaneously and transform as

$$\mathcal{M}_i \rightarrow U_\nu^\dagger \mathcal{M}_i U_\nu, \quad (2.45)$$

where $\mathcal{M}_i = \{A, B, C, D\}$. The simplest CP-odd invariants that can be formed out of this set are

$$\begin{aligned} & \text{Tr}[\mathcal{M}_i^p, \mathcal{M}_j^q]^n, \\ & \text{Tr}[\mathcal{M}_i^p, \mathcal{M}_j^q, \mathcal{M}_k^r]^m, \end{aligned} \quad (2.46)$$

where p, q, r are integer and n, m are odd; [...] denotes complete antisymmetrization of the matrix product. The first class of invariants is the familiar Jarlskog type ("J-type"), while the

⁴It can be also written as $\text{Im}(\det[A, B])$ [41].

second class (“ K -type”) appears, for example, in supersymmetric models [55]. A possible set of 6 independent weak basis invariants is given by⁵

$$\text{Tr}[A, B]^3, \quad (2.47)$$

$$\text{Tr}[A, C]^3, \quad (2.48)$$

$$\text{Tr}[A, D]^3, \quad (2.49)$$

$$\text{Tr}[A, C]B, \quad (2.50)$$

$$\text{Tr}[A, D]B, \quad (2.51)$$

$$\text{Tr}[A, D]C, \quad (2.52)$$

where $\text{Tr}[a, b, c] \propto \text{Tr}[a, b]c$ have been used. If the invariants are calculated in the basis (2.26), the first invariant is proportional to the sine of the Dirac phase (2.30). The remaining invariants are complicated functions of the phases in Eqs. (2.30)-(2.35). The independence of the 6 invariants can be shown by evaluating the Jacobian,

$$\text{Det}\left(\frac{\partial J_i}{\partial \phi_j}\right), \quad (2.53)$$

where J_i are the invariants above. A non-zero Jacobian indicates that the objects are independent. It is confirmed numerically that this is indeed the case.

It is instructive to consider the above invariants in a different basis, for example, where matrix A is diagonal,

$$A = \begin{pmatrix} A_1 & 0 & 0 \\ 0 & A_2 & 0 \\ 0 & 0 & A_3 \end{pmatrix}, \quad B = \begin{pmatrix} B_{11} & B_{12} & B_{13} \\ B_{12}^* & B_{22} & B_{23} \\ B_{13}^* & B_{23}^* & B_{33} \end{pmatrix}, \quad C = \begin{pmatrix} C_{11} & C_{12} & C_{13} \\ C_{12}^* & C_{22} & C_{23} \\ C_{13}^* & C_{23}^* & C_{33} \end{pmatrix}, \quad D = \dots \quad (2.54)$$

This basis is defined up to a rephasing

$$\tilde{U}_\nu = \text{diag}(\exp[i\alpha_1], \exp[i\alpha_2], \exp[i\alpha_3]). \quad (2.55)$$

The physical CP phases must be invariant under this residual symmetry and are of the form

$$\arg[B_{12}B_{23}B_{13}^*], \arg[C_{12}C_{23}C_{13}^*], \dots \quad (2.56)$$

$$\arg[B_{12}C_{12}^*], \arg[B_{23}C_{23}^*], \dots \quad (2.57)$$

The 4 Hermitian objects have altogether 12 phases. But the unitary symmetry can remove 5 phases, so that one ends up with 7 phases. This seems to be contradictory to the previous result, because one obtained 6 physical phases. The reason is that the Hermitian objects are built from 3 flavor objects, so that 1 phase is a functions of the other phases. Except from

$$\phi_0 \propto \arg[B_{12}B_{23}B_{13}^*]. \quad (2.58)$$

⁵The $\text{Im}(\dots)$ for each invariant is dropped in the following.

the phases in Eqs. (2.30)-(2.35) are complicated functions of the expressions in Eq. (2.56) and Eq. (2.57). For $\text{Tr}[A, B]^3$, one obtains the following explicit expression

$$6(A_1 - A_2)(A_2 - A_3)(A_3 - A_1)|B_{12}B_{23}B_{13}^*|\text{Arg}[B_{12}B_{23}B_{13}^*]. \quad (2.59)$$

If only A , B and C are taken, then only 4 phases can be extracted.

$$\arg[B_{12}B_{23}B_{13}^*], \arg[B_{13}C_{13}^*], \arg[B_{23}C_{23}^*], \arg[B_{12}C_{12}^*]. \quad (2.60)$$

The phase $\arg[C_{12}C_{23}C_{13}^*]$ is not an independent one, since it can be expressed in terms of the phases in Eq. (2.60),

$$\arg[C_{12}C_{23}C_{13}^*] = \arg[B_{12}B_{23}B_{13}^*] - \arg[B_{13}C_{13}^*] - \arg[B_{23}C_{23}^*] - \arg[B_{12}C_{12}^*]. \quad (2.61)$$

By constructing Hermitian objects, some informations got lost, so that it is necessary to include a further object D .

The necessary and sufficient conditions for CP conservation in the non-degenerate case are

$$J_i = 0, \quad (2.62)$$

where J_i are the invariants (2.47)-(2.52). This is equivalent to Eq.(2.37).

2.2.2 Low-energy theory

CP phases

At low energies, there are 2 flavor matrices Y_e and m_{eff} . Using the unitary freedom (2.21), both can be brought in the form

$$\begin{aligned} m_{\text{eff}} &= \text{real diagonal}, \\ Y^e &= \text{Hermitian}. \end{aligned} \quad (2.63)$$

In the non-degenerate case, there is no residual freedom in this basis due to the Majorana character of m_{eff} . The 3 off-diagonal phases of the Hermitian matrix Y^e are the physical phases

$$\phi_1^{\text{eff}} = \arg[h_{12}], \quad (2.64)$$

$$\phi_2^{\text{eff}} = \arg[h_{23}], \quad (2.65)$$

$$\phi_3^{\text{eff}} = \arg[h_{13}]. \quad (2.66)$$

Alternatively, one can choose a basis, in which Y^e is diagonal,

$$\begin{aligned} Y^e &= \text{real diagonal}, \\ m_{\text{eff}} &= \text{symmetric}, \end{aligned} \quad (2.67)$$

where the second equation is satisfied in any basis. The residual freedom is

$$\tilde{U}_l = \tilde{U}_e = \text{diag}(\exp[i\alpha_1], \exp[i\alpha_2], \exp[i\alpha_3]), \quad (2.68)$$

such that the 3 physical phases are of the form

$$\arg[(m_{\text{eff}})_{ii}(m_{\text{eff}})_{jj}(m_{\text{eff}})_{ij}^{*2}] \quad (2.69)$$

for $i \neq j$.

These phases can be separated into Majorana and Dirac ones. This can be done by expressing m_{eff} as

$$m_{\text{eff}} = U \text{ (real diagonal) } U^T, \quad (2.70)$$

where U is unitary. 5 of its phases can be factored out [62],

$$\begin{aligned} U &= \text{diag}(\exp[i\alpha_1], \exp[i\alpha_2], \exp[i\alpha_3]) \\ &\times U' \text{diag}(1, \exp[i\Phi_1], \exp[i\Phi_2]), \end{aligned} \quad (2.71)$$

with U' containing a single phase which cannot be factored out. The phases α_{1-3} are unphysical and can be removed by the residual symmetry transformations $m_{\text{eff}} \rightarrow \tilde{U}_l^\dagger m_{\text{eff}} \tilde{U}_l^*$, which is equivalent to rephasing the lepton fields. The ‘‘Majorana’’ phases $\Phi_{1,2}$ as well as the ‘‘Dirac’’ phase δ in U' are unaffected by this phase redefinition and are physical. They enter the PMNS matrix at the W-boson–lepton–lepton vertex [58]–[60].

The necessary and sufficient conditions for CP conservation in the non-degenerate case are given by

$$\phi_i^{\text{eff}} = 0 \quad (2.72)$$

for $i = 1, 2, 3$ which is equivalent to $\Phi_1 = \Phi_2 = \delta = 0$ (the phases are understood mod π).

CP violating invariants

As in the previous subsection, first Hermitian matrices are constructed, transforming under one of the unitary symmetries only. At low energies, U_l is the relevant symmetry and therefore the following Hermitian objects are chosen

$$\begin{aligned} \mathcal{A} &= Y^e Y^{e\dagger}, \\ \mathcal{B} &= m_{\text{eff}} m_{\text{eff}}^*, \\ \mathcal{C} &= m_{\text{eff}} (Y^e Y^{e\dagger})^* m_{\text{eff}}^*. \end{aligned} \quad (2.73)$$

They all transform as

$$\mathcal{M}_i \rightarrow U_l^\dagger \mathcal{M}_i U_l, \quad (2.74)$$

where $\mathcal{M}_i = \{\mathcal{A}, \mathcal{B}, \mathcal{C}\}$. Generally $\mathcal{A}, \mathcal{B}, \mathcal{C}$ are not diagonalizable in the same basis. They contain $3 \times 3 - 5 = 4$ invariant phases, 3 of which are independent and related to ϕ_i^{eff} . Again, using 2 Hermitian matrices, e.g. \mathcal{A} and \mathcal{B} , would only allow to extract information about 1 phase, so it is necessary to consider \mathcal{C} as well.

In principle, it is possible to construct weak basis invariants transforming under U_e ,

$$\mathcal{A}' = Y^{e\dagger} Y^e, \quad (2.75)$$

$$\mathcal{B}' = Y^{e\dagger} m_{\text{eff}} m_{\text{eff}}^* Y^e, \quad (2.76)$$

$$\mathcal{C}' = Y^{e\dagger} m_{\text{eff}} (Y^e Y^{e\dagger})^* m_{\text{eff}}^* Y^e, \quad (2.77)$$

but these expressions are quite cumbersome and in addition, U_e is not the relevant symmetry in the low-energy theory.

The CP-odd invariants can be chosen as

$$\text{Tr}[\mathcal{A}, \mathcal{B}]^3, \quad (2.78)$$

$$\text{Tr}[\mathcal{A}, \mathcal{C}]^3, \quad (2.79)$$

$$\text{Tr}[\mathcal{A}, \mathcal{B}] \mathcal{C}. \quad (2.80)$$

In the non-degenerate case, they are all independent and can be used to extract ϕ_i^{eff} . This is established by calculating the Jacobian $\text{Det}\left(\frac{\partial \mathcal{J}_i}{\partial \phi_j^{\text{eff}}}\right)$.

As expected, the Jarlskog-type invariant (2.78) is independent of the Majorana phases and is proportional to the Dirac phase,

$$\text{Tr}[\mathcal{A}, \mathcal{B}]^3 \propto \sin \delta. \quad (2.81)$$

The other invariants are complicated functions of the Dirac and Majorana phases.

The necessary and sufficient conditions for CP conservation in the non-degenerate case are

$$\mathcal{J}_i = 0, \quad (2.82)$$

where \mathcal{J}_i ($i = 1, 2, 3$) denote the invariants (2.78)-(2.80).

2.2.3 Degenerate case

So far it has been assumed that there are no degenerate eigenvalues in any of the matrices and that the mixing angles are non-zero. It is however instructive to consider the special case, where all the low-energy neutrino mass eigenvalues are equal, *i.e.* there exists a basis such that

$$m_{\text{eff}} = m \times \mathbf{1}, \quad (2.83)$$

where $\mathbf{1}$ is a 3×3 unit matrix and m is real and the mass of the neutrino, *i. e.* the eigenvalues of the effective Majorana mass matrix are degenerate. There is no residual phase symmetry left, but in this basis (2.63), there is an orthogonal symmetry,

$$\tilde{U}_l = \tilde{U}_e = O, \quad OO^T = \mathbf{1}, \quad (2.84)$$

which retains the Hermiticity of Y^e . The phases ϕ_i^{eff} are not all independent and can be parametrized by a single phase [61]. This means, that in the Majorana sector CP violation can be possible, even if the Majorana mass matrix is degenerate. This should be contrasted to the Dirac case. In the limit of degenerate eigenvalues or vanishing mixing angles, the invariant (2.81) vanishes.

In the basis (2.67) where Y_e is real and diagonal, it can be seen more explicitly, that there is 1 CP violating phase left. m_{eff} is expressed as follows

$$m_{\text{eff}} = m U_l^\dagger U_l^* = \text{symmetric unitary} , \quad (2.85)$$

since basis (2.67) must be unitarily related to the basis (2.83). m_{eff} is in the degenerate case a symmetric unitary matrix, parametrized by 4 phases (and 2 angles) [63]. Indeed, 3 of them can be factored out as [62]

$$\text{diag}(\exp[i\alpha_1], \exp[i\alpha_2], \exp[i\alpha_3]) U' \text{diag}(\exp[i\alpha_1], \exp[i\alpha_2], \exp[i\alpha_3]) , \quad (2.86)$$

while a symmetric unitary matrix U' contains a single phase. The explicit form of U' can be found in [61]. The phases α_{1-3} are removed by the residual phase symmetry (2.68) in this basis, leaving a single physical phase. This can be also understood by counting the parameter. Since there is only 1 Yukawa coupling and 1 unitary symmetric matrix, the number of physical phases is given by $9 + 4 - 12 = 1$.

Thus, in this degenerate case there is 1 physical Majorana phase. That this phase has to be Majorana is clear from the vanishing of the Jarlskog invariant $\text{Tr}[\mathcal{A}, \mathcal{B}]^3$. The only non-vanishing invariant is given by (2.79). In the basis where m_{eff} is diagonal, it is given by (up to a factor) [61]

$$\text{Tr}[Y^e Y^{e\dagger}, (Y^e Y^{e\dagger})^*]^3 \quad (2.87)$$

and is invariant under the residual orthogonal symmetry (2.84). It is non-zero in general since \mathcal{A} and \mathcal{A}^* are not diagonal in the same basis.

In principle, this analysis can be carried over to the ‘‘high energy theory’’ case. There are 4 physical CP phases, since $9 + 9 + 4 - 18 = 4$. But it is very tedious, since now the matrix element of M are related in a complicated way due to the additional unitary property.

The discussion of vanishing of CP phases due to degenerate Dirac masses is much simpler compared to the Majorana case and is discussed in [55].

2.3 MSSM with 3 right-handed neutrinos

The most general R-parity (or proton-hexality) conserving renormalizable superpotential [64] for the leptonic part is

$$\begin{aligned} \mathcal{W}_{\text{leptonic}} = & \hat{H}_2 Y_{ij}^\nu \hat{L}_i \hat{N}_j + \hat{H}_1 Y_{ij}^e \hat{L}_i \hat{E}_j \\ & + \frac{1}{2} M_{ij} \hat{N}_i \hat{N}_j . \end{aligned} \quad (2.88)$$

Here \hat{L} , \hat{E} and \hat{N} are the left-chiral superfields describing the lepton doublet, a charge conjugate of the right-handed electron and a charge conjugate of the right-handed neutrino, respectively. $\hat{\mathcal{H}}_1$ and $\hat{\mathcal{H}}_2$ are the Higgs doublet superfields. Again, in order to employ the seesaw mechanism, $M \gg M_Z$ is assumed. The relevant soft SUSY breaking terms are

$$\begin{aligned} \Delta V_{\text{soft}} = & (H_2 A_{ij}^\nu \tilde{l}_i \tilde{n}_j^* + H_1 A_{ij}^e \tilde{l}_i \tilde{e}_j^* \\ & + \frac{1}{2} B_{ij} \tilde{n}_i \tilde{n}_j + \text{h.c.}) \\ & + M_{ij}^{l2} \tilde{l}_i \tilde{l}_j^* + M_{ij}^{\nu 2} \tilde{n}_i \tilde{n}_j^* + M_{ij}^{e2} \tilde{e}_i \tilde{e}_j^* , \end{aligned} \quad (2.89)$$

where \tilde{l} , \tilde{e}^* and \tilde{n}^* are the scalar components of \hat{L} , \hat{E} and \hat{N} , respectively. \mathcal{H}_1 and \mathcal{H}_2 denote the Higgs doublets. The soft parameters $M_{ij}^{\nu 2}$ and B_{ij} are not constrained by naturalness, since both are connected to the right-handed sneutrino fields, being singlets under $SU(2) \times U(1)$ [65]. In the following, it is understood that the soft-terms B and $M^{\nu 2}$ are of the order of the Majorana mass scale M_R .

As in the Standard Model, the flavor symmetry is

$$U(3)_l \times U(3)_e \times U(3)_\nu , \quad (2.90)$$

which now applies to superfields. Fermions and sfermions are transformed with the same unitary flavor matrices, in order to avoid flavor mixing at a fermion-sfermion-gaugino vertex such as $e\tilde{\chi}^0$. The flavor objects transform as follows,

$$Y^\nu \rightarrow U_l^\dagger Y^\nu U_\nu , \quad (2.91)$$

$$Y^e \rightarrow U_l^\dagger Y^e U_e , \quad (2.92)$$

$$A^\nu \rightarrow U_l^\dagger A^\nu U_\nu , \quad (2.93)$$

$$A^e \rightarrow U_l^\dagger A^e U_e , \quad (2.94)$$

$$M^{l2} \rightarrow U_l^\dagger M^{l2} U_l , \quad (2.95)$$

$$M^{\nu 2} \rightarrow U_\nu^\dagger M^{\nu 2} U_\nu , \quad (2.96)$$

$$M^{e2} \rightarrow U_e^\dagger M^{e2} U_e , \quad (2.97)$$

$$M \rightarrow U_\nu^T M U_\nu , \quad (2.98)$$

$$B \rightarrow U_\nu^T B U_\nu . \quad (2.99)$$

The number of physical phases in the non-degenerate case is counted as follows: The Yukawa couplings Y^e and Y^ν and the corresponding soft terms A^e and A^ν are arbitrary complex matrices and give $9 + 9 + 9 + 9 = 36$ phases. The soft terms of the scalar leptons are Hermitian and the off-diagonal entries yield $3 + 3 + 3 = 9$ phases. Finally, the mass term of the right-handed neutrino superfield and its soft term are complex symmetric and contribute $6 + 6 = 12$ phases. Altogether, all flavor objects in the leptonic sector contain 57 phases. Out of these original phases, 18 phases can be removed by the symmetry transformation in Eq. (2.90). One is left with 39 physical phases.⁶

⁶If the Majorana matrices were absent, we would get $45 - 17 = 28$ physical CP phases.

2.3.1 SUSY CP phases and CP-odd invariants

First, the physical CP phases are constructed in a specific basis, which is the same as in the Standard Model extended with 3 right-handed neutrinos (2.26),

$$\begin{aligned} Y^\nu &= \text{real diagonal} , \\ Y^e &= \text{Hermitian} , \\ M &= \text{symmetric} . \end{aligned} \tag{2.100}$$

6 of the physical phases are also the same as in the previous case

$$\phi_0 = \arg[Y_{12}^e Y_{23}^e Y_{13}^{e*}] , \tag{2.101}$$

$$\phi_1 = \arg[M_{11} M_{22} M_{12}^{*2}] , \tag{2.102}$$

$$\phi_2 = \arg[M_{22} M_{33} M_{23}^{*2}] , \tag{2.103}$$

$$\phi_3 = \arg[M_{11} M_{33} M_{13}^{*2}] , \tag{2.104}$$

$$\phi_4 = \arg[Y_{13}^e M_{13} M_{33}^*] , \tag{2.105}$$

$$\phi_5 = \arg[Y_{23}^e M_{22} M_{23}^*] . \tag{2.106}$$

The additional physical CP phases due to the new supersymmetric flavor structures are given by

$$\arg\left(Y_{ij}^e A_{ij}^{\{e,\nu\}*}\right) , \tag{2.107}$$

$$\arg\left(Y_{ij}^e M_{ij}^{\{e,\nu,l\}2*}\right) , \tag{2.108}$$

$$\arg\left(M_{ij} B_{ij}^*\right) . \tag{2.109}$$

The first class of physical phases, originating from the A terms, provides 18 phases. The second class, involving the Hermitian soft slepton masses, gives additional 9 phases and the last class, covering the symmetric Majorana mass term and its soft term yields 6 phases.

In the second step, Hermitian objects are constructed. In the Standard Model case, all Hermitian objects transform under the same unitary symmetry, namely U_ν and U_l , respectively. Pursuing the same strategy in the supersymmetric case leads to very cumbersome Hermitian objects. Therefore, in the supersymmetric case, 3 separate groups of Hermitian objects are constructed, each transforming under one of unitary symmetry U_l , U_ν and U_e , respectively. These are listed in Table 2.1. This set is sufficient to provide a minimal set of weak basis invariants and therefore fixes all physical phases in the non-degenerate case. In the following, it is investigated on what CP phases these Hermitian matrices are sensitive to.

Consider for example Column 3. In the basis where $Y^{\nu\dagger} Y^\nu$ is diagonal, the CP phases invariant under the residual symmetry (2.27) are of the type

$$\arg((M_i)_{12} (M_i)_{23} (M_i)_{13}^*) , \tag{2.110}$$

$$\arg((M_i)_{12} (M_{i+1})_{12}^*) , \dots , \tag{2.111}$$

$U(3)_l$	$U(3)_e$	$U(3)_\nu$
$Y^e Y^{e\dagger}$	$Y^{e\dagger} Y^e$	$Y^{\nu\dagger} Y^\nu$
$Y^\nu Y^{\nu\dagger}$	$A^{e\dagger} A^e$	$A^{\nu\dagger} A^\nu$
$A^e A^{e\dagger}$	$Y^{e\dagger} A^e + \text{h.c.}$	$A^{\nu\dagger} Y^\nu + \text{h.c.}$
$A^\nu A^{\nu\dagger}$	M^{e2}	$M^{\nu2}$
$Y^e A^{e\dagger} + \text{h.c.}$		$M^* M$
$A^\nu Y^{\nu\dagger} + \text{h.c.}$		$M^* (Y^{\nu\dagger} Y^\nu)^* M$
M^{l2}		$B^* (Y^{\nu\dagger} Y^\nu)^* B$
		$B^* M + \text{h.c.}$

Table 2.1: The minimal set of Hermitian flavor objects.

where \mathcal{M}_i are the Hermitian matrices of the third Column of Table 2.1. Given $N > 1$ independent Hermitian matrices, one can construct $3N - 5$ independent invariant phases. These can be chosen as 1 CKM-type phase (2.110), taking a cyclic product of the the same matrix, and the rest of the form (2.111) by taking products of elements in the same positions in different matrices [55]. In this fashion, one obtains 19 invariant phases from Column 3. However, as it has been seen in the SM case, one has to be cautious in determining the correct number of *independent* phases, and not too many, since there are certain relations among these matrices.

In order to make the choice of Hermitian objects in Table 2.1 plausible and to better understand the counting of independent phases, consider first the hypothetical special case, when the only non-zero quantities are Y^e , Y^ν and $M^{\nu2}$. The arising Hermitian objects are: $Y^e Y^{e\dagger}$, $Y^\nu Y^{\nu\dagger}$ in the first column, $Y^{e\dagger} Y^e$ in the second column and $Y^{\nu\dagger} Y^\nu$ and $M^{\nu2}$ in the third column. In the basis (2.26) with $M = 0$, using the above counting arguments, one then obtains only 4 physical independent phases. These *can not* be recovered from the Hermitian quantities in the 3 columns of Table 2.1. It is only possible to get 1 phase of the form (2.110) in Column 1, and another phase of the same type from Column 3. In order to construct the 4 phases, it is thus necessary to include a more complicated Hermitian object, $Y^{\nu\dagger} Y^e Y^{e\dagger} Y^\nu$, in Column 3, as it was done in the Standard Model case. This brings in 3 extra phases, 2 of which are independent. This shows that, in the special case, extra Hermitian objects may have to be included.

Next the more involved case is considered, where apart from Y^e , Y^ν and $M^{\nu2}$, also $A^\nu \neq 0$. Again, by the counting argument, there exists 13 physical independent phases from the remaining Hermitian objects in Table 2.1 in the supersymmetric basis corresponding to (2.26). In order to construct the extra phases, additional Hermitian matrices can be written down, namely $A^\nu A^{\nu\dagger}$ and $A^\nu Y^{\nu\dagger} + \text{H.c.}$ in the first column, as well as $A^{\nu\dagger} A^\nu$ and $A^{\nu\dagger} Y^\nu + \text{H.c.}$ in the third column. These extra objects restore the deficit encountered above, *i.e.* one can now recover 13 physical phases from the Hermitian objects. The naïve counting gives 7 phases for Column 1 and 7 phases for Column 3, which is too many. However, of the matrices

$$A^\nu A^{\nu\dagger}, A^\nu Y^{\nu\dagger} + \text{H.c.}, A^{\nu\dagger} A^\nu, A^{\nu\dagger} Y^\nu + \text{H.c.}$$

only 3 are independent. One of these matrices, say $A^{\nu\dagger} Y^\nu + \text{H.c.}$, can be reconstructed from

the others. This can be seen more clearly by the following argument [55]. In a basis, where Y^ν is diagonal, the objects $A^\nu A^{\nu\dagger}$ and $A^{\nu\dagger} A^\nu$ fix the diagonalization matrices of A^ν up to a phase transformation,

$$A^\nu A^{\nu\dagger} \rightarrow U_l^\dagger A^\nu A^{\nu\dagger} U_l = \text{diag}(a_1^{\nu 2}, a_2^{\nu 2}, a_3^{\nu 2}), \quad (2.112)$$

$$A^{\nu\dagger} A^\nu \rightarrow U_\nu^\dagger A^{\nu\dagger} A^\nu U_\nu = \text{diag}(a_1^{\nu 2}, a_2^{\nu 2}, a_3^{\nu 2}). \quad (2.113)$$

A^ν is then expressed in terms of its eigenvalues and the diagonalization matrices,

$$A^\nu = U_\nu^\dagger \text{diag}(a_1^\nu, a_2^\nu, a_3^\nu) U_l. \quad (2.114)$$

Due to the residual phase symmetry, the diagonalization matrices are defined up to phase transformation

$$U_l \rightarrow \text{diag}(\exp[i\delta_1], \exp[i\delta_2], \exp[i\delta_3]) U_l, \quad (2.115)$$

$$U_\nu \rightarrow \text{diag}(\exp[i\phi_1], \exp[i\phi_2], \exp[i\phi_3]) U_\nu. \quad (2.116)$$

$\delta_i = \phi_i$ does not change A^ν , but $\delta_i = -\phi_i$ changes A^ν , so that the phases of A^ν are not fixed. This can be resolved by fixing $A^\nu Y^{\nu\dagger} + \text{h.c.}$ such that A^ν can be reconstructed. In other words, $A^{\nu\dagger} Y^\nu + \text{h.c.}$ can be reconstructed from $A^\nu A^{\nu\dagger}$, $A^{\nu\dagger} A^\nu$ and $A^\nu Y^{\nu\dagger} + \text{h.c.}$. This means that the CKM-type phase associated with $A^{\nu\dagger} Y^\nu + \text{H.c.}$, namely

$$\arg\left((A^{\nu\dagger} Y^\nu + \text{H.c.})_{12} (A^{\nu\dagger} Y^\nu + \text{H.c.})_{23} (A^{\nu\dagger} Y^\nu + \text{H.c.})_{13}^*\right) \quad (2.117)$$

is not an independent phase and should not be counted. Although it may seem that $A^{\nu\dagger} Y^\nu + \text{H.c.}$ should be excluded altogether, this is not correct since it allows one to restore the (otherwise missing) phases of $M^{\nu 2}$ through the rephasing invariant combinations

$$\arg\left((M^{\nu 2})_{12} (A^{\nu\dagger} Y^\nu + \text{H.c.})_{12}^*\right), \text{ etc.} \quad (2.118)$$

The other 3 phases can be chosen as

$$\arg\left((A^{\nu\dagger} A^\nu)_{12} (A^{\nu\dagger} Y^\nu + \text{H.c.})_{12}^*\right), \text{ etc.} \quad (2.119)$$

One thus ends up with 6 phases from the Hermitian matrices of Column 3 and 7 phases from those of Column 1. Similar considerations apply when adding A^e to Column 2, where the CKM-type phase for $A^{e\dagger} Y^e + \text{H.c.}$ is not independent.

In the Dirac case, where only $M = B = 0$ in (2.89), (2.90), *i.e.* also $M^l, M^\nu, M^e \neq 0$, these are the only complications and one gets 28 phases from the Hermitian objects of Table 2.1. Adding a non-trivial Majorana mass M results in 5 further physical phases. This is because, in the basis (2.26), M adds 6 phases while its overall phase can be eliminated by the residual symmetry transformation, which leaves Y^e and Y^ν invariant. To recover these 5 phases from the Hermitian objects, one must add 2 entries in Column 3, $M^* M$ and $M^* (Y^{\nu\dagger} Y^\nu)^* M$. This adds 6 invariant phases of the type (2.111), 5 of which are independent. Finally, inclusion of

B brings in 6 more physical phases of the type (2.111) in the basis (2.26), all of which are independent. Correspondingly, one adds $B^*(Y^{\nu\dagger}Y^\nu)^*B$ and $B^*M + \text{H.c.}$ to Column 3, which are sensitive to these phases. Note that the object of the form $B^*M + \text{H.c.}$ is necessary as it depends on the *physical* relative phase between B and M . In the end, the first, second and third Column provide 16, 6 and 17 independent phases, respectively.

The above choice of the Hermitian objects is not unique and there are many other possibilities. In particular, one may replace $A^{\nu\dagger}A^\nu$ in the third Column with $Y^{\nu\dagger}Y^eY^{e\dagger}Y^\nu$. In that case, the limit “soft terms” $\rightarrow 0$ reproduces the SM Hermitian matrices of Eqs. (2.41)-(2.44). On the other hand, the Hermitian objects in Table (2.1) are similar to the quark sector Hermitian objects of Ref. [55]. These choices are equivalent in the non-degenerate case.

The CP-odd invariants are constructed out of the Hermitian objects transforming under one of the unitary symmetries in Eq. (2.90), respectively. These can be chosen as 1 Jarlskog-type invariant and the rest K -invariants. The former is sensitive to the cyclic product of phases of each matrix while the latter are sensitive to the relative phases between Hermitian matrices [55]. Thus one has 39 independent invariants in the non-degenerate case,

$$\begin{aligned} J(H_1, H_2), \\ K(H_i^p, H_j^q, H_k^r), \end{aligned} \quad (2.120)$$

where $J(A, B) \equiv \text{Tr}[A, B]^3$, $K(A, B, C) \equiv \text{Tr}[A, B, C]$ and p, q, r are integers. In each invariant, only matrices H_a belonging to the same column appear. In the Appendix, an explicit example of 39 independent invariants is given. To prove that they are independent functions of the 39 physical phases (2.30)-(2.35) and (2.107)-(2.109), the Jacobian has been calculated

$$\text{Det}\left(\frac{\partial J_i}{\partial \phi_j}\right), \quad (2.121)$$

where J_i denotes collectively all the invariants (2.120) and ϕ_i are the physical phases. The Jacobian is non-zero. Thus, all the physical phases can be determined from these invariants.

The traditional Jarlskog invariants $\text{Tr}[H_i^p, H_j^q]^r$ are not sufficient to describe CP violation in supersymmetry. This is seen most easily in the case of 3 Hermitian matrices A, B, C (which can be, for example, $Y^eY^{e\dagger}$, $Y^\nu Y^{\nu\dagger}$ and M^{l2}). This system has 4 physical phases, however there are only 3 independent Jarlskog-type invariants $\text{Tr}[A, B]^3$, $\text{Tr}[B, C]^3$ and $\text{Tr}[C, A]^3$. All higher order Jarlskog-type invariants are proportional to these 3. This means that 1 CP phase cannot be picked up by such invariants and even if all of them vanish, CP violation is possible. It is thus necessary to include the K -type invariants [55].

The necessary and sufficient conditions for CP-conservation in the non-degenerate case amount to vanishing of the invariants (2.120). In that case, the 39 physical phases vanish and in some basis all the flavor objects are real. Clearly, there can then be no CP violation and any higher order CP-odd invariant, e.g. $\text{Tr}[A, B, C, D, E, \dots]$, would vanish as well.

The degenerate case is not discussed in detail. Suffice it to say that additional conditions such as $\text{Im}(\text{Tr}(A^e Y^{e\dagger})^n) = 0$, *etc.* arise [55].⁷

⁷It is assumed that different matrices are not diagonal in the same basis. In the degenerate case, this is not

$U(3)_l$	$U(3)_e$
$Y^e Y^{e\dagger}$	$Y^{e\dagger} Y^e$
$A^e A^{e\dagger}$	$A^{e\dagger} A^e$
$Y^e A^{e\dagger} + \text{h.c.}$	$Y^{e\dagger} A^e + \text{h.c.}$
M^{l2}	M^{e2}
$m_{\text{eff}} m_{\text{eff}}^*$	
$m_{\text{eff}} (Y^e Y^{e\dagger})^* m_{\text{eff}}^*$	

Table 2.2: The minimal set of Hermitian flavor objects in the low energy theory.

2.3.2 Low energy theory

Upon the electroweak scale, the right-handed (s)neutrinos decouple, and an effective mass matrix for the light neutrinos is generated. In the MSSM with right-handed superfields, the dimension-5 operator $LHLH$ generates the masses for the light neutrinos. The operator is R-parity invariant and also proton-hexality invariant. The Hermitian objects, transforming under either $U(3)_l$ or $U(3)_e$ are given in Table 2.2.

The physical phases are constructed in the basis (2.63). Since there is no residual phase symmetry left, all phases in the matrices Y^e , A^e , M^{l2} and M^{e2} are physical. The physical phases are given by Eqs. (2.64)-(2.66) and

$$\arg(A_{ij}^e) \rightarrow 9, \quad (2.122)$$

$$\arg(M_{ij}^{l2}) \rightarrow 3, \quad (2.123)$$

$$\arg(M_{ij}^{e2}) \rightarrow 3. \quad (2.124)$$

The corresponding invariants for the 18 physical phases are constructed from the Hermitian objects in Table 2.2. For each column, the weak basis invariants are constructed from the Hermitian matrices, transforming under the same flavor symmetry. A possible set is given in the Appendix. Again, the independence of the weak basis invariants is proved by calculating the Jacobian.

The necessary and sufficient conditions for CP conservation in the nondegenerate case is that all weak basis invariants vanish.

2.4 Observables and CP-odd invariants

In the Standard Model with an effective neutrino mass matrix, the Dirac-type CP violation can be expressed by the following weak basis invariant [51],

$$\text{Tr}[Y^e Y^{e\dagger}, m_{\text{eff}} m_{\text{eff}}^*]^3 = -6i \Delta_{21} \Delta_{32} \Delta_{31} \Delta m_{21}^2 \Delta m_{31}^2 \Delta m_{32}^2 \mathcal{J}_{CP}, \quad (2.125)$$

true and all J - and K -invariants can vanish even though there is physical CP violation. CP-odd invariants sensitive to the corresponding CP phases are, for example, $\text{Tr}[(A^e Y^{e\dagger})^n - \text{h.c.}]$.

where $\Delta_{21} = (m_\mu^2 - m_e^2)$, $\Delta_{32} = (m_\tau^2 - m_\mu^2)$ and $\Delta_{31} = (m_\tau^2 - m_e^2)$ and $\Delta m_{21}^2 = (m_2^2 - m_1^2)$. \mathcal{J}_{CP} is imaginary part of the product of 4 leptonic mixing matrix elements,

$$\mathcal{J}_{CP} = \text{Im}[U_{11}U_{22}U_{12}^*U_{21}^*]. \quad (2.126)$$

It can be expressed in terms of physical observables,

$$\mathcal{J}_{CP} = \frac{1}{8} \sin[2\theta_{12}] \sin[2\theta_{13}] \sin[2\theta_{23}] \cos[\theta_{13}] \sin \delta. \quad (2.127)$$

θ_{ij} , δ , denote the mixing angles and the Dirac CP phase, respectively. CP effects can be measured in the difference of the CP-conjugated neutrino oscillation probabilities,

$$P(\nu_e \rightarrow \nu_\mu) - P(\bar{\nu}_e \rightarrow \bar{\nu}_\mu). \quad (2.128)$$

The same invariant quartet also appears in Eq. (2.128). Thus both quantities are related. The explicit relation between the weak basis invariant and the CP violating process (2.128) can be found in [67]. The vanishing of the weak basis invariant provides the necessary and sufficient condition for observing (2.128).

In seesaw models, the baryon asymmetry is produced by the out of equilibrium decays of the right-handed neutrinos, provided the CP asymmetry is large enough. The CP violating asymmetry is given by,

$$\epsilon_1 = \frac{\Gamma_1 - \bar{\Gamma}_1}{\Gamma_1 + \bar{\Gamma}_1}, \quad (2.129)$$

Γ_1 and $\bar{\Gamma}_1$ are the decay rate of the lightest right-handed neutrino and the decay rate into CP conjugate particles, respectively. Ref. [66] related the CP asymmetry with a CP-odd weak basis invariant, provided the right handed neutrino masses are hierarchically ordered. Since a weak basis invariant can be expressed either in terms of left-handed or right-handed quantities, the CP asymmetry can be related to the phases arising in the PMNS matrix.

In the following, the neutralino induced electron electric dipole moment (EDM) (see [68] for recent analyses) is related to a "supersymmetric" weak basis invariant. In generic SUSY models, the EDM is often expressed in terms of the "mass insertion" $(\delta_{LR}^e)_{11}$ [69],

$$\Delta d_e \propto \text{Im}(\delta_{LR}^e)_{11}, \quad (2.130)$$

with

$$(\delta_{LR}^e)_{11} \approx \frac{\langle \mathcal{H}_1 \rangle A_{11}^e}{\tilde{m}^2}, \quad (2.131)$$

where the μ -term contribution is neglected. \tilde{m} is the average slepton mass and the A-terms are calculated in the basis where the charged lepton masses are diagonal and real.

To understand the connection to CP-odd invariants, a simple form for the A-terms is assumed in this basis,

$$A^e = \begin{pmatrix} A_{11}^e & A_{12}^e & 0 \\ 0 & 0 & 0 \\ 0 & 0 & 0 \end{pmatrix}. \quad (2.132)$$

Calculating the K -invariants with Hermitian matrices of Table 2.2, column 2, it turns out that this invariant controls the electron EDM.

$$\text{Tr} [Y^{e\dagger}Y^e, (Y^{e\dagger}A^e + \text{h.c.})]A^{e\dagger}A^e \propto \arg (A_{11}^e Y_{11}^{e*}) .$$

A few comments are in order. First, the reparametrization invariant phase $\arg (A_{11}^e Y_{11}^{e*})$ appears in the weak basis invariant. Second, this phase cannot be “picked up” by any Jarlskog-type invariant. This is because the A -matrix is effectively 2×2 and the CKM-type phases vanish. Finally, if $A_{12}^e = 0$, A^e and Y^e are diagonal simultaneously. In this (degenerate) case, the K -invariants vanish and CP violation comes from CP-odd invariants based on anti-hermitian objects like $\text{Tr} [(A^e Y^{e\dagger})^n - \text{h.c.}]$.

In general, even if all of the soft terms are real in some basis, that does not guarantee absence of dangerous SUSY contributions to EDMs. The SM flavour structures Y^e and m_{eff} may contain complex phases such that the reparametrization invariant phases are non-zero. In other words, K -invariants can be non-zero even if the soft terms are real. As a simple example, it is assumed that the soft term A^e is real. However, the following invariant,

$$\text{Tr}[m_{\text{eff}} m_{\text{eff}}^*, Y^e Y^{e\dagger}]A^e A^{e\dagger}, \quad (2.133)$$

is non-vanishing. This is similar to the quark sector where the CKM phase can result in large EDMs in the presence of real soft terms [70].

2.5 Conclusion

The generalization of the Jarlskog invariant to supersymmetric models with right-handed neutrinos has been constructed. CP violation in supersymmetric models is controlled by CP-odd invariants of the conventional Jarlskog-type (“ J -invariants”) as well as those involving anti-symmetric products of 3 Hermitian matrices (“ K -invariants”), which cannot be expressed in terms of the former.

The presence of right-handed neutrinos brings in new features, in particular, Majorana-type CP phases in supersymmetric as well as soft terms. The corresponding CP-odd invariants are built out of Hermitian objects involving a product of 2 or 4 flavor matrices as opposed to 2 in the Dirac case. This complicates the analysis, on one hand, but allows for interesting features, on the other hand. For example, CP violation is possible even if the neutrinos are all degenerate.

There are 39 physical CP phases and corresponding CP-odd invariants which control CP violation in the lepton sector of the MSSM with right-handed neutrinos. Below the seesaw scale, the low energy theory is described by 18 CP phases which can again be linked to 18 independent CP invariants. Basis-independent conditions for CP conservation in the non-degenerate case has been formulated.

Physical observables are in general complicated functions of CP-odd invariants, which has been illustrated with an example of the electron EDM. SUSY CP violation and, in particular, dangerous EDM contributions, are possible even if the soft terms are real in some basis.

Chapter 3

A simple baryon triality model for neutrino masses

3.1 Introduction

The first experimental evidence for physics beyond the Standard Model (SM) has been found in the neutrino sector [73]. The solar and atmospheric neutrino anomalies are best explained in terms of oscillating massive neutrinos [74], as opposed to for example lepton flavour-violating interactions [75]. Assuming massive neutrinos, based on a three neutrino fit including the recent MINOS [76] and the SK-II atmospheric data [77], the corresponding neutrino mass and mixing parameters at 1σ (3σ) C.L. are [78, 79]

$$\Delta m_{21}^2 = 7.9 \begin{matrix} +0.27 \\ -0.28 \end{matrix} \begin{pmatrix} +1.1 \\ -0.89 \end{pmatrix} \times 10^{-5} \text{eV}^2, \quad (3.1)$$

$$|\Delta m_{31}^2| = 2.6 \pm 0.2 (0.6) \times 10^{-3} \text{eV}^2, \quad (3.2)$$

$$\theta_{12} = 33.7 \pm 1.3 \begin{pmatrix} +4.3 \\ -3.5 \end{pmatrix}, \quad (3.3)$$

$$\theta_{23} = 43.3 \begin{matrix} +4.3 \\ -3.8 \end{matrix} \begin{pmatrix} +9.8 \\ -8.8 \end{pmatrix}, \quad (3.4)$$

$$\theta_{13} = 0 \begin{matrix} +5.2 \\ -0.0 \end{matrix} \begin{pmatrix} +11.5 \\ -0.0 \end{pmatrix}. \quad (3.5)$$

The angles are given in degrees. The most widely discussed extensions of the SM to include massive neutrinos involve the see-saw mechanism [80]. These require right-handed neutrinos, as well as a new, typically very large Majorana mass-scale. The see-saw mechanism can also be incorporated into the minimal supersymmetric SM (MSSM) [81], now requiring right-handed neutrino superfields, as well as the additional high mass scale.

However, within supersymmetry there is a simpler possibility to include massive neutrinos, namely via *renormalizable* lepton-number violating terms, $W_{\cancel{L}_i}$, in the superpotential [82],

$$W_{\cancel{L}_i} = \lambda_{ijk} \hat{L}_i \hat{L}_j \hat{E}_k + \lambda'_{ijk} \hat{L}_i \hat{Q}_j \hat{D}_k + \kappa_i \hat{L}_i \hat{H}_u, \quad (3.6)$$

$$W_{H_d} = h_{ij}^E \hat{L}_i \hat{H}_d \hat{E}_j + h_{ij}^D \hat{Q}_i \hat{H}_d \hat{D}_j + \mu \hat{H}_d \hat{H}_u. \quad (3.7)$$

For later use, the superpotential terms involving the down-like Higgs superfield are also included. The terms in $W_{\mathcal{L}_i}$ violate R -parity (a \mathbb{Z}_2 -symmetry) as well as proton hexality [64, 84] (a \mathbb{Z}_6 -symmetry), but conserve baryon triality (B_3 , a \mathbb{Z}_3 -symmetry, sometimes also misleadingly called baryon parity) [85, 31, 86]. The Majorana neutrino masses are generated via tree-level mixing with the neutralinos, as well as via radiative corrections [82, 87, 88, 89, 90, 91, 92]. There is an implicit see-saw mechanism in the neutralino-neutrino sector: $\kappa_i^2/M_{1/2}$, but with a much smaller hierarchy of mass scales. Furthermore, no new fields or mass scales are required.

Within a baryon triality supergravity model the largest neutrino mass is naturally small [83]. For universal soft breaking terms, the mixing, κ_i , with the neutralinos is zero at the unification scale. It is subsequently generated at the order of a few MeV via renormalization group equations. It is thus proportional to the product of a (small) down-like Higgs Yukawa coupling (for example of the bottom quark or the tau lepton), a (small) baryon triality coupling and the Higgs mixing parameter μ [93, 94, 95, 83]. The lighter neutrino masses are generated via radiative corrections, and are naturally further suppressed.

There are $9+27+3 = 39$ lepton-number violating (complex) parameters in the superpotential $W_{\mathcal{L}}$. There are also 39 corresponding soft-supersymmetry breaking parameters, which in principle are independent, but are usually related to those of $W_{\mathcal{L}}$ via universal soft-supersymmetry breaking [96]. In a top-down approach, *e.g.* based on the Froggatt-Nielsen mechanism [97], one can attempt to predict the order of magnitude of all superpotential parameters, *i.e.* $W_{\mathcal{L}_p}$ together with the Higgs Yukawa couplings, based on a spontaneously broken gauge symmetry, Ref. [98, 99] and references therein. See also Refs. [91, 100, 92, 101].

A baryon triality model of neutrino masses is proposed instead, based on a simple phenomenological ansatz [71], which relates the Higgs superpotential parameters to those that violate lepton-number. The justification for this is that the down-like Higgs doublet superfield and the lepton-doublet superfields have identical Standard Model gauge quantum numbers. No assumption are made about the possible underlying theory at the unification scale. This ansatz dramatically reduces the number of free parameters. If experimentally confirmed it would give a clear indication on how to construct the more fundamental unified theory.

In the literature there are other simple ansätze [102, 103, 104], the most common and also the most similar to the ansatz, used in this chapter, is pure bi-linear lepton-number violation, *i.e.* $\lambda_{ijk} = \lambda'_{ijk} = 0$, and $\kappa_i \neq 0$. For this there is an extensive literature, see for example [91, 87, 88, 100, 105, 106] and references therein. It is discussed how the simple baryon trilinear model differs from the bi-linear case in Sect. 3.3.

A special feature of baryon triality models for the neutrino masses, is that they lead to other observable effects at colliders and can thus be tested [107, 108, 104, 109, 110, 111, 112, 113, 114, 115, 116, 117, 118, 119, 120, 121, 122]. In the case of pure tri-linear couplings ($\kappa_i = 0$), a fit to the neutrino data, Eqs. (3.1)-(3.5), leads to values in the range $\lambda_{ijk}, \lambda'_{ijk} \sim 10^{-5} - 10^{-4}$ [123, 124, 125, 126]. These couplings are very small, in particular, too small for the resonant production of supersymmetric particles [127]. However, they do lead to the decay of the lightest

supersymmetric particle in the detector, possibly with a detached vertex. This model can be confirmed by measuring the branching ratios of the various lightest supersymmetric particle (LSP) decays and thereby measuring the couplings. However, several points have been missed in the literature. In the case of a pure fit, *i.e.* not a model, it is possible to have larger couplings, which do not contribute to the neutrino masses, or which are not required for the fit. In this case, the LSP decay which dominates the collider signals will be completely independent of the neutrino sector. Thus pure fit models can only be tested if the neutrino mass parameters dominate the B_3 sector. Here a complete model is considered, where the fit to the neutrino data fixes *all* the B_3 parameters. Second, it has hitherto been assumed, that the LSP is the lightest neutralino. Here a scalar tau LSP [83, 128] is considered.

The analysis is structured as follows: In Sect. 3.2, the model is presented in detail. Then the neutrino masses in baryon triality models is briefly reviewed, Sect. 3.4. In Sect. 3.5, the values of the free parameters are estimated which result in acceptable neutrino masses. In Sect. 3.6, the new parameters are numerically evaluated in the model, such that the neutrino masses and mixing angles fall in the required experimental ranges, *cf* Eqs. (3.1)-(3.5). In order to obtain at least two non-vanishing neutrino masses, at least two lepton numbers must be violated. This typically leads to significantly stricter bounds on the products of couplings [129, 130, 131, 132]. In Sect. 3.7, it is investigated, whether the model is consistent with these bounds. In Sect. 3.8, possible future tests of the ansatz at colliders are discussed, in particular the LHC. In Sect. 3.9 the conclusion is given.

3.2 Simple B_3 -model

In the MSSM, the lepton doublet superfields \hat{L}_i and the down-type Higgs superfield \hat{H}_d have the same gauge quantum numbers. They are distinguished through a discrete symmetry: lepton number. However, in the case of baryon triality, lepton number is violated and not well defined. In the most general baryon triality superpotential with the MSSM superfields, \hat{H}_d and \hat{L}_i have exactly corresponding terms in the superpotential, as can be seen in Eqs. (3.6) and (3.7). Due to this correspondence the following simple ansatz is motivated for the Yukawa coupling constants

$$\lambda_{ijk} \equiv \ell_i \cdot h_{jk}^E - \ell_j \cdot h_{ik}^E, \quad (3.8)$$

$$\lambda'_{ijk} \equiv \ell'_i \cdot h_{jk}^D, \quad (3.9)$$

$$\kappa_i \equiv c_i \cdot \mu. \quad (3.10)$$

Here, ℓ_i, ℓ'_i are c -numbers. Eq. (3.8) has the required form to maintain the anti-symmetry of the λ_{ijk} in the first two indices. The ansatz for the dimensionful mixing terms, Eq. (3.10), is no simplification and the κ_i are taken as free parameters. Given the ansatz of Eqs. (3.8), (3.9), and assuming the Higgs-Yukawa coupling constants are known (leading to the SM fermion mass matrices), then the 36 couplings $\lambda_{ijk}, \lambda'_{ijk}$, are parameterized in terms of the six numbers ℓ_i, ℓ'_j .

Since \hat{L}_i and \hat{H}_d have the same *gauge* quantum numbers, the ansatz in Eqs. (3.8), (3.9) is given in the $SU(2) \times U(1)$ *current*-eigenstate basis. Thus when computing neutrino masses and comparing the required Yukawa coupling constants to low-energy bounds, one must rotate to

the mass-eigenstate basis [157, 133]. This requires a bi-unitary transformation in generation space. The transformation of the left-handed and right-handed fermions (not superfields) are given by

$$\mathbf{e}_L = \mathbf{V}_e \mathbf{e}'_L, \quad \mathbf{d}_L = \mathbf{V}_d \mathbf{d}'_L, \quad \mathbf{u}_L = \mathbf{V}_u \mathbf{u}'_L, \quad (3.11)$$

$$\mathbf{e}_R = \mathbf{U}_e \mathbf{e}'_R, \quad \mathbf{d}_R = \mathbf{U}_d \mathbf{d}'_R, \quad \mathbf{u}_R = \mathbf{U}_u \mathbf{u}'_R, \quad (3.12)$$

where $\mathbf{V}_{e,d,u}$, $\mathbf{U}_{e,d,u}$ are 3×3 matrices in generation space and the prime denotes the mass-eigenstates. The charged lepton and quark states are combined into three-component vectors in generation space, *e.g.* $\mathbf{e}_L \equiv (e_L, \mu_L, \tau_L)$. The sfermion partners are rotated by the same matrices in flavor space. By construction, these transformations diagonalize the SM Yukawa coupling matrices

$$\mathbf{U}_e^\dagger \cdot (\mathbf{h}^E)^T \cdot \mathbf{V}_e = \frac{\sqrt{2}}{v_d} \mathbf{diag}(m_e, m_\mu, m_\tau), \quad (3.13)$$

$$\mathbf{U}_d^\dagger \cdot (\mathbf{h}^D)^T \cdot \mathbf{V}_d = \frac{\sqrt{2}}{v_d} \mathbf{diag}(m_d, m_s, m_b), \quad (3.14)$$

$$\mathbf{U}_u^\dagger \cdot (\mathbf{h}^U)^T \cdot \mathbf{V}_u = \frac{\sqrt{2}}{v_u} \mathbf{diag}(m_u, m_c, m_t), \quad (3.15)$$

where the normalization of the Higgs vacuum expectation value is $v = \sqrt{|v_u|^2 + |v_d|^2} = 246$ GeV and $\tan \beta \equiv v_u/v_d$.

In the following, it is assumed that the charged lepton mass- and weak-eigenstates are the same. The corresponding charged lepton rotation matrices are then given by $\mathbf{V}_e = \mathbf{U}_e = \mathbf{1}$. Thus in this simple ansatz, in the leptonic sector the mixing takes place entirely in the neutrino sector, *cf.* the discussion in Refs. [131, 133]. Using Eqs. (3.8), and (3.13), the $\hat{L}\hat{L}\hat{E}$ couplings can then be expressed in terms of the lepton masses and the three parameters ℓ_i

$$\lambda_{ijk} = \ell_i \frac{\sqrt{2} m_{e^j}}{v_d} \delta_{jk} - \ell_j \frac{\sqrt{2} m_{e^i}}{v_d} \delta_{ik}, \quad (3.16)$$

where $m_{e^j} \equiv (m_e, m_\mu, m_\tau)^j$. Explicitly the couplings are given in Table 3.1, as a function of the free parameters ℓ_i . As an example, the numerical coefficients are also given in the case where $\tan \beta = 10$, which fixes $v_d = 24.5$ GeV. Overall, of course, all couplings are proportional to the free parameters ℓ_i .

There are some very specific predictions for the $\hat{L}\hat{L}\hat{E}$ couplings in the model.

$$\lambda_{123} = \lambda_{132} = \lambda_{231} = 0 \quad (3.17)$$

$$\frac{\lambda_{121}}{\lambda_{233}} = -\frac{m_e}{m_\tau}, \quad \frac{\lambda_{122}}{\lambda_{133}} = \frac{m_\mu}{m_\tau}, \quad \frac{\lambda_{131}}{\lambda_{232}} = \frac{m_e}{m_\mu}. \quad (3.18)$$

Coupling	Model Value	Numerical Value ($\tan \beta = 10$)
λ_{121}	$-\ell_2 \sqrt{2} m_e / v_d$	$-2.9 \cdot 10^{-5} \cdot \ell_2$
λ_{122}	$\ell_1 \sqrt{2} m_\mu / v_d$	$6.1 \cdot 10^{-3} \cdot \ell_1$
λ_{123}	0	0
λ_{131}	$-\ell_3 \sqrt{2} m_e / v_d$	$-2.9 \cdot 10^{-5} \cdot \ell_3$
λ_{132}	0	0
λ_{133}	$\ell_1 \sqrt{2} m_\tau / v_d$	$1.0 \cdot 10^{-1} \cdot \ell_1$
λ_{231}	0	0
λ_{232}	$-\ell_3 \sqrt{2} m_\mu / v_d$	$-6.1 \cdot 10^{-3} \cdot \ell_3$
λ_{233}	$\ell_2 \sqrt{2} m_\tau / v_d$	$1.0 \cdot 10^{-1} \cdot \ell_2$

Table 3.1: Predictions for the $\hat{L}\hat{L}\hat{E}$ in the simple ansatz as a function of the free parameters ℓ_i .

Besides the vanishing couplings, the couplings satisfy the strict constraints

$$\lambda_{121} < 2.0 \cdot 10^{-5} \frac{m_{\tilde{\tau}_R}}{100 \text{ GeV}}, \quad (3.19)$$

$$\lambda_{122} < 3.6 \cdot 10^{-4} \sqrt{\frac{m_{\tilde{\tau}}}{100 \text{ GeV}}}, \quad (3.20)$$

$$\lambda_{131} < 3.4 \cdot 10^{-4} \frac{m_{\tilde{\mu}_R}}{100 \text{ GeV}}, \quad (3.21)$$

where the low-energy bounds are implemented in [131] for λ_{133} , λ_{233} , λ_{232} and inserted the PDG lepton masses [134].

Throughout the model is considered only at the weak scale. In principle it should be embedded in a unified model at the grand unified scale or above [99, 98]. In that case, the predictions in Eqs. (3.17), (3.18) would be modified by renormalization group effects. In particular the couplings in Eq. (3.17) would get non-zero contributions [95], which however are extremely small, as they are proportional to the product of three non-zero $\hat{L}\hat{L}\hat{E}$ couplings.

When expanding the $\hat{L}\hat{L}\hat{E}$ term in the Lagrangian into its mass-eigenstate components, one obtains (summation over generation indices implied)

$$\begin{aligned} \mathcal{L}_{LLE} = & \left[-\lambda_{ijk} \tilde{e}_R^{k*} \tilde{\nu}^{ic} P_L e^j - \lambda_{ijk} \tilde{e}_L^j \tilde{e}^k P_L \nu^i \right. \\ & \left. - \lambda_{ijk} \tilde{\nu}_L^i \tilde{e}^k P_L e^j \right] + h.c.. \end{aligned} \quad (3.22)$$

Next the $\hat{L}\hat{Q}\hat{D}$ term is considered in the Lagrangian. Expanding out the $SU(2)_L$ doublet superfields, one obtains

$$\mathcal{L}_{LQD} = \lambda'_{ijk} N_{Li} D_{Lj} \bar{D}_{Rk} - \lambda'_{ijk} E_{Li} U_{Lj} \bar{D}_{Rk}. \quad (3.23)$$

Rotating the quark superfields in the first term into the superfield basis where the quarks are in the mass-eigenstate and using Eqs. (3.9) and (3.13) one obtains

$$\begin{aligned}
\lambda'_{ijk} N_{Li} D_{Lj} D_{Rk} &= \lambda'_{ijk} [\mathbf{U}_d^\dagger]_{rk} [\mathbf{V}_d]_{js} N_{Li} D_{Ls}' D'_{Rr} \\
&= \ell'_i [\mathbf{U}_d^\dagger (\mathbf{h}^D)^T \mathbf{V}_d]_{rs} N_{iL} D'_{Ls} D'_{Rr} \\
&= \frac{\sqrt{2} \ell'_i}{v_d} m_{d^r} \delta_{rs} N_{iL} D'_{Ls} D'_{Rr}.
\end{aligned} \tag{3.24}$$

For the second term in Eq.(3.23), one obtains analogously

$$\begin{aligned}
\lambda'_{ijk} E_{Li} U_{Lj} D_{Rk} &= \ell'_i [\mathbf{U}_d^\dagger (\mathbf{h}^D)^T \mathbf{V}_d]_{rt} [\mathbf{V}_d^\dagger \mathbf{V}_u]_{ts} E'_{Li} U_{Ls}' D'_{Rr} \\
&= \frac{\sqrt{2} \ell'_i}{v_d} m_{d^r} [\mathbf{V}^\dagger]_{sr} E'_{Li} U_{Ls}' D'_{Rr},
\end{aligned} \tag{3.25}$$

where $\mathbf{V}_{CKM} = \mathbf{V}_u^\dagger \mathbf{V}_d$ is the Cabibbo-Kobayashi-Maskawa matrix. Combining Eqs. (3.24) and (3.25), one can then write the Lagrangian for the $\hat{L}\hat{Q}\hat{D}$ interactions in the mass-eigenstate basis and expanded in superfield components¹

$$\begin{aligned}
\mathcal{L}_{LQD} &= \left[-\tilde{\lambda}'_{ijk} \left(\tilde{\nu}_L^i \bar{d}^j P_L d^k + \tilde{d}_L^j \bar{d}^k P_L \nu^i + \tilde{d}_R^{j*} \bar{\nu}^{ic} P_L d^k \right) \right. \\
&\quad \left. + \tilde{\lambda}'_{ijk} V_{rj}^* \left(\tilde{e}_L^i \bar{d}^k P_L u^r + \tilde{u}_L^r \bar{d}^k P_L e^i + \tilde{d}_R^{k*} \bar{e}^{ic} P_L u^r \right) \right] \\
&\quad + h.c.,
\end{aligned} \tag{3.26}$$

with the coupling defined by

$$\tilde{\lambda}'_{ijk} \equiv \ell'_i \frac{\sqrt{2} m_{d_k}}{v_d} \delta_{jk}. \tag{3.27}$$

Following notation is introduced

$$\tilde{\lambda}'_{ijk} \equiv \ell'_i \frac{\sqrt{2} m_{d_k}}{v_d} [\mathbf{V}]_{jk}. \tag{3.28}$$

Note that the (s)neutrino interactions are flavor diagonal in the down-(s)quarks, whereas the charged (s)lepton interactions involve generation off-diagonal (s)quark interactions [133].

The flavor violation is suppressed by small Yukawa couplings and moreover, the charged currents are suppressed by the CKM-matrix [86].

An estimate of the couplings $\tilde{\lambda}'$ and $\tilde{\lambda}'$ has been given, modulo the ℓ_i in Table 3.2. It is again assumed $\tan\beta = 10$. Furthermore, the central PDG values for the quark masses are

¹The primes, denoting the mass-eigenstates, are omitted in the following.

Index	$\tilde{\lambda}'/\ell'_i$	$\tilde{\lambda}'/\ell'_i$
(i11)	$3.5 \cdot 10^{-4}$	$3.4 \cdot 10^{-4}$
(i12)	0	$1.4 \cdot 10^{-3}$
(i13)	0	$9.7 \cdot 10^{-4}$
(i21)	0	$8.0 \cdot 10^{-5}$
(i22)	$6.0 \cdot 10^{-3}$	$5.8 \cdot 10^{-3}$
(i23)	0	$1.0 \cdot 10^{-2}$
(i31)	0	$2.8 \cdot 10^{-6}$
(i32)	0	$2.5 \cdot 10^{-4}$
(i33)	0.24	0.24

Table 3.2: Predictions for the LQD in the ansatz as a function of the free parameters ℓ'_i . In the right column it is assumed $\tan\beta = 10$.

taken: $m_d = 6 \text{ MeV}$, $m_s = 103 \text{ MeV}$, $m_b = 4.2 \text{ GeV}$, and the central values of the global PDG fit for the CKM matrix entries (2 significant figures) [134]

$$\mathbf{V}_{CKM} = \begin{pmatrix} 0.97 & 0.23 & 0.0040 \\ 0.23 & 0.97 & 0.042 \\ 0.0081 & 0.042 & 1.0 \end{pmatrix}. \quad (3.29)$$

As can be seen from Table 3.2, there are also simple predictions for the $\tilde{\lambda}'$ couplings in terms of quark masses and \mathbf{V}_{CKM} entries and independent of $\tan\beta$,

$$\frac{\tilde{\lambda}'_{ijk}}{\tilde{\lambda}'_{ijl}} = \frac{m_{d^k} V_{jk}}{m_{d^l} V_{jl}}, \quad \frac{\tilde{\lambda}'_{ijk}}{\tilde{\lambda}'_{ilk}} = \frac{V_{jk}}{V_{lk}} \quad (3.30)$$

Eqs. (3.16), (3.27) (3.28) can be used to translate between the parameters ℓ_i , ℓ'_i and the B_3 couplings, where in the latter case, care must be taken to include the CKM-mixing for the charged (s)lepton interactions.

It is investigated whether with this reduced freedom in the B_3 sector, one can still obtain neutrino masses and mixings, which are, first of all, consistent with Eqs. (3.1)-(3.5) and second, where the resulting coupling constants are consistent with the existing low-energy bounds. In Sect. 3.8, the possible observable consequences of the absolute values of the couplings as well as of the relative values are studied.

3.3 Other ansätze

In Ref. [103, 104, 119] the hierarchy in the SM Higgs Yukawa couplings was taken to motivate a similar hierarchy in the LQD (and separately in the LLE couplings). The authors restrict themselves to the couplings λ'_{i33} and λ_{i33} . Here this interesting work is extended in several

respects. The most recent neutrino data are included in the fit; Eqs. (3.1)-(3.5). Furthermore, the CKM mixing in the ansatz are included, thus having a prediction for the full range of the couplings. This is particularly important for the observable consequences of the model, *i.e.* the LSP decays. Combined fits including all the couplings are done, *i.e.* the λ and the λ' couplings and also the κ_i , the Models **I** and **II** below in Sect 3.6.

The most widely considered simple ansatz are B_3 models, where $\lambda_{ijk} = \lambda'_{ijk} = 0$ and $\kappa_i \neq 0$, often denoted bi-linear R -parity violation. This clearly has only three free parameters compared to the six or nine, in the models, used in this work. In order to compare the two ansätze in more detail, the fields are combined $\mathcal{L}_\alpha = (\mathcal{L}_0, \mathcal{L}_i) = (H_d, L_i)$, where $\alpha = 0, \dots, 3$ and $i = 1, 2, 3$. The bi-linear R -parity violating superpotential is then

$$W = h_{ij}^E \mathcal{L}_i \mathcal{L}_0 \bar{E}_j + h_{ij}^D Q_i \mathcal{L}_0 \bar{D}_j + \mu \mathcal{L}_0 H_u + \kappa_i L_i H_u, \quad (3.31)$$

Following field redefinition can be made

$$\mathcal{L} \rightarrow \mathcal{L}' = \mathbf{R}\mathcal{L}, \quad (3.32)$$

such that the bi-linear lepton-number violating terms are eliminated from the superpotential. The explicit form for \mathbf{R} is given in Ref. [83, 98, 88]. One then obtains the superpotential

$$\begin{aligned} \tilde{W} &= h_{ij}^E [\mathbf{R}]_{i\alpha} [\mathbf{R}]_{0\beta} \mathcal{L}_\alpha \mathcal{L}_\beta \bar{E}_j \\ &+ h_{ij}^D [\mathbf{R}]_{0\alpha} Q_i \mathcal{L}_\alpha \bar{D}_j + \tilde{\mu} \mathcal{L}_0 H_u. \end{aligned} \quad (3.33)$$

The transformed parameters (denoted by a tilde) are then given by

$$\tilde{\mu} = \mu [\mathbf{R}]_{00} + \kappa_i [\mathbf{R}]_{i0} \quad (3.34)$$

$$\tilde{h}_{ij}^D = h_{ij}^D [\mathbf{R}]_{00} \quad (3.35)$$

$$\tilde{h}_{ij}^E = h_{ij}^E \left\{ [\mathbf{R}]_{li} [\mathbf{R}]_{00} - [\mathbf{R}]_{l0} [\mathbf{R}]_{0i} \right\} \quad (3.36)$$

$$\tilde{\lambda}'_{ijk} = h_{jk}^D [\mathbf{R}]_{0i} = \frac{[\mathbf{R}]_{0i}}{[\mathbf{R}]_{00}} \tilde{h}_{jk}^D \quad (3.37)$$

$$\begin{aligned} \tilde{\lambda}_{ijk} &= h_{lk}^E \left\{ [\mathbf{R}]_{lj} [\mathbf{R}]_{0i} - [\mathbf{R}]_{li} [\mathbf{R}]_{0j} \right\} \\ &= [\mathbf{R}]_{0i} \left(h_{lk}^E [\mathbf{R}]_{lj} \right) - [\mathbf{R}]_{0j} \left([\mathbf{R}]_{li} h_{lk}^E \right). \end{aligned} \quad (3.38)$$

In the last equation the parentheses are included to emphasize the sum over l . Note that not only are the tri-linear couplings λ_{ijk} , λ'_{ijk} generated, but also the Higgs Yukawa couplings are modified

$$h_{ij}^{E,D} \longrightarrow \tilde{h}_{ij}^{E,D}. \quad (3.39)$$

From Eq. (3.37) one can see that

$$\lambda'_{ijk} = \ell'_i \tilde{h}_{jk}^D, \quad \text{with} \quad \ell'_i = \frac{[\mathbf{R}]_{0i}}{[\mathbf{R}]_{00}} = \frac{\kappa_i}{\mu}. \quad (3.40)$$

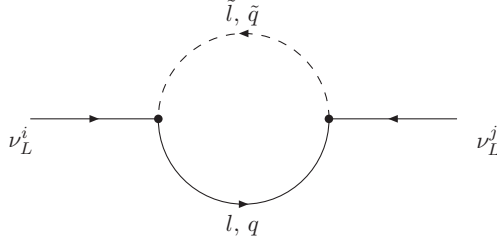


Figure 3.1: The radiative slepton-lepton and squark-quark contribution to the neutrino mass.

In the last equation, the explicit form of the matrix is employed \mathbf{R} . Next it will be shown that

$$\tilde{\lambda}_{ijk} = \ell_i \tilde{h}_{jk}^E - \ell_j \tilde{h}_{ik}^E. \quad (3.41)$$

For this \tilde{h}^E from Eq. (3.36) is inserted and factor $\ell_{i,j}$

$$\begin{aligned} \tilde{\lambda}_{ijk} &= \ell_j [\mathbf{R}]_{00} \left(h_{lk}^E[\mathbf{R}]_{li} \right) - \ell_i [\mathbf{R}]_{00} \left(h_{lk}^E[\mathbf{R}]_{lj} \right) \\ &\quad + \ell_j [\mathbf{R}]_{0i} \left(h_{lk}^E[\mathbf{R}]_{l0} \right) - \ell_i [\mathbf{R}]_{0j} \left(h_{lk}^E[\mathbf{R}]_{l0} \right) \end{aligned} \quad (3.42)$$

If one now sets

$$\ell_i = \frac{[\mathbf{R}]_{0i}}{[\mathbf{R}]_{00}} \quad \text{and} \quad \ell_j = \frac{[\mathbf{R}]_{0j}}{[\mathbf{R}]_{00}}. \quad (3.43)$$

the last two terms in Eq. (3.42) cancel and the first two terms agree with Eq. (3.38). In particular, one can see that B_3 models with only bi-linear terms are a special case of the simple ansatz with $\ell_i = \ell'_i$.

3.4 B_3 neutrino masses

The general, lepton number violating superpotential in a B_3 -model is given in Eq.(3.6). As stated in the introduction, due to the κ_i , the neutrinos mix with the Higgsino components of the neutralinos, resulting in one massive neutrino at tree-level. The mass matrix, with rows and columns corresponding to $\{\tilde{B}, \tilde{W}^3, \tilde{h}_u, \tilde{h}_d, \nu_1, \nu_2, \nu_3\}$, is given by²

$$M_{\tilde{\chi}^0-\nu} = \begin{pmatrix} M_1 & 0 & m_Z s_\beta s_W & -m_Z c_\beta s_W & 0 & 0 & 0 \\ 0 & M_2 & -m_Z s_\beta c_W & m_Z c_\beta c_W & 0 & 0 & 0 \\ m_Z s_\beta s_W & -m_Z s_\beta c_W & 0 & -\mu & -\kappa_1 & -\kappa_2 & -\kappa_3 \\ -m_Z c_\beta s_W & m_Z c_\beta c_W & -\mu & 0 & 0 & 0 & 0 \\ 0 & 0 & -\kappa_1 & 0 & 0 & 0 & 0 \\ 0 & 0 & -\kappa_2 & 0 & 0 & 0 & 0 \\ 0 & 0 & -\kappa_3 & 0 & 0 & 0 & 0 \end{pmatrix}, \quad (3.44)$$

²As in [89], it is assumed that here a rotation into the basis where the sneutrino vacuum expectation values vanish. In principle this requires a detailed minimization of the scalar potential as discussed for example in Ref. [91, 87, 83].

The resulting mass matrix is perturbatively given by [89, 90, 135]

$$\begin{aligned} (m_\nu^{\text{tree}})_{ij} &= \frac{m_Z^2 M_{\tilde{\gamma}} \cos^2 \beta}{\bar{\mu} (m_Z^2 M_{\tilde{\gamma}} \sin 2\beta - M_1 M_2 \bar{\mu})} \kappa_i \kappa_j, \\ &\equiv C_{\tilde{S}} \kappa_i \kappa_j. \end{aligned} \quad (3.45)$$

Here m_Z and $M_{1,2}$ denote the mass of the Z^0 gauge boson and the soft supersymmetry breaking, electroweak gaugino mass parameters, respectively. The photino mass is given by $M_{\tilde{\gamma}} \equiv M_1 \cos^2 \theta_W + M_2 \sin^2 \theta_W$, where θ_W is the electroweak mixing angle. $|\bar{\mu}| \equiv \sqrt{\mu^2 + \sum_i |\kappa_i|^2}$. One will see below that $\sum_i |\kappa_i|^2 = \mathcal{O}(1 \text{ MeV}^2)$ and thus to a high precision $\bar{\mu} \approx \mu$ [93, 89, 83]. For later convenience, the constant $C_{\tilde{S}}$ is introduced to summarize the dependence on the supersymmetric parameters.

Within B_3 -supersymmetry, the other two neutrinos obtain masses through radiative corrections from both the bi-linear [87, 88] and the tri-linear terms in the superpotential [89, 90]. In the following, the focus is on the radiative corrections due to the tri-linear terms, since it is expected that these to dominate for small κ_i [83], however realistic neutrino mass models based only on bi-linear terms have been constructed [91, 87, 88].

There are two distinct radiative contributions to the neutrino masses from the tri-linear couplings for which the Feynman diagrams are shown in Fig. (3.1). One is proportional to $\lambda'_{ik\ell} \lambda'_{j\ell k}$, where a squark and a quark propagate in the loop. A second is given by a slepton-lepton loop, and is proportional to $\lambda_{ik\ell} \lambda_{j\ell k}$. For the squark-quark loop, the bottom-sbottom contribution dominates ($k = \ell = 3$), since for the down-like quark masses $m_b^2 \gg m_s^2, m_d^2$. This results in the mass matrix³

$$(m_\nu^d)_{ij} \approx \frac{2N_c \lambda'_{i33} \lambda'_{j33} m_b^2 A_b}{16\pi^2} \frac{f(x_b)}{M_{\tilde{b}_2}^2}, \quad (3.46)$$

where $N_c = 3$ is the colour factor and

$$f(x_b) \equiv \frac{x_b \ln x_b}{x_b - 1}, \quad \text{with} \quad x_b = \left(\frac{M_{\tilde{b}_2}}{M_{\tilde{b}_1}} \right)^2. \quad (3.47)$$

$M_{\tilde{b}_s}$, $s = 1, 2$, denote the sbottom mass-eigenstates, where $M_{\tilde{b}_1} < M_{\tilde{b}_2}$. $A_b \equiv A_b^0 - \bar{\mu} \tan \beta$, where A_b^0 is the tri-linear soft-supersymmetry breaking bottom coupling. $i, j = 1, 2, 3$ are generation indices. In calculating explicit values for Eq. (3.46), the mixing of the left and right handed bottom squarks is taken into account but generation mixing is neglected due to the strict constraints from flavor changing neutral currents. For later numerical estimates, it is found that

$$f(1) = 1, \quad f(100) \approx 4.65, \quad (3.48)$$

where the latter value corresponds to the fairly extreme value of $M_{\tilde{b}_2} = 10 \cdot M_{\tilde{b}_1}$. Note, there are no neutrino mass contributions proportional to $m_b m_s$. The subleading contribution is proportional to $\lambda'_{i22} \lambda'_{j22} m_s^2$. This could in principle be dominant for $\lambda'_{i22} > (m_b/m_s) \lambda'_{i33} \approx$

³The extra factor of two arises from two distinct contributions to the mass which are equal for $k = \ell$ [90].

$45 \cdot \lambda'_{i33}$. However due to the relation Eq. (3.27), this is not possible in the simple ansatz, cf Table 3.2.

The contribution from the slepton-lepton loop is analogously given by ($N_c = 1$)

$$(m_\nu^e)_{ij} \approx \frac{\lambda_{i33}\lambda_{j33}}{8\pi^2} m_\tau^2 A_\tau \frac{f(x_\tau)}{M_{\tilde{\tau}_2}^2}. \quad (3.49)$$

Here m_τ is the tau mass and $x_\tau = (M_{\tilde{\tau}_2}/M_{\tilde{\tau}_1})^2$, $M_{\tilde{\tau}_1} < M_{\tilde{\tau}_2}$ are the stau masses. $A_\tau \equiv A_\tau^0 - \bar{\mu} \tan \beta$, where A_τ^0 is the trilinear soft breaking term for the τ . Since λ_{ijk} is antisymmetric in the first two indices, one must restrict the indices $i, j = 1, 2$ in Eq. (3.49). For $i = j = 3$ the leading contribution⁴ is from the smuon-muon loop, proportional to $\lambda_{322}^2 m_\mu^2$.

At any given energy scale, the mass parameters κ_i in Eq. (3.6) can be rotated away [136]. Depending on the scale and mechanism of supersymmetry breaking, the corresponding soft supersymmetry breaking terms will then also vanish [83]. When this occurs, there is pure tri-linear B_3 -models, which have been widely discussed in the literature. The leading neutrino mass contributions must then arise solely from the above loop-diagrams. In the following, thus two models embedded in the simple ansatz are discussed. In Model **I**, the case of pure tri-linear interactions is considered, *i.e.* $\kappa_i = 0$. The neutrino masses are then solely given through the combined loop contributions in Eqs. (3.46) and (3.49). In Model **II**, the more general case with $\kappa_i \neq 0$, as well as $\lambda, \lambda' \neq 0$ is considered. In this case, either the complete Majorana neutrino mass matrix is given by the sum of all three contributions, Eqs. (3.45), (3.46) and (3.49) or one of the loop contributions is absent. In both models, the neutrino masses and mixing angles are then obtained upon diagonalization.

In the following, first the resulting neutrino masses in both Models **I** and **II** are estimated and then the masses and mixing angles are determined by numerically diagonalising the complete mass matrix.

3.5 Neutrino masses from the simple B_3 -model

The simple ansatz is inserted into the neutrino mass formulæ above and give an estimate for the ℓ_i, ℓ'_j . The tree-level contribution, Eq. (3.45), is unchanged. The one-loop contributions, Eqs. (3.46) and (3.49), are given by

$$(\mathbf{M}_\nu^d)_{ij} \approx \frac{3\ell'_i\ell'_j m_b^4}{4\pi^2 v_d^2} A_b \frac{f(x_b)}{M_{b_2}^2} \equiv 3\ell'_i\ell'_j C_b, \quad (3.50)$$

$$(\mathbf{M}_\nu^e)_{ij} \approx \frac{\ell_i\ell_j m_\tau^4}{4\pi^2 v_d^2} A_\tau \frac{f(x_\tau)}{M_{\tilde{\tau}_2}^2} \equiv \ell_i\ell_j C_\tau, \quad (3.51)$$

⁴In principle, one could also have a contribution proportional to $\lambda_{i22}\lambda_{j22}m_\mu^2 \propto \ell_3^2 m_\mu^4/v_d^2$. This can be large since ℓ_3 is a free parameter in the ansatz. However, in order to have a comparable contribution, one must have $\ell_3 \approx (m_\tau/m_\mu)^2 \approx 300$. Comparing with Table 3.1, one sees that the resulting λ_{232} typically violates the low-energy experimental bounds [131].

where in the last equation $i, j \neq 3$. For later convenience the constants $C_{b,\tau}$ are introduced. In order to estimate the order of magnitude of the ℓ_i, ℓ'_j , hierarchical neutrino masses are assumed. In Model **I**, the neutrino masses are generated alone from the loop corrections and the mass matrix is then

$$[\mathbf{M}_\nu]_{ij} = \ell_i \ell_j C_\tau + 3\ell'_i \ell'_j C_b, \quad (3.52)$$

which results in two massive neutrinos, since $i, j \neq 3$ for C_τ . One can obtain a third massive neutrino if the subleading term proportional to $\ell_i \ell_j C_\mu$ are included, for which there is a contribution for $i, j = 3$.

In order to obtain an estimate, $\tan \beta = 10$ is set and $A_b^0 = A_\tau^0 = M_{\tilde{b}, \tilde{\tau}} = m_{soft} = 100$ GeV is assumed, which results in $f(x) \rightarrow 1$. One then has $C_b \approx 130$ keV and $C_\tau = 4.1$ keV. The heaviest neutrino is in agreement with the atmospheric neutrino anomaly, Eq. (3.1), for

$$\ell \approx 3.5 \cdot 10^{-3}, \quad \text{or} \quad \ell' \approx 3.6 \cdot 10^{-4}, \quad (3.53)$$

$$\lambda_{i33} \approx 3.6 \cdot 10^{-4}, \quad \text{or} \quad \lambda'_{i33} \approx 8.7 \cdot 10^{-5}. \quad (3.54)$$

Correspondingly, the mass required by the solar neutrino anomaly is generated by the other term. One obtains $m_\nu \approx 0.01$ eV, for

$$\ell \approx 1.6 \cdot 10^{-3}, \quad \text{or} \quad \ell' \approx 1.6 \cdot 10^{-4}, \quad (3.55)$$

$$\lambda_{i33} \approx 1.6 \cdot 10^{-4}, \quad \text{or} \quad \lambda'_{i33} \approx 3.9 \cdot 10^{-5}, \quad (3.56)$$

For both the atmospheric and solar anomalies Eqs. (3.16) and (3.27) has been used to translate back to the corresponding values for λ_{i33} and λ'_{i33} .

In Model **II**, the largest neutrino mass is generated by the tree-level contribution. Taking the trace of Eq. (3.45), and assuming $M_1 = M_2 = \mu = m_{soft}$, one has approximately

$$m_\nu \approx \frac{m_Z^2 \cos^2 \beta \sum_i \kappa_i^2}{m_{soft}^3}. \quad (3.57)$$

From Eq. (3.1), one then obtains [93]

$$\sqrt{\sum \kappa_i^2} = \mathcal{O}(1 \text{ MeV}). \quad (3.58)$$

With the same assumptions as in Model **I**, the radiative contributions then generate the solar neutrino mass for the values given in Eqs. (3.55), (3.56).

3.6 Numerical evaluation of the neutrino masses

3.6.1 General outline

Next the parameters of the simple ansatz are determined more precisely, *i.e.* the $\ell_i, \ell'_i, \kappa_i$, by fitting them to the neutrino data. They in turn fix the B_3 parameters. In order to learn more

about the importance of various parameters, two cases are considered. In Model **I**, the case of pure tri-linear terms is considered. The free parameters are

$$\text{Model I: } \quad \ell_i, \ell'_i. \quad (3.59)$$

In Model **II**, $\kappa_i \neq 0$ is included; the respective free parameters are given by

$$\text{Model II: } \quad \kappa_i, \ell_i, \ell'_i \quad (3.60)$$

Clearly, Model **II** is the most general case.

The full neutrino mass matrix $(\mathbf{M}_\nu)_{ij}$ is given by the sum of Eqs. (3.45), (3.50) and (3.51), where depending on the model, the coefficient of $C_{\tilde{s}}$ can be zero. In the case of Model **I**, the real symmetric mass matrix has the form of

$$\begin{aligned} \mathbf{M}_\nu^{\text{I}} &= \quad (3.61) \\ &C_b \begin{pmatrix} \ell'_1 \ell'_1 & \ell'_1 \ell'_2 & \ell'_1 \ell'_3 \\ \ell'_2 \ell'_1 & \ell'_2 \ell'_2 & \ell'_2 \ell'_3 \\ \ell'_3 \ell'_1 & \ell'_3 \ell'_2 & \ell'_3 \ell'_3 \end{pmatrix} + C_\tau \begin{pmatrix} \ell_1 \ell_1 & \ell_1 \ell_2 & 0 \\ \ell_2 \ell_1 & \ell_2 \ell_2 & 0 \\ 0 & 0 & 0 \end{pmatrix}, \end{aligned}$$

which is a function of five parameters. However, due to the simple form of the matrices, there are only two non-vanishing neutrino mass eigenvalues. This is sufficient to explain the atmospheric and solar neutrino anomalies. In principle, a massless lightest eigenstate can also lead to an observable effect. If both the massless and the massive, second lightest neutrino have significant electron-neutrino admixtures, then the corresponding Kurie plot will have a dip at the electron energy $Q - m_2$, with m_2 being the second lightest neutrino mass. The maximal electron energy however will be Q , within experimental uncertainties [137]. Depending on the parameter values this could be observable by the KATRIN experiment [138].

In Model **II**, one obtains three non-zero neutrino masses from the real symmetric mass matrix,

$$\begin{aligned} \mathbf{M}_\nu^{\text{II}} &= C_{\tilde{s}} \begin{pmatrix} \kappa_1 \kappa_1 & \kappa_1 \kappa_2 & \kappa_1 \kappa_3 \\ \kappa_2 \kappa_1 & \kappa_2 \kappa_2 & \kappa_2 \kappa_3 \\ \kappa_3 \kappa_1 & \kappa_3 \kappa_2 & \kappa_3 \kappa_3 \end{pmatrix} + \quad (3.62) \\ &C_b \begin{pmatrix} \ell'_1 \ell'_1 & \ell'_1 \ell'_2 & \ell'_1 \ell'_3 \\ \ell'_2 \ell'_1 & \ell'_2 \ell'_2 & \ell'_2 \ell'_3 \\ \ell'_3 \ell'_1 & \ell'_3 \ell'_2 & \ell'_3 \ell'_3 \end{pmatrix} + C_\tau \begin{pmatrix} \ell_1 \ell_1 & \ell_1 \ell_2 & 0 \\ \ell_2 \ell_1 & \ell_2 \ell_2 & 0 \\ 0 & 0 & 0 \end{pmatrix}. \end{aligned}$$

which depends on 8 independent parameters.

In the numerical evaluation, the coefficients $C_{\tilde{s}}$, C_b and C_τ are determined by assuming a BC1 mass spectrum [128], which has a scalar tau LSP. The resulting neutrino mass matrix $(\mathbf{M}_\nu)_{ij}$ is diagonalized by the orthogonal rotation matrix \mathbf{V}

$$\mathbf{V}^T \mathbf{M}_\nu \mathbf{V} = \begin{pmatrix} m_1 & 0 & 0 \\ 0 & m_2 & 0 \\ 0 & 0 & m_3 \end{pmatrix}, \quad (3.63)$$

where $m_1 \leq m_2 \leq m_3$ and \mathbf{V} is given by the standard parameterization

$$\mathbf{V} = \begin{pmatrix} c_{12}c_{13} & s_{12}c_{13} & s_{13} \\ -s_{12}c_{23} - c_{12}s_{23}s_{13} & c_{12}c_{23} - s_{12}s_{23}s_{13} & s_{23}c_{13} \\ s_{12}s_{23} - c_{12}c_{23}s_{13} & -c_{12}s_{23} - s_{12}c_{23}s_{13} & c_{23}c_{13} \end{pmatrix}, \quad (3.64)$$

with $c_{ij} = \cos \theta_{ij}$ and $s_{ij} = \sin \theta_{ij}$. The complex Dirac phase δ_{13} and the two Majorana phases $\alpha_{1/2}$ are omitted. The experimental ranges of the masses and the mixing parameters θ_{12} and θ_{23} are given in Eqs. (3.1)-(3.4). In addition, the bound on the mixing angle θ_{13} from the CHOOZ experiment Eq. (3.5) is taken into account. It is convenient in presenting the results instead of using the angles as in [78, 79], to use $\tan^2 \theta_{12}$, $\tan^2 \theta_{23}$ and $\sin^2 \theta_{13}$. The corresponding 1σ ranges are given by

$$\tan^2 \theta_{12} \in [0.403, 0.490], \quad (3.65)$$

$$\tan^2 \theta_{23} \in [0.680, 1.20], \quad (3.66)$$

$$\sin^2 \theta_{13} < 0.0082. \quad (3.67)$$

In performing the fit, $\log_{10}(\ell_i)$ and $\log_{10}(\ell'_j)$ are randomly sampled, thus guaranteeing that the full hierarchy of couplings is explored. Only couplings $\ell_i, \ell'_j \geq 1 \cdot 10^{-7}$ are considered, as smaller couplings have no effect on the neutrino observables. Furthermore it is required

$$\ell_i \ell_j \cdot C_\tau \leq 0.1 \text{ eV} \quad (3.68)$$

$$\ell'_i \ell'_j \cdot C_b \leq 0.1 \text{ eV} \quad (3.69)$$

$$\kappa_i \kappa_j \cdot C_S \leq 0.1 \text{ eV}. \quad (3.70)$$

For given values of the parameters $\ell_i, \ell'_j, \kappa_k$, the resulting mass matrix is computed. The numerical diagonalization of the mass matrix yields the mass eigenvalues m_1, m_2, m_3 and the orthogonal transformation matrix V and thus the mixing angles θ_{12}, θ_{23} and θ_{13} . Afterwards, all experimental requirements, Eqs. (3.1)-(3.5), are applied on the mass eigenvalues and on the mixing angles. Models are deleted, which do not fall within the 1σ ranges. Throughout a hierarchical mass spectrum is assumed. The results are summarized in Tables 3.3 and 3.4, which will be discussed in the next section.

3.6.2 Discussion of the results

Model I

In Table 3.3, the fit values for the parameters ℓ_i, ℓ'_j in Model **I** are presented. In the five columns on the right, the resulting neutrino mass and mixing parameters are included. Of the large number of solutions, only those are presented, where the parameters $|\ell_i|$ take on extremal values. For example in the first row of Table 3.3, $|\ell_1|$ takes on the largest value. One can now see in the five columns on the right, that $\tan^2 \theta_{12}$ and Δm_{21}^2 , are at the upper limit of their allowed ranges, Eqs. (3.1) and (3.65), respectively. This is as one would expect from

	ℓ_1	ℓ_2	ℓ'_1	ℓ'_2	ℓ'_3	$\tan^2 \theta_{12}$	$\tan^2 \theta_{23}$	$\sin^2 \theta_{13}$	Δm_{21}^2	Δm_{23}^2
ℓ_1 max	$9.38 \cdot 10^{-4}$	$1.69 \cdot 10^{-3}$	$-1.60 \cdot 10^{-7}$	$4.01 \cdot 10^{-4}$	$-5.22 \cdot 10^{-4}$	0.48	0.99	0.0078	0.081	2.5
ℓ_1 min	$7.10 \cdot 10^{-4}$	$-1.76 \cdot 10^{-3}$	$9.27 \cdot 10^{-5}$	$4.16 \cdot 10^{-4}$	$-5.09 \cdot 10^{-4}$	0.42	1.10	0.0037	0.077	2.6
ℓ_2 max	$-7.12 \cdot 10^{-4}$	$1.78 \cdot 10^{-3}$	$-9.42 \cdot 10^{-5}$	$-4.10 \cdot 10^{-4}$	$5.04 \cdot 10^{-4}$	0.42	1.11	0.0038	0.081	2.5
ℓ_2 min	$9.23 \cdot 10^{-4}$	$1.58 \cdot 10^{-3}$	$1.82 \cdot 10^{-6}$	$3.83 \cdot 10^{-4}$	$-5.60 \cdot 10^{-4}$	0.49	0.72	0.0056	0.078	2.7
ℓ'_1 max	$7.10 \cdot 10^{-4}$	$-1.76 \cdot 10^{-3}$	$9.27 \cdot 10^{-5}$	$4.16 \cdot 10^{-4}$	$-5.09 \cdot 10^{-4}$	0.42	1.10	0.0037	0.077	2.6
ℓ'_1 min	$-9.14 \cdot 10^{-4}$	$-1.67 \cdot 10^{-3}$	$1.00 \cdot 10^{-7}$	$4.11 \cdot 10^{-4}$	$-5.35 \cdot 10^{-4}$	0.47	0.95	0.0065	0.077	2.7
ℓ'_2 max	$9.01 \cdot 10^{-4}$	$-1.77 \cdot 10^{-3}$	$1.10 \cdot 10^{-7}$	$4.28 \cdot 10^{-4}$	$5.16 \cdot 10^{-4}$	0.43	1.18	0.0077	0.078	2.8
ℓ'_2 min	$8.73 \cdot 10^{-4}$	$1.62 \cdot 10^{-3}$	$4.00 \cdot 10^{-7}$	$3.61 \cdot 10^{-4}$	$-5.53 \cdot 10^{-4}$	0.41	0.68	0.0053	0.080	2.4
ℓ'_3 max	$8.69 \cdot 10^{-4}$	$1.61 \cdot 10^{-3}$	$-5.50 \cdot 10^{-7}$	$3.82 \cdot 10^{-4}$	$5.71 \cdot 10^{-4}$	0.42	0.69	0.0043	0.078	2.8
ℓ'_3 min	$-7.12 \cdot 10^{-4}$	$1.78 \cdot 10^{-3}$	$-9.42 \cdot 10^{-5}$	$-4.10 \cdot 10^{-4}$	$5.04 \cdot 10^{-4}$	0.42	1.11	0.0038	0.081	2.5

Table 3.3: Explicit solutions for Model **I**, where $\kappa_i = 0$. Only values are shown where one of the $|\ell_i|$, $|\ell'_j|$ takes on an extremal absolute value, *i.e.* the highest or lowest value obtained in the fits. Note that due to the sampling constraints, values are not probed for the ℓ_i , $\ell'_j < 10^{-7}$. In the five columns on the far right, the resulting neutrino parameters are shown. The values for Δm_{21}^2 and Δm_{23}^2 are given units 10^{-3} eV^2 . Comparing with Eqs. (3.1)-(3.5), one can see which physical parameter is at its experimentally allowed limit. Thus for example in the first row, where ℓ_1 is maximal, $\tan^2 \theta_{12}$ and Δm_{21}^2 are at the edge of their allowed values. Pushing ℓ_1 any higher would violate these constraints.

	ℓ_1	ℓ_2	ℓ'_1	ℓ'_2	ℓ'_3	κ_1	κ_2	κ_3
ℓ_1 max	$1.08 \cdot 10^{-3}$	$-1.17 \cdot 10^{-3}$	$1.80 \cdot 10^{-6}$	$-4.39 \cdot 10^{-4}$	$4.57 \cdot 10^{-4}$	-0.128	0.00551	-3.40
ℓ_1 min	$1.30 \cdot 10^{-7}$	$1.45 \cdot 10^{-5}$	$-6.50 \cdot 10^{-7}$	$-4.30 \cdot 10^{-4}$	$5.35 \cdot 10^{-4}$	1.93	2.82	1.09
ℓ_2 max	$-8.15 \cdot 10^{-4}$	$1.77 \cdot 10^{-3}$	$4.06 \cdot 10^{-5}$	$4.14 \cdot 10^{-4}$	$-5.01 \cdot 10^{-4}$	-0.159	-0.541	-0.103
ℓ_2 min	$4.50 \cdot 10^{-7}$	$1.20 \cdot 10^{-7}$	$1.42 \cdot 10^{-4}$	$3.22 \cdot 10^{-4}$	$4.10 \cdot 10^{-7}$	1.02	-4.65	6.11
ℓ'_1 max	$-8.80 \cdot 10^{-7}$	$1.34 \cdot 10^{-3}$	$1.84 \cdot 10^{-4}$	$2.28 \cdot 10^{-4}$	$2.20 \cdot 10^{-6}$	0.401	-4.64	6.01
ℓ'_1 min	$-4.65 \cdot 10^{-6}$	$9.62 \cdot 10^{-6}$	$2.20 \cdot 10^{-7}$	$-5.28 \cdot 10^{-4}$	$-4.04 \cdot 10^{-4}$	-2.07	-0.0320	3.72
ℓ'_2 max	$-1.50 \cdot 10^{-6}$	$-7.07 \cdot 10^{-6}$	$-8.85 \cdot 10^{-5}$	$5.31 \cdot 10^{-4}$	$-4.10 \cdot 10^{-4}$	1.70	0.100	-3.81
ℓ'_2 min	$-9.49 \cdot 10^{-4}$	$1.66 \cdot 10^{-3}$	$-9.70 \cdot 10^{-6}$	$1.30 \cdot 10^{-7}$	$1.10 \cdot 10^{-4}$	0.219	4.92	5.98
ℓ'_3 max	$8.82 \cdot 10^{-4}$	$1.64 \cdot 10^{-3}$	$3.60 \cdot 10^{-7}$	$3.91 \cdot 10^{-4}$	$5.55 \cdot 10^{-4}$	-0.457	0.0604	-0.218
ℓ'_3 min	$4.50 \cdot 10^{-7}$	$1.20 \cdot 10^{-7}$	$1.42 \cdot 10^{-4}$	$3.22 \cdot 10^{-4}$	$4.10 \cdot 10^{-7}$	1.02	-4.65	6.11
κ_1 max	$1.43 \cdot 10^{-4}$	$-1.30 \cdot 10^{-3}$	$-2.69 \cdot 10^{-6}$	$4.47 \cdot 10^{-4}$	$-4.77 \cdot 10^{-4}$	2.06	-0.0125	-3.03
κ_1 min	$-1.87 \cdot 10^{-6}$	$-2.30 \cdot 10^{-5}$	$-1.74 \cdot 10^{-4}$	$-4.23 \cdot 10^{-5}$	$2.99 \cdot 10^{-4}$	0.0149	-5.90	-5.32
κ_2 max	$1.21 \cdot 10^{-4}$	$3.77 \cdot 10^{-5}$	$-1.65 \cdot 10^{-4}$	$-1.04 \cdot 10^{-4}$	$2.27 \cdot 10^{-4}$	0.139	6.18	5.26
κ_2 min	$9.03 \cdot 10^{-4}$	$-1.19 \cdot 10^{-3}$	$-2.15 \cdot 10^{-5}$	$4.56 \cdot 10^{-4}$	$-4.49 \cdot 10^{-4}$	-0.556	0.0338	3.16
κ_3 max	$-7.67 \cdot 10^{-4}$	$-1.23 \cdot 10^{-3}$	$-8.03 \cdot 10^{-5}$	$-1.07 \cdot 10^{-4}$	$1.31 \cdot 10^{-4}$	-0.0348	5.00	6.42
κ_3 min	$9.00 \cdot 10^{-4}$	$-1.60 \cdot 10^{-3}$	$2.30 \cdot 10^{-6}$	$-3.75 \cdot 10^{-4}$	$-5.64 \cdot 10^{-4}$	0.0656	-0.0242	0.0140

Table 3.4: The same as Table 3.3 for Model **II**. Now the values of κ_i as well as the extremal values of $|\kappa_i|$ are shown. The κ_i are given in units of MeV.

Eq. (3.62), where one sees that ℓ_1 influences the first two generations. On the other hand, for example in the seventh row, where $|\ell'_2|$ is maximal, one sees that $\tan^2 \theta_{23}$ and Δm_{32}^2 are at the upper limit of their allowed ranges. Similarly, in the second row, where $|\ell_1|$ is minimal, one sees that Δm_{21}^2 is at the *lower* end of its allowed range. For the eighth row, where $|\ell'_2|$ is minimal, Δm_{32}^2 is at the *lower* end of its allowed range. Overall, one sees that $\tan^2 \theta_{12}$ is at its upper limit for $[\ell_1 \text{ max}]$ and also for $[\ell_2 \text{ min}]$. $\tan^2 \theta_{23}$ is at its upper limit for $[\ell'_2 \text{ max}]$ and at its lower limit for $[\ell'_2 \text{ min}]$ and $[\ell'_3 \text{ max}]$. $\sin^2 \theta_{13}$ is always well within its limits and thus does not pose a real constraint on the fit. However, one does predict a value between 0.003 and the current upper bound. For Δm_{21}^2 , one is at the upper end of the allowed range for $[\ell_1 \text{ max}]$, $[\ell_2 \text{ max}]$, and $[\ell'_3 \text{ min}]$. One is close to the lower range for $[\ell_1 \text{ min}]$, $[\ell'_1 \text{ max}]$, and $[\ell'_1 \text{ min}]$. For Δm_{23}^2 , one

	$\tan^2 \theta_{12}$	$\tan^2 \theta_{23}$	$\sin^2 \theta_{13}$	Δm_{21}^2	Δm_{23}^2
ℓ_1 max	0.48	0.80	0.0061	0.077	2.4
ℓ_1 min	0.45	0.79	0.0012	0.081	2.5
ℓ_2 max	0.41	1.19	0.0007	0.078	2.5
ℓ_2 min	0.44	0.93	0.0031	0.080	2.4
ℓ'_1 max	0.41	1.06	0.0003	0.079	2.4
ℓ'_1 min	0.47	1.04	0.0072	0.081	2.6
ℓ'_2 max	0.44	1.03	0.0009	0.080	2.7
ℓ'_2 min	0.47	1.04	0.0075	0.080	2.6
ℓ'_3 max	0.44	0.78	0.0053	0.079	2.7
ℓ'_3 min	0.44	0.93	0.0031	0.080	2.4
κ_1 max	0.40	0.83	0.0034	0.080	2.6
κ_1 min	0.47	0.81	0.0056	0.081	2.7
κ_2 max	0.49	1.18	0.0001	0.078	2.6
κ_2 min	0.42	0.95	0.0051	0.081	2.4
κ_3 max	0.44	0.74	0.0014	0.081	2.8
κ_3 min	0.45	0.69	0.0055	0.080	2.6

Table 3.5: Model **II** (continued). Again, the values for Δm_{21}^2 and Δm_{23}^2 are given units 10^{-3} eV^2 .

is at the upper end of the allowed range for $[\ell'_2 \text{ max}]$ and $[\ell'_3 \text{ max}]$. Thus one gets the strongest constraints from the allowed mass ranges and from $\tan^2 \theta_{23}$.

In the case of Model **I**, there are only five free parameters. With these one must fit the two neutrino masses, two mixing angles and one upper bound. It is thus perhaps not surprising, that except for ℓ'_1 , the allowed ranges for the five parameters are quite narrow. $\ell'_{1 \text{ min}}$ is consistent with zero. In summary, one finds from Table 3.3

$$7.10 \cdot 10^{-4} < |\ell_1| < 9.38 \cdot 10^{-4} \quad (3.71)$$

$$1.58 \cdot 10^{-3} < |\ell_2| < 1.78 \cdot 10^{-3} \quad (3.72)$$

$$1.00 \cdot 10^{-7} < |\ell'_1| < 9.27 \cdot 10^{-5} \quad (3.73)$$

$$3.61 \cdot 10^{-4} < |\ell'_2| < 4.28 \cdot 10^{-4} \quad (3.74)$$

$$5.04 \cdot 10^{-4} < |\ell'_3| < 5.71 \cdot 10^{-4}. \quad (3.75)$$

The central values of these regions are employed in the discussion of the resulting collider signals, below.

Model II

In Table 3.4, the results of the fit to Model **II** are shown. Now there are total of eight free-parameters. The values of the mass mixing parameters are varied in the interval

$$0.01 \text{ MeV} \leq \kappa_i \leq 10 \text{ MeV}. \quad (3.76)$$

	$\lambda_{122}\lambda'_{211}$	$\lambda_{132}\lambda'_{311}$	$\lambda_{121}\lambda'_{111}$	$\lambda_{231}\lambda'_{311}$
Bound	$4.0 \cdot 10^{-8}$	$4.0 \cdot 10^{-8}$	$4.0 \cdot 10^{-8}$	$4.0 \cdot 10^{-8}$

	$\lambda'_{i12}\lambda'_{i21}$	$\lambda'_{i13}\lambda'_{i31}$	$\lambda'_{i13}\lambda'_{i31}$	$\lambda'_{1k1}\lambda'_{2k1}$	$\lambda'_{11j}\lambda'_{21j}$
Bound	10^{-9}	$3 \cdot 10^{-8}$	$8 \cdot 10^{-8}$	$8.0 \cdot 10^{-8}$	$8.5 \cdot 10^{-8}$

Table 3.6: Bounds on the products of B_3 couplings [131]. The first four and the last two bounds arise from contributions to the process $\mu\text{Ti} \rightarrow e\text{Ti}$. The fifth bound arises from contributions to Δm_K and the sixth and seventh from contributions to Δm_B .

Due to the enhanced freedom, one sees that now there exists solutions, where $\ell_i, \ell'_j = \mathcal{O}(10^{-7})$, which is consistent with zero, in the numerical evaluation. One sees that one pushes the upper boundary of $\tan^2 \theta_{12}$ for $[\ell_1 \text{ max}]$ and $[\kappa_2 \text{ max}]$ and the lower boundary for $[\kappa_1 \text{ max}]$. For $\tan^2 \theta_{23}$ one pushes the upper and lower limits for $[\kappa_2 \text{ max}]$ and for $[\kappa_3 \text{ min}]$, respectively. From $\sin^2 \theta_{13}$, one again has basically no constraint on the model, beyond those of the other parameters, *i.e.* one is always well within the CHOOZ bound.

One is pushing the upper end of the allowed range of Δm_{21}^2 for $[\ell_1 \text{ min}]$, $[\ell'_1 \text{ min}]$, $[\kappa_{1,2} \text{ min}]$, and $[\kappa_3 \text{ max}]$. For Δm_{23}^2 , one is at the upper end for $[\ell'_2 \text{ max}]$, $[\ell'_3 \text{ max}]$, and $[\kappa_1 \text{ min}]$. One is at the *lower* end of Δm_{23}^2 for $[\ell_1 \text{ max}]$, $[\ell_2 \text{ min}]$, $[\ell'_1 \text{ max}]$, $[\ell'_3 \text{ min}]$, and $[\kappa_2 \text{ min}]$. Thus the mass ranges set the strictest limits on the parameters, the angles are fairly easy to accommodate.

Due to the enhanced freedom, one sees that any one of the parameters can consistently be set to zero. This is of particular interest when trying to extract typical collider signatures, below. In Model **II**, it is thus difficult to discern an identifying experimental signature.

3.7 Bounds on the products of the parameters of the simple B_3 -model

Before discussing the consequences of the model, first the low-energy constraints are considered. Typical bounds on single B_3 couplings are of order 0.1 to 0.01 [139, 31]. However, one necessarily has multiple couplings in the models and thus must take into account the bounds on products of couplings [129, 130, 131, 132], which are also typically much stricter, due to lepton flavor violating effects. The strictest product bounds ($< 10^{-7}$) of Table II in Ref. [131] are given in Table 3.6.

Now it can be investigated whether the couplings satisfy the bounds in Table 3.6. For this

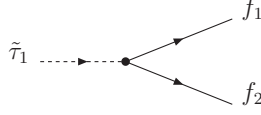


Figure 3.2: The two-body decay of a scalar particle into two fermions.

the values in Tables 3.1 and 3.2 are used and it is assumed $\tan\beta = 10$. One finds

$$\lambda_{122}\lambda'_{211} = 2.1 \cdot 10^{-6} \ell_1 \ell'_2 \quad (3.77)$$

$$\lambda_{132}\lambda'_{311} = 0 \quad (3.78)$$

$$\lambda_{121}\lambda'_{111} = -9.9 \cdot 10^{-9} \ell_2 \ell'_1 \quad (3.79)$$

$$\lambda_{231}\lambda'_{311} = 0 \quad (3.80)$$

$$\lambda'_{i12}\lambda'_{i21} = 1.1 \cdot 10^{-7} (\ell'_i)^2 \quad (3.81)$$

$$\lambda'_{113}\lambda'_{131} = 2.7 \cdot 10^{-9} (\ell'_1)^2 \quad (3.82)$$

$$\lambda'_{i13}\lambda'_{i31} = 2.7 \cdot 10^{-9} (\ell'_i)^2 \quad (3.83)$$

$$\lambda'_{1k1}\lambda'_{2k1} = 1.2 \cdot 10^{-7} \ell'_1 \ell'_2, \quad k = 1 \quad (3.84)$$

$$\lambda'_{11j}\lambda'_{21j} = 2.0 \cdot 10^{-6} \ell'_1 \ell'_2, \quad j = 2 \quad (3.85)$$

In the last two cases the chosen indices result in the largest possible value. The strictest bounds result from Eqs. (3.77) and (3.81): $\ell_1 \ell'_2 < 0.02$, and $\ell'_i < 0.1$. From Tables 3.3 and 3.4, one sees that these are always satisfied in our numerical solutions.

3.8 Collider tests

An essential feature of B_3 neutrino models, is that they necessarily lead to observable consequences at colliders. Resonant slepton or squark production requires couplings of order 10^{-3} or larger [127]. As can be seen from Tables 3.1 and 3.2 together with the numerical results presented in Tables 3.3, 3.4, this is not possible in the models. However, it is well known, that at the LHC squark and gluino production provide the largest supersymmetric cross sections. This is independent of whether P_6 or B_3 is the relevant symmetry. The produced squarks and gluinos then cascade decay within the detector to the LSP. In particular, this also holds for the BC benchmark points [128], where $\tilde{\tau}_1$ is the LSP. In this paper, the focus is on stau-LSP scenarios, as outlined in Ref. [128]. Only the essential features are focused on, a full phenomenological analysis goes beyond the scope of this work and will be presented in the future [140]. The neutralino LSP case requires a full treatment of the scalar potential in order to determine the relevant couplings and masses. This in turn requires assumptions about the soft-supersymmetry breaking sector, which also goes well beyond the scope of this work. It will be considered elsewhere [140].

3.8.1 Stau LSP decays

As discussed in detail in Refs. [83, 128], there are extensive regions of mSUGRA parameter space, where the scalar tau is the LSP. The final state collider signals will be determined by the dominant decays of the stau. The lightest stau, $\tilde{\tau}_1$, is an admixture of right and left stau.

$$\tilde{\tau}_1 = \cos \theta_{\tilde{\tau}} \tilde{\tau}_R + \sin \theta_{\tilde{\tau}} \tilde{\tau}_L \quad (3.86)$$

with $\theta_{\tilde{\tau}}$ the mixing angle. In Ref. [128], it was found that in the representative benchmark points (BC1-BC4) the $\tilde{\tau}_1$ is dominantly a right-handed stau with $|\theta_{\tilde{\tau}}| < 0.3$ (in radians), *i.e.* the $\tilde{\tau}_1$ -LSP is more than 91% $\tilde{\tau}_R$ and $\sin^2 \theta_{\tilde{\tau}} < 0.09$.

In the model, there is a wide range of non-zero B_3 couplings, where the corresponding operators couple directly to the stau. The stau can thus decay via the two-body mode into two spin-1/2 fermions $f_{1,2}$ shown in Fig. 3.2. The corresponding partial decay rate is in given in leading order by [141]

$$\Gamma(\tilde{\tau}_1 \rightarrow f_1 f_2) = \frac{N_c |\Lambda|^2 \Theta^2 p_{cm}}{8\pi M_{\tilde{\tau}_1}^2} (M_{\tilde{\tau}_1}^2 - m_1^2 - m_2^2) \quad (3.87)$$

$$\approx \frac{N_c |\Lambda|^2 \Theta^2}{16\pi} M_{\tilde{\tau}_1}, \quad (3.88)$$

where

$$p_{cm}^2 = \frac{[M_{\tilde{\tau}_1}^2 - (m_1 + m_2)^2] [M_{\tilde{\tau}_1}^2 - (m_1 - m_2)^2]}{4M_{\tilde{\tau}_1}^2}. \quad (3.89)$$

$m_{1,2}$ denote the final state masses. Λ denotes one of the following B_3 couplings relevant for tree-level stau decay

$$\Lambda \in \{\lambda_{131}, \lambda_{133}, \lambda_{232}, \lambda_{233}, \lambda'_{3jk}\}, \quad (3.90)$$

and N_c is the colour factor. $N_c = 1$ for the decay via the $LL\bar{E}$ operators, and $N_c = 3$ for the $LQ\bar{D}$ operators. $\Theta = (\cos \theta_{\tilde{\tau}}, \sin \theta_{\tilde{\tau}})$, depending on whether the $\tilde{\tau}_1$ couples via the right- or the left-handed stau component. Eq. (3.88) is taken for the case where $m_{1,2} \rightarrow 0$. This is a good approximation for $M_{\tilde{\tau}_1} < m_{\text{top}}$, which is the case for all the BC benchmark points.

Given the above decay formula one can now compute the decay rates for the dominant decay modes using the numerical values in Tables 3.1 and 3.2 for the relevant coupling. One expects the decays where the right-handed stau component couples directly to dominate, due to the small mixing angle in the stau sector. Furthermore, for λ'_{333} which is a potentially large coupling the large top quark mass kinematically blocks the decay, for the stau masses considered here. The results are presented for the decays in terms of the ℓ_i, ℓ'_j in Table 3.7. For completeness, the couplings involving ℓ_3 are included, which are neglected in the neutrino parameter fits. One sees that for substantial decays via the corresponding operators, one requires, *e.g.* $\ell_3 \gg \ell_{1,2}$.

Model I

If one considers the BC1 benchmark point, one has $M_{\tilde{\tau}_1} = 148.38$ GeV. Using Tables 3.3, 3.4 one can then compute explicit values for the partial widths and the branching ratios. In Model

Operator	Decay Mode	$\Gamma(\tilde{\tau}_1^- \rightarrow bc)/M_{\tilde{\tau}_1}$
$L_1 L_3 E_1$	$\tilde{\tau}_1^- \rightarrow e^- \nu_e$	$1.5 \cdot 10^{-12} \ell_3^2$
$L_1 L_3 E_3$	$\tilde{\tau}_1^- \rightarrow \tau^- \nu_e$	$2.0 \cdot 10^{-4} \ell_1^2$
$L_1 L_3 E_3$	$\tilde{\tau}_1^- \rightarrow e^- \nu_\tau$	$1.8 \cdot 10^{-4} \ell_1^2$
$L_2 L_3 E_2$	$\tilde{\tau}_1^- \rightarrow \mu^- \nu_\mu$	$6.7 \cdot 10^{-8} \ell_3^2$
$L_2 L_3 E_3$	$\tilde{\tau}_1^- \rightarrow \tau^- \nu_\mu$	$2.0 \cdot 10^{-4} \ell_2^2$
$L_2 L_3 E_3$	$\tilde{\tau}_1^- \rightarrow \mu^- \nu_\tau$	$1.8 \cdot 10^{-4} \ell_2^2$
$L_3 Q_2 D_3$	$\tilde{\tau}_1^- \rightarrow c b$	$5.4 \cdot 10^{-7} (\ell_3')^2$
$L_3 Q_2 D_2$	$\tilde{\tau}_1^- \rightarrow c s$	$1.8 \cdot 10^{-7} (\ell_3')^2$
$L_3 Q_1 D_2$	$\tilde{\tau}_1^- \rightarrow u s$	$1.1 \cdot 10^{-8} (\ell_3')^2$

Table 3.7: Decay modes and partial decay widths of a stau LSP given as a function of the relevant ℓ_i, ℓ'_j . In the second and the fifth decay modes the two contributions from the doublet and the singlet stau are added. $\theta_{\tilde{\tau}} = 0.3$ (in radians) as obtained for BC1.

I, $|\ell_1| \approx 8 \cdot 10^{-4}$, $|\ell_2| \approx 2 \cdot 10^{-3}$ and $|\ell'_3| \approx 5 \cdot 10^{-4}$. Using these values, one then obtains the total decay width and lifetime in Model **I** at BC1

$$\Gamma(\tilde{\tau}_1) = 260 \text{ eV}, \quad \tau(\tilde{\tau}_1) = 2.5 \cdot 10^{-18} \text{ sec}. \quad (3.91)$$

One sees that the stau-LSP always decays within the detector. It also will not lead to a detached vertex. For the branching ratios of the decay modes in Table 3.7, one obtains

$$\text{Br}(\tilde{\tau}_1 \rightarrow \tau^- \nu_e) = 0.072 \quad (3.92)$$

$$\text{Br}(\tilde{\tau}_1 \rightarrow e^- \nu_\tau) = 0.065 \quad (3.93)$$

$$\text{Br}(\tilde{\tau}_1 \rightarrow \tau^- \nu_\mu) = 0.45 \quad (3.94)$$

$$\text{Br}(\tilde{\tau}_1 \rightarrow \mu^- \nu_\tau) = 0.41 \quad (3.95)$$

The other decay modes are negligible. The branching ratios are independent of $M_{\tilde{\tau}_1}$, *i.e.* in Model **I** they only depend on the ℓ_i, ℓ'_j . As the neutrinos are not visible, one has a combined branching ratio into charged tau leptons of about 52%. For squark or gluino pair production, one expects two stau's in the decay chains. The probability for then having two charged electrons/muons in the final state is about 23%. Since the gluino/squark pair production cross section is very large for accessible supersymmetric masses, this should lead to an easily visible signal rate.

Model II

In Model **II**, there are eight free parameters and thus a much larger freedom. Furthermore for $\kappa_3 \neq 0$ the stau can mix with the charged Higgs boson, leading to additional decay modes. In order to compute these properly, one must minimize the full scalar potential. This is beyond the scope of this work. One can estimate the stau-Higgs mixing to be κ_3/μ . Using the Feynman rules in Fig. 8 of Ref. [142] for the charged Higgs coupling to the tau lepton, one then typically

finds a product of mixing times couplings of order 10^{-7} , for $\kappa_3 = 1$ MeV, $\tan\beta = 10$ and $\mu = 200$ GeV. This would lead to an additional decay $\tilde{\tau} \rightarrow \tau\nu$. The couplings to the second generation quarks are another order of magnitude smaller. These Higgs-mixing couplings are negligible compared to the direct stau decay couplings, in most cases. However, in general they must be included. A proper complete treatment will be given in Ref. [140]. Here it shall suffice to present one example case from Table 3.4 employing only the direct decays from Table 3.7. An example is chosen, such that $\ell_{1,2} \ll \ell'_3$, which differs from Model **I**.

The case: [ℓ'_1 min], where $\ell_1 = -4.65 \cdot 10^{-6}$, $\ell_2 = 9.62 \cdot 10^{-6}$ and $\ell'_3 = -4.04 \cdot 10^{-4}$ is considered. One finds for the total decay rate and the lifetime

$$\Gamma(\tilde{\tau}_1) = 2.4 \cdot 10^{-2} \text{ eV}, \quad (3.96)$$

$$\tau(\tilde{\tau}_1) = 2.7 \cdot 10^{-14} \text{ sec}. \quad (3.97)$$

One sees that the width is now substantially smaller and thus the lifetime correspondingly larger. For a Lorentz boost $\gamma_L = 10$, one has a decay length of about $100\mu\text{m}$. This is on the boarderline of visibility for a detached vertex. For the branching ratios one finds

$$\text{Br}(\tilde{\tau}_1 \rightarrow \text{hadrons}) = 0.73 \quad (3.98)$$

$$\text{Br}(\tilde{\tau}_1 \rightarrow \tau^- \nu_e) = 0.026 \quad (3.99)$$

$$\text{Br}(\tilde{\tau}_1 \rightarrow e^- \nu_\tau) = 0.023 \quad (3.100)$$

$$\text{Br}(\tilde{\tau}_1 \rightarrow \tau^- \nu_\mu) = 0.11 \quad (3.101)$$

$$\text{Br}(\tilde{\tau}_1 \rightarrow \mu^- \nu_\tau) = 0.10 \quad (3.102)$$

The stau now dominantly decays hadronically. In this specific case, one can have still a roughly 25% branching ratio to charged leptons. Or a probability of roughly 6% for two charged leptons in the final state. However, recall that only couplings are scanned down to 10^{-7} . Thus one would expect solutions with even smaller $\ell_{1,2}$. In this case one would have purely hadronic final states and one must resort to the techniques used in Ref. [143], where the *UDD* R-parity violating operators were studied.

3.9 Conclusions and outlook

A simple ansatz for the B_3 Yukawa couplings has been presented, relating them directly to the corresponding Higgs Yukawa couplings via a small set of parameters ℓ_i, ℓ'_j . This results in simple relations between the B_3 couplings presented in Tables 3.1 and 3.2. Estimates of these parameters are given in order to obtain the correct neutrino masses and then has been numerically determined the precise values. These are summarised in Tables 3.3, 3.4. The resulting collider signals for the case of a stau LSP are discussed. Depending on the fit values, a wide range for the possible branching ratios of the stau-LSP has been found.

Chapter 4

Electroweak contributions to squark pair production at the LHC

4.1 Introduction

The large hadron collider (LHC) will start in 2008. Supersymmetry at the TeV scale will then be decisively tested [144]. In typical mSUGRA scenarios, the squarks are among the heaviest supersymmetric particles. However, the production cross section of squark pairs is very large. The leading term of the cross section is of the order α_s^2 and there are contributions with 2 valence quarks [19]. The expressions for the cross section of squark production from initial quarks is very similar to the standard QCD case, where the final states are 2 quarks [20]. For a rough estimate of the cross section at the LHC, one can use the cross section for quark pairs from the Standard Model QCD contribution. It has a t-channel gluon contribution for the production of 2 different quarks,

$$\sigma \approx \frac{2\pi\alpha_s^2}{9\hat{s}}. \quad (4.1)$$

The main difference between the cross section for quark and squark pair production is the propagator. In the Standard Model case, the propagator yields \hat{t}^{-2} . In the supersymmetric case, the gluino is massive and therefore the propagator is replaced with $(\hat{t} - m_{\tilde{g}}^2)^{-2}$. Assuming $\alpha_s \approx 0.15$ and $\sqrt{\hat{s}} \approx 5$ TeV, one obtains from Eq. (4.1)

$$\sigma \approx 0.25 \text{ pb} \quad (4.2)$$

This is a very rough estimate, since the cross section must be convoluted with the parton density functions $f(x)$. In Fig. 4.1, $x f(x)$ is plotted as function of Bjorken- x for various partons. If one wants to produce squarks with a mass of about $m_{\tilde{q}} = 1$ TeV, one needs at least the center of mass energy of $E_{\text{CMS}} = 2$ TeV. The partonic Mandelstam variable \hat{s} and s are related by

$$\hat{s} = x_1 x_2 s. \quad (4.3)$$

Assuming $\sqrt{s} = 14$ TeV and $x_1 = x_2$, one obtains

$$x_1 = x_2 \approx 1/7. \quad (4.4)$$

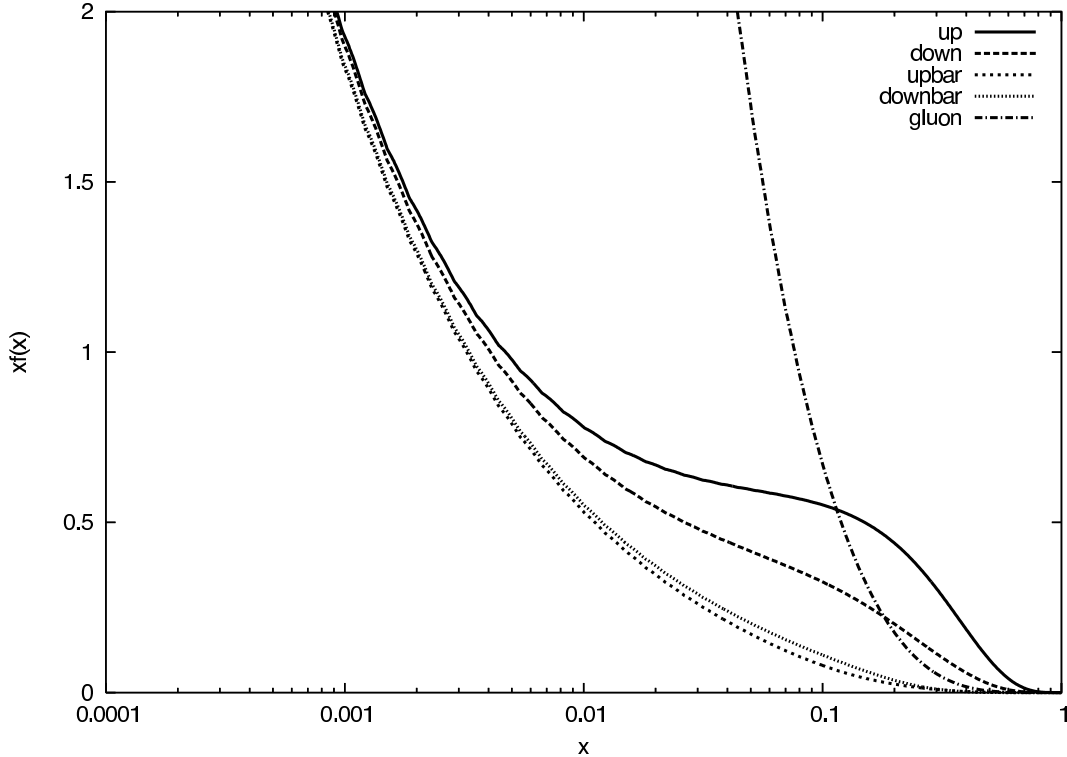


Figure 4.1: The parton distribution functions for quarks, antiquarks and gluons in a proton for $Q = 250 \text{ GeV}^2$. CTEQ5L has been used [147].

In this region, the quark flux starts to dominate over the gluon flux. Thus gluon fusion contribution to squark pair production is subdominant, if the squark masses are very large. The gluon fusion contribution for squark pair production increases the contribution from 2 initial quarks by 14 (6.7, 1.4)% for the benchmark mSUGRA scenarios SPS 1a(1b,2) [152].

It turns out that the typical cross section for degenerate first and second generation squarks is about,

$$\sigma \approx 0.5 \text{ pb} \quad (4.5)$$

for squarks with a mass of about 1 TeV. If one assumes a low luminosity \mathcal{L} of about 10 fb^{-1} per year, one still obtains

$$N_{\text{Events}} = \mathcal{L}\sigma = 5000 \quad (4.6)$$

events. Ref. [145] calculated the leading order (LO) QCD cross sections for squark pair production. The lowest order cross sections strongly depend on the renormalization and factorization scale. By including the next to leading order (NLO) corrections [146], the scale dependence is strongly reduced. For the LHC with $m_{\tilde{q}} = 600 \text{ GeV}$ and $m_t = 175 \text{ GeV}$, where renormalization and factorization scale are assumed to be the same, the LO cross section increases by 35% in the interval between $Q = m_{\tilde{q}}$ and $m_{\tilde{q}}/2$. Taking account the NLO corrections the variation of the cross section is reduced to 5 – 10%. Taking $Q = m_{\tilde{q}/2}$ leads to quite small NLO corrections

to the LO QCD contribution.

In our work, the leading order electroweak (EW) contributions to squark production is calculated at the LHC. The cross section for 2 (anti-) squark pair production of the first 2 generations with 2 (anti-) quarks in initial states are calculated. There are no leading order EW contributions to the gluon fusion channel.

In the following section, explicit expressions are presented for the squared amplitudes for all processes with 2 quarks in the initial state and 2 squarks in the final state, where antiparticles are included. In Sec. 4.5, the numerical results for the total cross section as well as the $p_{T,\bar{q}}$ distribution are presented. In Sec. 4.6 the experimental signal is briefly discussed before concluding in Sec. 4.7. A list of employed couplings is given in the Appendix.

4.2 General formula

In this subsection the squared spin and color averaged matrix elements are presented for squark pair production. Gluon fusion is not considered. Since only production of first and second generation squarks is considered, all quark mass effects are neglected, including mixing between $SU(2)$ doublet and singlet squarks.

The functions are specified that describe the contributions from various kinds of matrix elements. Φ and χ describe squared t - and u -channel (gaugino exchange) diagrams¹, while Ψ describes the interference between a t -channel and a u -channel diagram. Similarly, s -channel (gauge boson exchange) and the interference between s - and t -channel diagrams are described by Υ and Ω , respectively:

$$\begin{aligned}
\Phi(\tilde{q}_{i\alpha}, \tilde{q}'_{j\beta}, a) &= \frac{1}{4} \sum_{l,k} c_a(l, k) \frac{1}{\hat{t} - m_l^2} \frac{1}{\hat{t} - m_k^2} \left\{ A(l, k, \tilde{q}_{i\alpha}, \tilde{q}'_{j\beta}) \right. \\
&\quad \left. \times (\hat{t}\hat{u} - m_{\tilde{q}_{i\alpha}}^2 m_{\tilde{q}'_{j\beta}}^2) + B(l, k, \tilde{q}_{i\alpha}, \tilde{q}'_{j\beta}) m_l m_k \hat{s} \right\}, \\
\chi(\tilde{q}_{i\alpha}, \tilde{q}'_{j\beta}, a) &= \frac{1}{4} \sum_{l,k} c_a(l, k) \frac{1}{\hat{u} - M_l^2} \frac{1}{\hat{u} - M_k^2} \left\{ C(l, k, \tilde{q}_{i\alpha}, \tilde{q}'_{j\beta}) \right. \\
&\quad \left. \times (\hat{t}\hat{u} - m_{\tilde{q}_{i\alpha}}^2 m_{\tilde{q}'_{j\beta}}^2) + D(l, k, \tilde{q}_{i\alpha}, \tilde{q}'_{j\beta}) M_l M_k \hat{s} \right\}, \\
\Psi(\tilde{q}_{i\alpha}, \tilde{q}'_{j\beta}, a) &= \frac{1}{4} \sum_{l,k} c_a(l, k) \frac{1}{\hat{t} - m_l^2} \frac{1}{\hat{u} - M_k^2} F(l, k, \tilde{q}_{i\alpha}, \tilde{q}'_{j\beta}) m_l M_k \hat{s}, \\
\Upsilon(q_g, q'_h, \tilde{q}_{i\alpha}, \tilde{q}'_{j\beta}, a) &= \frac{1}{4} \sum_{l,k} c_a(l, k) \frac{1}{\hat{s} - M_l^2} \frac{1}{\hat{s} - M_k^2} G(l, k, q_g, q'_h, \tilde{q}_{i\alpha}, \tilde{q}'_{j\beta}) \\
&\quad \times \left\{ (m_{\tilde{q}'_{j\beta}}^2 - m_{\tilde{q}_{i\alpha}}^2 + \hat{t} - \hat{u})(m_{\tilde{q}'_{j\beta}}^2 - m_{\tilde{q}_{i\alpha}}^2 + \hat{u} - \hat{t}) \right. \\
&\quad \left. - \hat{s}(2m_{\tilde{q}_{i\alpha}}^2 + 2m_{\tilde{q}'_{j\beta}}^2 - \hat{s}) \right\}, \\
\Omega(q_g, q'_h, \tilde{q}_{i\alpha}, \tilde{q}'_{j\beta}, a) &= -\frac{1}{4} \sum_{l,k} c_a(l, k) \frac{1}{\hat{s} - M_l^2} \frac{1}{\hat{t} - m_k^2} H(l, k, q_g, q'_h, \tilde{q}_{i\alpha}, \tilde{q}'_{j\beta}) \\
&\quad \times \left\{ (m_{\tilde{q}'_{j\beta}}^2 - \hat{t})(m_{\tilde{q}_{i\alpha}}^2 - m_{\tilde{q}'_{j\beta}}^2 + \hat{u} - \hat{t}) \right. \\
&\quad \left. - \hat{s}(\hat{s} - 3m_{\tilde{q}'_{j\beta}}^2 - m_{\tilde{q}_{i\alpha}}^2) + (m_{\tilde{q}'_{j\beta}}^2 - \hat{u})(m_{\tilde{q}_{i\alpha}}^2 - m_{\tilde{q}'_{j\beta}}^2 + \hat{t} - \hat{u}) \right\}. \tag{4.7}
\end{aligned}$$

\hat{t} , \hat{u} and \hat{s} denote the partonic Mandelstam variables. $m_{l,k}$, $M_{l,k}$ and $m_{\tilde{q}_{i\alpha}, j\beta}$ are the masses of the propagating particles and the final states squarks, respectively; capital letters are used for the masses of particles exchanged in the u - or s -channel, and lower case letters for masses in t -channel propagators. The electrically neutral gauge bosons, all of which can contribute to the same processes, are labeled through the indices $l, k = 1, 2, 3$ for γ , Z and gluon, respectively; W -boson exchange can only occur in different reactions than the exchange of the neutral gauge

¹This includes products of two different t - or u -channel diagrams.

bosons. Similarly, the four neutralinos and the gluino, which can contribute to the same process, are labeled by $l, k = 1, 2, 3, 4, 5$; alternatively, the two charginos are represented by $l, k = 1, 2$. The flavour of the quarks and squarks is given by $q, q' = u, d$. $g, h, i, j = 1, 2$ are generation indices. $\alpha, \beta = 1, 2$ label $SU(2)$ doublet (L -type) and singlet (R -type) squarks, respectively. $c_a(l, k)$ are the colour factors for the different contributions, where a labels the various exchange topologies; note that unlike l and k , a is not summed. Finally, the functions A, B, C, D, F, G and H are products of the various coupling constants appearing in the matrix elements for the different processes. Their general structure is given by

$$\begin{aligned}
A(l, k, \tilde{q}_{i\alpha}, \tilde{q}'_{j\beta}) &= a(l, \tilde{q}_{i\alpha})a(k, \tilde{q}_{i\alpha})b'(l, \tilde{q}'_{j\beta})b'(k, \tilde{q}'_{j\beta}) \\
&\quad + b(l, \tilde{q}_{i\alpha})b(k, \tilde{q}_{i\alpha})a'(l, \tilde{q}'_{j\beta})a'(k, \tilde{q}'_{j\beta}), \\
B(l, k, \tilde{q}_{i\alpha}, \tilde{q}'_{j\beta}) &= a(l, \tilde{q}_{i\alpha})a(k, \tilde{q}_{i\alpha})a'(l, \tilde{q}'_{j\beta})a'(k, \tilde{q}'_{j\beta}) \\
&\quad + b(l, \tilde{q}_{i\alpha})b(k, \tilde{q}_{i\alpha})b'(l, \tilde{q}'_{j\beta})b'(k, \tilde{q}'_{j\beta}), \\
C(l, k, \tilde{q}_{j\beta}, \tilde{q}'_{i\alpha}) &= c(l, \tilde{q}_{j\beta})c(k, \tilde{q}_{j\beta})d'(l, \tilde{q}'_{i\alpha})d'(k, \tilde{q}'_{i\alpha}) \\
&\quad + d(l, \tilde{q}_{j\beta})d(k, \tilde{q}_{j\beta})c'(l, \tilde{q}'_{i\alpha})c'(k, \tilde{q}'_{i\alpha}), \\
D(l, k, \tilde{q}_{j\beta}, \tilde{q}'_{i\alpha}) &= c(l, \tilde{q}_{j\beta})c(k, \tilde{q}_{j\beta})c'(l, \tilde{q}'_{i\alpha})c'(k, \tilde{q}'_{i\alpha}) \\
&\quad + d(l, \tilde{q}_{j\beta})d(k, \tilde{q}_{j\beta})d'(l, \tilde{q}'_{i\alpha})d'(k, \tilde{q}'_{i\alpha}), \\
F(l, k, \tilde{q}_{i\alpha}, \tilde{q}'_{j\beta}) &= a(l, \tilde{q}_{i\alpha})c(k, \tilde{q}_{j\beta})a'(l, \tilde{q}'_{j\beta})c'(k, \tilde{q}'_{i\alpha}) \\
&\quad + b(l, \tilde{q}_{i\alpha})d(k, \tilde{q}_{j\beta})b'(l, \tilde{q}'_{j\beta})d'(k, \tilde{q}'_{i\alpha}), \\
G(l, k, q_g, q'_h, \tilde{q}_{i\alpha}, \tilde{q}'_{j\beta}) &= c(l, \tilde{q}_{i\alpha}, \tilde{q}'_{j\beta})c(k, \tilde{q}_{i\alpha}, \tilde{q}'_{j\beta}) \\
&\quad \times \{e(l, q_g, q'_h)e(k, q_g, q'_h) + f(l, q_g, q'_h)f(k, q_g, q'_h)\}, \\
H(l, k, q_g, q'_h, \tilde{q}_{i\alpha}, \tilde{q}'_{j\beta}) &= c(l, \tilde{q}_{i\alpha}, \tilde{q}'_{j\beta})\{e(l, q_g, q'_h)b'(k, \tilde{q}'_{j\beta})a(k, \tilde{q}_{i\alpha}) \\
&\quad + f(l, q_g, q'_h)a'(k, \tilde{q}'_{j\beta})b(k, \tilde{q}_{i\alpha})\}. \tag{4.8}
\end{aligned}$$

Here l and k again label the exchanged (s)particles. a, b, c, d, a', b', c' and d' denote couplings of the relevant gaugino–quark–squark vertices; a, c, a' and c' denote left–handed couplings, i.e. the corresponding vertex factors are multiplied with the left–chiral projector $P_L = (1 - \gamma_5)/2$, while b, d, b' and d' denote right–handed couplings. Similarly, e and f are left– and right–handed gauge boson–quark–anti-quark couplings, respectively, and c is a gauge boson–squark–anti-squark coupling.

In the subsequent description of the contributing classes of subprocesses the contributing diagrams will be specified, color factors, and couplings; explicit expressions for the latter are given in the Appendix.

4.3 $qq' \rightarrow \tilde{q}\tilde{q}'$

Processes with two squarks or two anti-squarks in the final state are discussed. There are no s -channel contributions to this class of processes. All squark–quark–neutralino and squark–quark–gluino couplings are flavor–diagonal. Similarly, CKM mixing is ignored for charged currents, i.e. it is assumed that quark–squark–chargino couplings only occur within one gener-

ation. In the given class of reactions the flavor in the initial and final state is therefore always the same.

4.3.1 $u_i u_j \rightarrow \tilde{u}_{i\alpha} \tilde{u}_{j\beta}$

These processes proceed through the exchange of a neutralino or gluino in the t - or u -channel, as shown in Fig. 4.2.

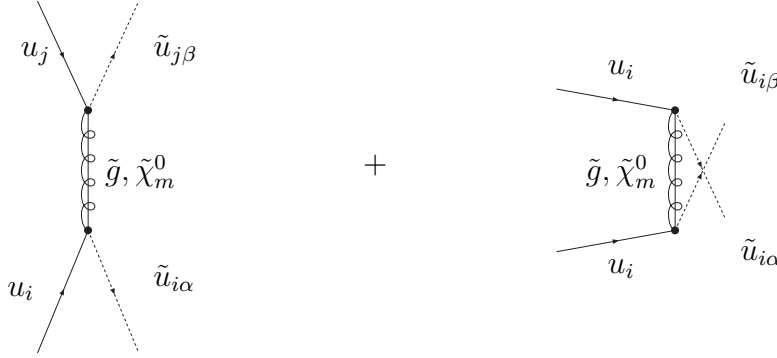


Figure 4.2: Feynman diagrams contributing to $u_i u_j \rightarrow \tilde{u}_{i\alpha} \tilde{u}_{j\beta}$. Here i and j are flavor indices, while α and β label the ‘chirality’ of the squarks, with 1 (2) standing for L -type (R -type) squarks. The index $m \in \{1, 2, 3, 4\}$ labels the exchanged neutralino. The second, u -channel, diagram only exists for $i = j$.

In the notation of Eq.(4.7) the squared spin- and color-averaged matrix element is given by

$$|\overline{M}|^2 = \Phi(\tilde{u}_{i\alpha}, \tilde{u}_{j\beta}, 1) + \chi(\tilde{u}_{i\alpha}, \tilde{u}_{i\beta}, 1)\delta_{ij} + \Psi(\tilde{u}_{i\alpha}, \tilde{u}_{i\beta}, 2)\delta_{ij}. \quad (4.9)$$

If the final state squarks are identical, a statistics factor of $\frac{1}{2}$ must be included. The colour factors of the t - and the u -channel are given by $c_1(l, k)$, while the factors for the interference term are given by $c_2(l, k)$. Explicitly,

$$c_1(l, k) = \begin{pmatrix} 1 & 1 & 1 & 1 & 0 \\ 1 & 1 & 1 & 1 & 0 \\ 1 & 1 & 1 & 1 & 0 \\ 1 & 1 & 1 & 1 & 0 \\ 0 & 0 & 0 & 0 & 2/9 \end{pmatrix}, \quad c_2(l, k) = \begin{pmatrix} 1 & 1 & 1 & 1 & 4/9 \\ 1 & 1 & 1 & 1 & 4/9 \\ 1 & 1 & 1 & 1 & 4/9 \\ 1 & 1 & 1 & 1 & 4/9 \\ 4/9 & 4/9 & 4/9 & 4/9 & -2/27 \end{pmatrix}. \quad (4.10)$$

The relevant neutralino-squark-quark and gluino-squark-quark-couplings to be inserted in

Eqs.(4.8) are

$$\begin{aligned}
a(l, \tilde{u}_{i\alpha}) &= a_{\tilde{\chi}_l^0/\tilde{g}}(\tilde{u}_{i\alpha}), & b(l, \tilde{u}_{i\alpha}) &= b_{\tilde{\chi}_l^0/\tilde{g}}(\tilde{u}_{i\alpha}), \\
a'(l, \tilde{u}_{j\beta}) &= a_{\tilde{\chi}_l^0/\tilde{g}}(\tilde{u}_{j\beta}), & b'(l, \tilde{u}_{j\beta}) &= b_{\tilde{\chi}_l^0/\tilde{g}}(\tilde{u}_{j\beta}), \\
c(l, \tilde{u}_{i\beta}) &= a_{\tilde{\chi}_l^0/\tilde{g}}(\tilde{u}_{i\beta}), & d(l, \tilde{u}_{i\beta}) &= b_{\tilde{\chi}_l^0/\tilde{g}}(\tilde{u}_{i\beta}), \\
c'(l, \tilde{u}_{i\alpha}) &= a_{\tilde{\chi}_l^0/\tilde{g}}(\tilde{u}_{i\alpha}), & d'(l, \tilde{u}_{i\alpha}) &= b_{\tilde{\chi}_l^0/\tilde{g}}(\tilde{u}_{i\alpha}).
\end{aligned} \tag{4.11}$$

As indicated earlier, $l \in \{1, 2, 3, 4\}$ refers to the l -th neutralino, while $l = 5$ refers to the gluino. Explicit expressions for the neutralino and gluino couplings appearing in Eq.(4.11) can be found in the Appendix, Eqs.(B.1) and (B.2).

Eqs.(4.9) and (4.10) also hold for the charge conjugate process. However, the appropriate anti-(s)quark couplings has to be used in Eqs.(4.8), which are given by

$$a_{\tilde{\chi}_l^0/\tilde{g}}(\tilde{\bar{u}}_{i\alpha}) = \left[b_{\tilde{\chi}_l^0/\tilde{g}}(\tilde{u}_{i\alpha}) \right]^*, \quad b_{\tilde{\chi}_l^0/\tilde{g}}(\tilde{\bar{u}}_{i\alpha}) = \left[a_{\tilde{\chi}_l^0/\tilde{g}}(\tilde{u}_{i\alpha}) \right]^*, \tag{4.12}$$

where $\tilde{\bar{q}}$ denotes an anti-squark and the stars stand for complex conjugation. Note that even in a CP-conserving scenario some neutralino couplings have to be complex (more exactly, purely imaginary) if we insist on using positive neutralino masses in all propagators [150]. If CP is violated, all chargino, neutralino and gluino couplings may be complex. Finally, recall that a right-handed anti-quark is an $SU(2)$ doublet; its couplings are therefore related to those of left-handed quarks, and vice versa.

4.3.2 $d_i d_j \rightarrow \tilde{d}_{i\alpha} \tilde{d}_{j\beta}$

The process $d_i d_j \rightarrow \tilde{d}_{i\alpha} \tilde{d}_{j\beta}$ and its charge-conjugated process are given by Eqs.(4.9) to (4.12), with the obvious replacement $\tilde{u} \rightarrow \tilde{d}$ everywhere.

4.3.3 $u_i d_j \rightarrow \tilde{u}_{i\alpha} \tilde{d}_{j\beta}$

This process receives contributions from the t -channel exchange of a neutralino or gluino; if both (s)quarks are from the same generation, $i = j$, there is also a u -channel chargino exchange contribution. The corresponding Feynman diagrams are shown in Fig. 4.3.

The squared spin- and color-averaged matrix element is given by

$$\overline{|M|^2} = \Phi(\tilde{u}_{i\alpha}, \tilde{d}_{j\beta}, 1) + \chi(\tilde{u}_{i\alpha}, \tilde{d}_{i\beta}, 2)\delta_{ij} + \Psi(\tilde{u}_{i\alpha}, \tilde{d}_{i\beta}, 3)\delta_{ij}. \tag{4.13}$$

The color factors for the squared t -channel neutralino and gluino contributions, squared u -channel chargino contributions and of the interference terms are given by

$$c_1(l, k) = \begin{pmatrix} 1 & 1 & 1 & 1 & 0 \\ 1 & 1 & 1 & 1 & 0 \\ 1 & 1 & 1 & 1 & 0 \\ 1 & 1 & 1 & 1 & 0 \\ 0 & 0 & 0 & 0 & 2/9 \end{pmatrix}, \quad c_2(l, k) = \begin{pmatrix} 1 & 1 \\ 1 & 1 \end{pmatrix}, \quad c_3(l, k) = \begin{pmatrix} 1 & 1 \\ 1 & 1 \\ 1 & 1 \\ 4/9 & 4/9 \end{pmatrix}. \tag{4.14}$$

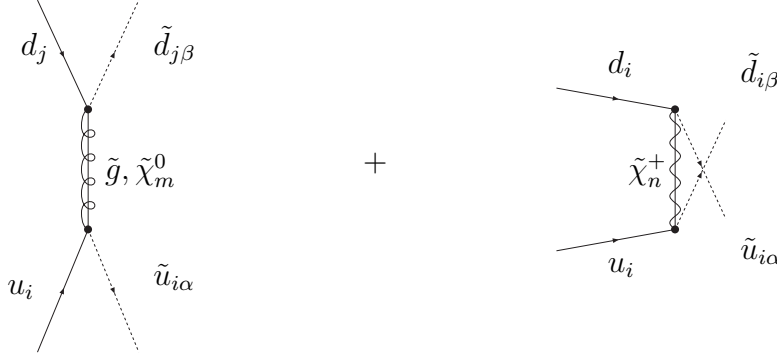


Figure 4.3: Feynman diagrams contributing to $u_i d_j \rightarrow \tilde{u}_{i\alpha} \tilde{d}_{j\beta}$. The notation in the t -channel diagram is as in Fig. 4.2. In the second, u -channel, diagram, which only exists of $i = j$, the chargino index n runs from 1 to 2.

In the squared t -channel diagrams the indices l, k labeling the exchanged particles run from 1 to 5 for the four neutralinos and gluino, whereas in the squared u -channel chargino-exchange contribution the indices run from 1 to 2. In the interference contribution the index l labeling the particle exchanged in the t -channel again runs from 1 to 5, while k takes the values 1 or 2. The couplings to be inserted in Eqs.(4.8) are given by

$$\begin{aligned}
 a(l, \tilde{u}_{i\alpha}) &= a_{\tilde{\chi}_l^0/\tilde{g}}(\tilde{u}_{i\alpha}), & b(l, \tilde{u}_{i\alpha}) &= b_{\tilde{\chi}_l^0/\tilde{g}}(\tilde{u}_{i\alpha}), \\
 a'(l, \tilde{d}_{j\beta}) &= a_{\tilde{\chi}_l^0/\tilde{g}}(\tilde{d}_{j\beta}), & b'(l, \tilde{d}_{j\beta}) &= b_{\tilde{\chi}_l^0/\tilde{g}}(l, \tilde{d}_{j\beta}), \\
 c(l, \tilde{d}_{i\beta}) &= a_{\tilde{\chi}_l^+}(\tilde{d}_{i\beta}), & d(l, \tilde{d}_{i\beta}) &= b_{\tilde{\chi}_l^+}(\tilde{d}_{i\beta}), \\
 c'(l, \tilde{u}_{i\alpha}) &= a_{\tilde{\chi}_l^+}(\tilde{u}_{i\alpha}), & d'(l, \tilde{u}_{i\alpha}) &= b_{\tilde{\chi}_l^+}(\tilde{u}_{i\alpha})
 \end{aligned} \quad . \quad (4.15)$$

The explicit expressions for the couplings appearing in Eqs.(4.15) can be found in Eqs.(B.1), (B.2) and (B.3) in the Appendix.

The cross section for the charge-conjugated process can again be obtained by using the appropriate couplings for anti-(s)quarks in Eqs.(4.8):

$$\begin{aligned}
 a_{\tilde{\chi}_l^0/\tilde{g}/\tilde{\chi}_l^+}(\tilde{\bar{d}}_{i\alpha}) &= \left[b_{\tilde{\chi}_l^0/\tilde{g}/\tilde{\chi}_l^+}(\tilde{d}_{i\alpha}) \right]^*, & b_{\tilde{\chi}_l^0/\tilde{g}/\tilde{\chi}_l^+}(\tilde{\bar{d}}_{i\alpha}) &= \left[a_{\tilde{\chi}_l^0/\tilde{g}/\tilde{\chi}_l^+}(\tilde{d}_{i\alpha}) \right]^*, \\
 a_{\tilde{\chi}_l^0/\tilde{g}/\tilde{\chi}_l^+}(\tilde{\bar{u}}_{i\alpha}) &= \left[b_{\tilde{\chi}_l^0/\tilde{g}/\tilde{\chi}_l^+}(\tilde{u}_{i\alpha}) \right]^*, & b_{\tilde{\chi}_l^0/\tilde{g}/\tilde{\chi}_l^+}(\tilde{\bar{u}}_{i\alpha}) &= \left[a_{\tilde{\chi}_l^0/\tilde{g}/\tilde{\chi}_l^+}(\tilde{u}_{i\alpha}) \right]^* .
 \end{aligned} \quad (4.16)$$

4.3.4 $u_i d_j \rightarrow \tilde{d}_{i\alpha} \tilde{u}_{j\beta}$, $i \neq j$

This process differs from the one considered in the previous subsection only if the two (s)quarks are from *different* generation, with the d -type squark in the final state being from the same

generation as the initial u -type quark. In this case only the chargino exchange diagram shown in Fig. 4.4 contributes. The momenta are labelled such that this is a t -channel diagram.

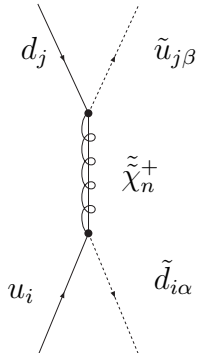


Figure 4.4: Feynman diagram contributing to $u_i d_j \rightarrow \tilde{u}_{j\alpha} \tilde{d}_{i\beta}$ with $i \neq j$. The notation is as in the chargino exchange diagram of Fig. 4.3.

The squared spin- and color-averaged matrix element is given by

$$\overline{|M|}^2 = \Phi(\tilde{d}_{i\alpha}, \tilde{u}_{j\beta}, 1). \quad (4.17)$$

The colour factor is trivial,

$$c_1 = \begin{pmatrix} 1 & 1 \\ 1 & 1 \end{pmatrix}. \quad (4.18)$$

The couplings to be inserted in Eqs.(4.8) are,

$$\begin{aligned} a(l, \tilde{d}_{i\alpha}) &= a_{\tilde{\chi}_i^+}(\tilde{d}_{i\alpha}), & b(l, \tilde{d}_{i\alpha}) &= b_{\tilde{\chi}_i^+}(\tilde{d}_{i\alpha}), \\ a'(l, \tilde{u}_{j\beta}) &= a_{\tilde{\chi}_i^+}(\tilde{u}_{j\beta}), & b'(l, \tilde{u}_{j\beta}) &= b_{\tilde{\chi}_i^+}(\tilde{u}_{j\beta}). \end{aligned} \quad (4.19)$$

The cross section for the charge conjugated process can be obtained by using the appropriate anti-(s)quark couplings, which have already been given in Eqs.(4.16).

4.4 $q\bar{q}' \rightarrow \tilde{q}\tilde{q}'$

Processes with one squark and one anti-squark in the final state are considered. Since now the initial and final state have vanishing baryon charge, s -channel diagrams may contribute.

4.4.1 $u_i \bar{u}_j \rightarrow \tilde{u}_{i\alpha} \tilde{\bar{u}}_{j\beta}$

This process receives contributions from the exchange of a gluino or neutralino in the t -channel; if $i = j$, there are also s -channel gluon, photon and Z exchange contributions. The corresponding Feynman diagrams are shown in Fig. 4.5.

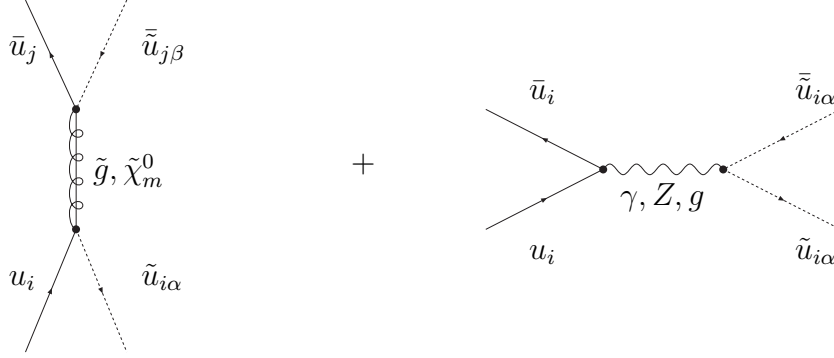


Figure 4.5: Feynman diagrams contributing to $u_i \bar{u}_j \rightarrow \tilde{u}_{i\alpha} \tilde{\bar{u}}_{j\beta}$. The notation for the t -channel diagram is as in Fig.4.2. The gauge boson exchanged in the second, s -channel, diagram, which only exists if $i = j$, can be a gluon, a photon or a Z boson.

The squared spin- and color-averaged matrix element is given by

$$\overline{|M|^2} = \Phi(\tilde{u}_{i\alpha}, \tilde{\bar{u}}_{j\beta}, 1) + \Upsilon(u_i, \bar{u}_i, \tilde{u}_{i\alpha}, \tilde{\bar{u}}_{i\alpha}, 2) \delta_{ij} \delta_{\alpha\beta} + \Omega(u_i, \bar{u}_i, \tilde{u}_{i\alpha}, \tilde{\bar{u}}_{i\alpha}, 3) \delta_{ij} \delta_{\alpha\beta}. \quad (4.20)$$

The color factors of the pure t -channel neutralino and gluino contributions, the s -channel γ, Z , gluon contributions and the interference terms are given by

$$c_1(l, k) = \begin{pmatrix} 1 & 1 & 1 & 1 & 0 \\ 1 & 1 & 1 & 1 & 0 \\ 1 & 1 & 1 & 1 & 0 \\ 1 & 1 & 1 & 1 & 0 \\ 0 & 0 & 0 & 0 & 2/9 \end{pmatrix}, \quad c_2(l, k) = \begin{pmatrix} 1 & 1 & 0 \\ 1 & 1 & 0 \\ 0 & 0 & 2/9 \end{pmatrix},$$

$$c_3(l, k) = \begin{pmatrix} 1 & 1 & 1 & 1 & 4/9 \\ 1 & 1 & 1 & 1 & 4/9 \\ 4/9 & 4/9 & 4/9 & 4/9 & -2/27 \end{pmatrix}. \quad (4.21)$$

The couplings to be inserted in Eqs.(4.8) are given by:

$$\begin{aligned}
a(l, \tilde{u}_{i\alpha}) &= a_{\tilde{\chi}_l^0/\tilde{g}}(\tilde{u}_{i\alpha}), & b(l, \tilde{u}_{i\alpha}) &= b_{\tilde{\chi}_l^0/\tilde{g}}(\tilde{u}_{i\alpha}), \\
a'(l, \tilde{\bar{u}}_{j\beta}) &= \left[b_{\tilde{\chi}_l^0/\tilde{g}}(\tilde{u}_{j\beta}) \right]^*, & b'(l, \tilde{\bar{u}}_{j\beta}) &= \left[a_{\tilde{\chi}_l^0/\tilde{g}}(\tilde{u}_{j\beta}) \right]^*, \\
e(l, u_i, \bar{u}_i) &= e_{\gamma/Z/g}(u_i, \bar{u}_i), & f(l, u_i, \bar{u}_i) &= q_{\gamma/Z/g}(u_i, \bar{u}_i), \\
c(l, \tilde{u}_{i\alpha}, \tilde{\bar{u}}_{i\alpha}) &= c_{\gamma/Z/g}(\tilde{u}_{i\alpha}, \tilde{\bar{u}}_{i\alpha}).
\end{aligned} \tag{4.22}$$

Recall that in s -channel diagrams $l = 1$ stands for a photon, $l = 2$ for a Z -boson, and $l = 3$ for a gluon. The explicit expressions for the couplings of these gauge bosons can be found in Eqs.(B.4) and (B.5) in the Appendix.

4.4.2 $u_i \bar{u}_i \rightarrow \tilde{q}_{j\alpha} \tilde{\bar{q}}_{j\alpha}, \quad i \neq j$

Since the flavor in the initial and final state is different, only the s -channel diagrams of Fig.4.5 contribute. The squared spin- and color-averaged matrix element is thus simply given by

$$\overline{|M|^2} = \Upsilon(u_i, \bar{u}_i, \tilde{q}_{i\alpha}, \tilde{\bar{q}}_{i\alpha}, 1). \tag{4.23}$$

The colour factors are

$$c_1(l, k) = \begin{pmatrix} 1 & 1 & 0 \\ 1 & 1 & 0 \\ 0 & 0 & 2/9 \end{pmatrix}. \tag{4.24}$$

The couplings to be inserted in Eqs.(4.8) can be read off from Eqs.(4.22).

4.4.3 $u_i \bar{u}_j \rightarrow \tilde{d}_{i\alpha} \tilde{\bar{d}}_{j\beta}$

This process receives contributions from chargino exchange in the t -channel; if $i = j$, there are also s -channel contributions with gluon, photon and Z -exchange. The corresponding Feynman diagrams are shown in Fig. 4.6.

The squared spin- and color-averaged matrix element is given by

$$\overline{|M|^2} = \Phi(\tilde{d}_{i\alpha}, \tilde{\bar{d}}_{j\beta}, 1) + \Upsilon(u_i, \bar{u}_i, \tilde{d}_{i\alpha}, \tilde{\bar{d}}_{i\alpha}, 2)\delta_{ij}\delta_{\alpha\beta} + \Omega(u_i, \bar{u}_i, \tilde{d}_{i\alpha}, \tilde{\bar{d}}_{i\alpha}, 3)\delta_{ij}\delta_{\alpha\beta}. \tag{4.25}$$

The respective colour factors for the squared t -channel, squared s -channel and the interference terms are given by

$$c_1 = \begin{pmatrix} 1 & 1 \\ 1 & 1 \end{pmatrix}, \quad c_2(l, k) = \begin{pmatrix} 1 & 1 & 0 \\ 1 & 1 & 0 \\ 0 & 0 & 2/9 \end{pmatrix}, \quad c_3(l, k) = \begin{pmatrix} 1 & 1 \\ 1 & 1 \\ 4/9 & 4/9 \end{pmatrix}. \tag{4.26}$$

The couplings to be inserted in Eqs.(4.8) are given by

$$\begin{aligned}
a(l, \tilde{d}_{i\alpha}) &= a_{\tilde{\chi}_l^+}(\tilde{d}_{i\alpha}), & a'(l, \tilde{\bar{d}}_{j\beta}) &= \left[b_{\tilde{\chi}_l^+}(\tilde{d}_{j\beta}) \right]^*, \\
b(l, \tilde{d}_{i\alpha}) &= b_{\tilde{\chi}_l^+}(\tilde{d}_{i\alpha}), & b'(l, \tilde{\bar{d}}_{j\beta}) &= \left[a_{\tilde{\chi}_l^+}(\tilde{d}_{j\beta}) \right]^*, \\
e(l, u_i, \bar{u}_i) &= e_{\gamma/Z/g}(u_i, \bar{u}_i), & f(l, u_i, \bar{u}_i) &= q_{\gamma/Z/g}(u_i, \bar{u}_i), \\
c(l, \tilde{d}_{i\alpha}, \tilde{\bar{d}}_{i\alpha}) &= c_{\gamma/Z/g}(\tilde{d}_{i\alpha}, \tilde{\bar{d}}_{i\alpha}).
\end{aligned} \tag{4.27}$$

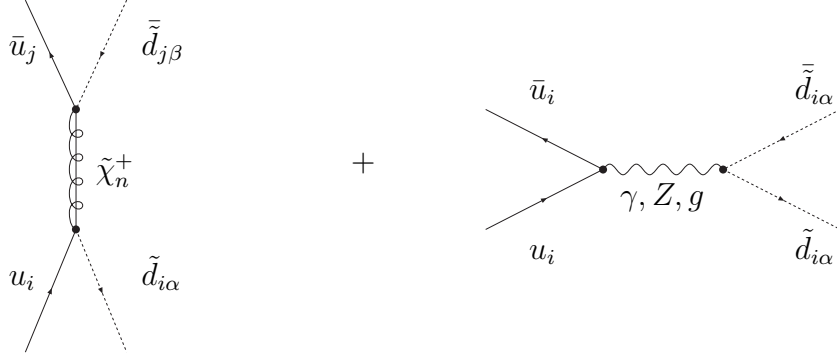


Figure 4.6: Feynman diagrams contributing to $u_i \bar{u}_j \rightarrow \tilde{d}_{i\alpha} \tilde{\bar{d}}_{j\beta}$. The notation for the t -channel diagram is as in Fig.4.4. The notation for the second, s -channel, diagram, which only exists if $i = j$, is as in Fig. 4.5.

4.4.4 $d_i \bar{d}_j \rightarrow \tilde{q} \tilde{\bar{q}}$

Each of the last three processes has an analogue where all u -type (s)quarks are replaced by d -type (s)quarks and vice versa. The cross sections for these reactions can be described by simply replacing $u \rightarrow d$ and $d \rightarrow u$ everywhere.

4.4.5 $d_i \bar{u}_j \rightarrow \tilde{d}_{i\alpha} \tilde{\bar{u}}_{j\beta}$

This process receives contributions from the exchange of a gluino or neutralino in the t -channel; if $i = j$, there is also an s -channel W exchange contribution. The corresponding Feynman diagrams are shown in Fig. 4.7.

The squared spin- and color-averaged matrix element is given by

$$\overline{|M|^2} = \Phi(\tilde{d}_{i\alpha}, \tilde{\bar{u}}_{j\beta}, 1) + \Upsilon(d_i, \bar{u}_i, \tilde{d}_{i\alpha}, \tilde{\bar{u}}_{i\alpha}, 2) \delta_{ij} \delta_{\alpha\beta} + \Omega(d_i, \bar{u}_i, \tilde{d}_{i\alpha}, \tilde{\bar{u}}_{i\alpha}, 3) \delta_{ij} \delta_{\alpha\beta}. \quad (4.28)$$

The color factors for the pure t -channel, pure s -channel and interference terms are

$$c_1(l, k) = \begin{pmatrix} 1 & 1 & 1 & 1 & 0 \\ 1 & 1 & 1 & 1 & 0 \\ 1 & 1 & 1 & 1 & 0 \\ 1 & 1 & 1 & 1 & 0 \\ 0 & 0 & 0 & 0 & 2/9 \end{pmatrix}, \quad c_2 = 1, \quad c_3 = (1 \ 1 \ 1 \ 1 \ 4/9). \quad (4.29)$$

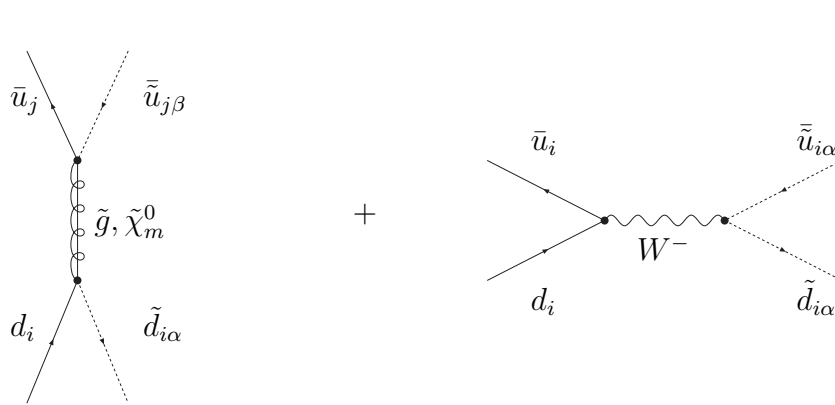


Figure 4.7: Feynman diagrams contributing to $d_i \bar{u}_j \rightarrow \tilde{d}_{i\alpha} \tilde{\bar{u}}_{j\beta}$. The notation for the t -channel diagram is as in Fig.4.4. The second, s -channel, diagram, which only exists if $i = j$, proceeds via the exchange of a charged W boson.

The couplings to be inserted in Eqs.(4.8) are

$$\begin{aligned}
a(l, \tilde{d}_{i\alpha}) &= a_{\tilde{\chi}_l^0/\tilde{g}}(\tilde{d}_{i\alpha}), & a'(l, \tilde{\bar{u}}_{j\beta}) &= \left[b_{\tilde{\chi}_l^0/\tilde{g}}(\tilde{u}_{j\beta}) \right]^*, \\
b(l, \tilde{d}_{i\alpha}) &= b_{\tilde{\chi}_l^0/\tilde{g}}(\tilde{d}_{i\alpha}), & b'(l, \tilde{\bar{u}}_{j\beta}) &= \left[a_{\tilde{\chi}_l^0/\tilde{g}}(\tilde{u}_{j\beta}) \right]^*, \\
e(d_i, \bar{u}_i) &= e_W(d_i, \bar{u}_i), & f(d_i, \bar{u}_i) &= f_W(l, d_i, \bar{u}_i), \\
c(l, \tilde{d}_{i\alpha}, \tilde{\bar{u}}_{i\alpha}) &= c_W(\tilde{d}_{i\alpha}, \tilde{\bar{u}}_{i\alpha})
\end{aligned} \tag{4.30}$$

Explicit expressions for the couplings of the W boson can be found in Eqs.(B.6) and (B.7) in the Appendix.

Unlike for the processes discussed so far in this Subsection, charge conjugation here leads to a physically different reaction. The cross section for this process can be obtained from Eqs.(4.28)–(4.30) by replacing (s)quark couplings with anti-(s)quark couplings and vice versa. The new couplings appearing in the t -channel diagrams can e.g. be read off from Eqs.(4.16), whereas the couplings in the s -channel diagram remain unchanged.

4.4.6 $d_i \bar{u}_i \rightarrow \tilde{d}_{j\alpha} \tilde{\bar{u}}_{j\beta}$, $i \neq j$

This process can only proceed through the exchange of a charged W boson in the s -channel. The corresponding Feynman diagram has already been shown in Fig. 4.7. The squared spin- and color-averaged matrix element is simply given by

$$\overline{|M|^2} = \Upsilon(d_i, \bar{u}_i, \tilde{d}_{j\alpha}, \tilde{\bar{u}}_{j\beta}, 1). \tag{4.31}$$

Scenario	m_0	$m_{1/2}$	$m_{\tilde{q}}$	QCD		QCD + EW		ratio	
				Total	LL	Total	LL	Total	LL
SPS 1a	100	250	560	12.11	3.09	12.55	3.50	1.036	1.133
SPS 1b	200	400	865	1.57	0.42	1.66	0.499	1.055	1.186
SPS 2	1450	300	1590	0.0553	0.0132	0.0567	0.0144	1.025	1.091
SPS 3	90	400	845	1.74	0.464	1.83	0.551	1.055	1.188
SPS 4	400	300	760	3.10	0.813	3.22	0.927	1.040	1.141
SPS 5	150	300	670	5.42	1.41	5.66	1.62	1.042	1.152

Table 4.1: Total cross sections at the LHC for combined first and second generation squark pair production from quark initial states in 6 mSUGRA benchmark scenarios [152]. All masses are in GeV, m_0 and $m_{1/2}$ being the common soft breaking scalar and gaugino masses, respectively, at the scale of Grand Unification, and $m_{\tilde{q}}$ giving the average mass of first generation $SU(2)$ doublet squarks. All cross sections are in pb. The last 2 columns show the ratio (QCD + EW) / QCD. Results are shown for the sum over all squark pairs (“total”), as well as for the sum over all combinations of 2 $SU(2)$ doublet squarks (“LL”); in both cases squarks and anti-squarks are included. The cross sections have been calculated in leading order, using the CTEQ5L parton distribution functions [147].

The color factor is trivial, $c_1 = 1$. The couplings to be inserted in Eqs.(4.8) are

$$\begin{aligned}
e(l, d_i, \bar{u}_i) &= e_W(d_i, \bar{u}_i), & f(l, d_i, \bar{u}_i) &= f_W(l, d_i, \bar{u}_i), \\
c(l, \tilde{d}_{j\alpha}, \tilde{\bar{u}}_{j\beta}) &= c_W(\tilde{d}_{j\alpha}, \tilde{\bar{u}}_{j\beta}).
\end{aligned}
\tag{4.32}$$

The squared matrix element for the charge conjugated process is identical.

4.5 Numerical results

4.5.1 Preliminary remarks

The cross section for production of the first 2 generation of squark pairs at the LHC is presented, where the leading order (LO) electroweak (EW) contribution to the QCD prediction is taken into account.

In performing the numerical analysis, the masses of the particles in the different mSUGRA points [152] are calculated by SoftSUSY [151]. In addition, the electroweak gauge couplings are taken from SoftSUSY. The masses of the gluino and the squarks are on-shell pole masses and the couplings are given in the \overline{MS} scheme at the squark mass scale. The CTEQ5L parton density functions [147] are used, since only electroweak corrections to the QCD predictions at leading order are considered. The one-loop expression for the QCD coupling α_s is used, where $\Lambda_{\text{QCD}} = 142$ MeV, and 5 active flavors are chosen. The factorization scale and renormalization scale are chosen to be equal and are fixed to the value $\mu_F = \mu_R = m_{\tilde{q}}/2$. This leads to small QCD NLO corrections to the LO QCD prediction [146].

4.5.2 Results

The numerical results are given in Table 4.1. For several mSUGRA scenarios [152], the cross section for squark pair production with and without LO EW contributions to QCD are listed, whereas the cross section for 2 SU(2) doublet squarks in the final state is separately given. All squarks and antisquarks of the first and second generation are considered. The mSUGRA parameters m_0 and $m_{1/2}$, see Eq. (1.32), are displayed for each benchmark scenario and the average squark mass is given. In addition, the enhancement, expressed as the ratio (QCD+EW)/QCD, are listed.

The cross section heavily depends on the squark mass scale, since the cross section scales like

$$\sigma \propto \frac{1}{m_{\tilde{q}}^2}, \quad (4.33)$$

on parton level, provided the running of the strong coupling constant is not taken into account and the ratios of sparticle masses are fixed. In addition, for large squark masses, i. e. for large Bjorken- x , the parton density functions of the quarks decrease quickly, see Fig. 4.1. and hence further suppress the cross section.

The corrections depend on the gluino mass $m_{\tilde{g}} \approx 2.5m_{1/2}$ and varying the gluino mass between $0.5m_{\tilde{q}}$ and $1.2m_{\tilde{q}}$ changes the QCD cross section between 15% and 20%. The EW contribution also depends on the ratio $m_{1/2}/m_0$ and for a constant ratio $m_{1/2}/m_0$, the EW contributions become larger for heavier squarks. The dependence on the gaugino mass is for the EW contributions much stronger than for the QCD case.

The full EW contributions to the QCD predictions are quite small. It never exceeds 6%. However, the electroweak contributions for the production of 2 SU(2) doublet squarks are much more important and can reach up to 20% for SPS 3. This can only be partly explained by the smaller hypercharge interaction compared to the SU(2) gauge interaction. The squared SU(2) gauge coupling $g'^2 = e^2/\cos^2\theta_W$ is compared to the squared U(1) $_Y$ coupling $g^2 = e^2/\sin^2\theta_W$ by a factor $\cot^2\theta_W \approx 3.3$ larger. If one considers the results for SPS 1a in Table 4.1, the cross section for the production of 2 SU(2) doublet squarks is 3.5 pb for QCD and EW contribution. The pure QCD cross section is 3.09 pb. Hence, the enhancement due to EW contribution is 0.41 pb. The enhancement of the EW contribution to the pure QCD prediction for the production of all squarks is 0.44 pb. Thus, the cross section, where both final states are not SU(2) doublet squarks, is 0.03 pb, where the exchanged gauge/gaugino is a U(1) $_Y$ boson. It will be shown that destructive interference effects diminish the U(1) $_Y$ contributions. In the next subsection, the origin of all these effects is explained.

4.5.3 Discussion

There are 3 classes of processes, contributing to the squark pair production. Basically, there are reactions, where t- and u-channel can interfere, where there are strong and electroweak contributions from both the t- and u-channel diagrams. The next class of processes is specified by interference between the t- and s-channel diagrams. Again, there can be electroweak and

strong contributions to t - and s -channel diagrams. In the last class of processes, there is no interference between electroweak and strong contributions possible.

In Table 4.2, all processes are listed, which are separated into the 3 groups. Only the first generation is considered and the mSUGRA benchmark SPS 1a [152] is chosen.

t - and u -channel contributions

First, start with the processes, where interference between t - and u -channel is possible. The first 7 processes in Table 4.2 belong to this group. Apart from the seventh process, there are both strong and electroweak contributions from both t - and u -channel. In the last process, there is only a gluino t -channel contribution, but for the electroweak part, there are both contributions. In this class of processes, there are 2 distinct reactions. There are reactions, which either require a helicity flip or do not need it. E. g., the process $uu \rightarrow \tilde{u}_L \tilde{u}_L$ requires a helicity flip, i. e. the corresponding amplitude is proportional to the mass of the exchanged gaugino. Since the quark-squark-gaugino gauge couplings couple L-type squarks to left-handed quarks, both initial state quarks are left-handed. Therefore, a helicity flip is required for the exchanged gaugino and the cross section is proportional to the mass of the exchanged gaugino. Because of unification of the gaugino masses at the unified scale, the $SU(2)$ and $U(1)_Y$ gaugino masses are about 3 and 7 times smaller than the gluino mass, see Eq. (1.38), so that the electroweak contributions are further suppressed. However, since both helicities are the same, the total angular momentum is zero ($J = 0$), so that the squarks are in a S-wave. Thus the cross section receives only a single power of the threshold factor²

$$\beta = \sqrt{1 - 4 \frac{m_{\tilde{q}}^2}{\hat{s}}}. \quad (4.34)$$

This β -factor originates from the phase space.

The situation is different, if one L-type and one R-type squark are produced. In the case of $\tilde{u}_L \tilde{u}_R$ (process no. 3 in Table 4.2), both initial state up quarks have opposite helicities. Since the exchanged gaugino does not change its helicity, the amplitude is not proportional to the gaugino mass and thus the amplitude is non-vanishing in the limit, where the gaugino is massless. Both spins of the quarks point in the same direction, so that $J = 1$. The final state squarks are now in a P-wave, so that the cross section is proportional to β^3 . One factor of β comes from the phase space and the squared matrix element is proportional to β^2 . Therefore processes, which do not require a helicity flip, are suppressed by 2 additional powers of β .

In the case, where antiparticles are involved, one has to treat an R-type anti-squark as an L-type squark, since

$$\overline{q}_R = (\bar{q})_L. \quad (4.35)$$

The R-type anti-squark couples to a left-handed particle. Similarly, an L-type anti-squark acts like an R-type squark.

²For simplicity, equal squark masses are assumed.

No.	Process	diagrams		helicity flip?	threshold	cross section [pb]		ratio
		QCD	EW			QCD	QCD + EW	
1	$uu \rightarrow \tilde{u}_L \tilde{u}_L$	t, u	t, u	yes	β	0.683	0.794	1.162
2	$uu \rightarrow \tilde{u}_R \tilde{u}_R$	t, u	t, u	yes	β	0.761	0.796	1.045
3	$uu \rightarrow \tilde{u}_L \tilde{u}_R$	t, u	t, u	no	β^3	0.929	0.931	1.002
4	$dd \rightarrow \tilde{d}_L \tilde{d}_L$	t, u	t, u	yes	β	0.198	0.232	1.171
5	$dd \rightarrow \tilde{d}_R \tilde{d}_R$	t, u	t, u	yes	β	0.234	0.237	1.012
6	$dd \rightarrow \tilde{d}_L \tilde{d}_R$	t, u	t, u	no	β^3	0.243	0.243	1.000
7	$ud \rightarrow \tilde{u}_L \tilde{d}_L$	t	t, u	yes	β	0.969	1.22	1.261
8	$u\bar{u} \rightarrow \tilde{u}_L \tilde{u}_L$	s, t	s, t	no	β^3	0.165	0.140	0.848
9	$u\bar{u} \rightarrow \tilde{u}_R \tilde{u}_R$	s, t	s, t	no	β^3	0.187	0.170	0.909
10	$d\bar{d} \rightarrow \tilde{d}_L \tilde{d}_L$	s, t	s, t	no	β^3	0.0925	0.0784	0.847
11	$d\bar{d} \rightarrow \tilde{d}_R \tilde{d}_R$	s, t	s, t	no	β^3	0.109	0.106	0.972
12	$u\bar{u} \rightarrow \tilde{d}_L \tilde{d}_L$	s	s, t	no	β^3	0.0341	0.0353	1.035
13	$d\bar{d} \rightarrow \tilde{u}_L \tilde{u}_L$	s	s, t	no	β^3	0.0207	0.0219	1.057
14	$u\bar{d} \rightarrow \tilde{u}_L \tilde{d}_L$	t	s, t	no	β^3	0.178	0.162	0.910
15	$ud \rightarrow \tilde{u}_L \tilde{d}_R$	t	t	no	β^3	0.484	0.485	1.001
16	$ud \rightarrow \tilde{u}_R \tilde{d}_L$	t	t	no	β^3	0.477	0.479	1.002
17	$ud \rightarrow \tilde{u}_R \tilde{d}_R$	t	t	yes	β	1.113	1.114	1.001
18	$u\bar{u} \rightarrow \tilde{u}_L \tilde{u}_R$	t	t	yes	β	0.569	0.569	1.000
19	$d\bar{d} \rightarrow \tilde{d}_L \tilde{d}_R$	t	t	yes	β	0.331	0.331	1.000
20	$u\bar{d} \rightarrow \tilde{u}_L \tilde{d}_R$	t	t	yes	β	0.491	0.491	1.000
21	$u\bar{d} \rightarrow \tilde{u}_R \tilde{d}_L$	t	t	yes	β	0.480	0.480	1.000
22	$u\bar{d} \rightarrow \tilde{u}_R \tilde{d}_R$	t	t	no	β^3	0.202	0.203	1.004
23	$u\bar{u} \rightarrow \tilde{d}_R \tilde{d}_R$	s	s	–	β^3	0.0420	0.0421	1.002
24	$d\bar{d} \rightarrow \tilde{u}_R \tilde{u}_R$	s	s	–	β^3	0.0240	0.0240	1.000

Table 4.2: The 24 different squark pair production processes involving first generation (s)quarks only; charge conjugate reactions are included in the cross section if they differ from the listed ones. The letters s, t, u stand for the existence of s -, t - and u -channel diagrams, respectively; this is listed separately for strong and electroweak interactions. It is also listed whether the exchange of a fermion in the t - and/or u -channel requires a helicity flip. The fifth column describes the threshold behavior of the cross section, in terms of the squark velocity β in the center-of-mass frame; a behavior $\propto \beta$ (β^3) indicates an S - (P -)wave cross section. The values of the cross sections are for scenario SPS 1a (see Table 4.1). The last column shows the relative size of the electroweak contributions.

The electroweak contributions of the first group in Table 4.2 enhance the cross section. This can be seen in Eq. (4.7), where the function Ψ is given. The relevant products of couplings

and color factors are positive for the interference between t- and u-channel diagrams. The remaining function is also positive. Thus the interference is constructive.

As explained above, the electroweak contributions are sizable, if both squarks are SU(2) doublet squarks. However the process $uu \rightarrow \tilde{u}_R \tilde{u}_R$ also yields a contribution, which is not negligible. This is due to the large hypercharge. The largest contribution is given by the process $ud \rightarrow \tilde{u}_L \tilde{d}_L$. In this reaction, there is interference from t- and u-channel electroweak diagrams and interference between a t-channel gluino and u-channel chargino diagram. In the limit, where one of the charginos is a pure charged wino, the coupling to a quark and a squark is given by Eq. (B.3)

$$a_{\tilde{\chi}_1^+}(\tilde{u}_L) = -gV_{11}. \quad (4.36)$$

The corresponding neutralino coupling is given by Eq. (B.1),

$$a_{\tilde{\chi}_2^0}(\tilde{u}_L) = \sqrt{2}g\frac{1}{2}N_{22}^*. \quad (4.37)$$

The chargino coupling is by a factor $\sqrt{2}$ larger compared to the corresponding neutralino coupling. Thus, the electroweak contribution to $\tilde{u}_L \tilde{d}_L$ should be twice as large as the electroweak contributions to $\tilde{u}_L \tilde{u}_L$ or $\tilde{d}_L \tilde{d}_L$. Actually, the enhancement is smaller, since the relative importance of the electroweak contributions to $\tilde{u}_L \tilde{u}_L$ and $\tilde{d}_L \tilde{d}_L$ is enhanced by the destructive interference between both QCD t-channel and u-channel diagrams, see e. g. Eq. (4.21).

All processes, where 2 SU(2) doublet squarks are produced require a helicity flip. In mSUGRA, the electroweak gauginos are much lighter than the gluino due to gaugino mass unification, so that the EW contribution are much smaller than a naive guess based on couplings constant. However, the color factor for the interference terms is 2 times bigger than for the pure QCD amplitudes, see e. g. Eq. (4.10).

One last remark is about the different absolute sizes of the cross section for these 7 processes. In principle, this can be explained by 4 effects. The production of 2 identical particles is suppressed by a statistical factor of 1/2. However, for the production of $\tilde{u}_L \tilde{u}_R$ and $\tilde{d}_L \tilde{d}_R$, the produced squarks require at least a P-wave. Thus the cross section is suppressed by 2 additional powers of β . This yields a similar suppression as the statistical factor for 2 identical particles and can even lead to a larger suppression, if the squarks are heavier. The flux of valence u-quarks is about 2 times larger than that for the valence d-quarks in the proton. For increasing Bjorken-x, see Fig. 4.1, the ratio of both parton density functions increases. Therefore, for heavier squarks, the dominance of the produced u-squarks over d-squarks is larger for heavier squarks. In mSUGRA, the SU(2) doublet squarks are heavier than the SU(2) singlet squarks, since the masses of the SU(2) doublet squarks receive radiative corrections from the SU(2) gauginos. Thus the pure QCD cross section are somewhat bigger for the production of SU(2) singlet squarks than for SU(2) doublet squarks. If one considers the electroweak contributions to the QCD predictions, the cross sections for the production of SU(2) doublet squarks and SU(2) singlet squarks is about the same, since the electroweak contributions are more important for SU(2) doublet squarks and thus cancel the difference of the cross sections due to the different masses of the SU(2) doublet and singlet squark masses.

t- and s-channel contributions

The 7 processes in this group require an antiquark in the initial state. Pure s-channel reactions require the produced squarks to be in a P-wave, i. e. the cross sections are proportional to the third power of the threshold factor β . Since one initial parton is an anti-quark, the cross sections are further suppressed by the parton density function. The resulting cross section is therefore considerably smaller than the processes with t- and u-channel interference of the first group. The interference between QCD s-channel and EW t-channel diagrams and EW s-channel and QCD t-channel diagrams is destructive. This can be easily seen in Eq. (4.7), where the function Ω describes the interference between s- and t-channel diagrams. For interference between QCD and EW, the products of couplings and color factor is positive. However, the remainder of the function Ω is again negative.

The largest negative contributions yield $q\bar{q} \rightarrow \tilde{q}_L\bar{\tilde{q}}_L$ ($q = u, d$). As in the previous case, the SU(2) doublet contributions are the most dominant. The process $u\bar{u} \rightarrow \tilde{u}_R\bar{\tilde{u}}_R$ also gives a sizable contribution due its large hypercharge. The SU(2) neutralino coupling receives a factor 1/2 from weak isospin, which is smaller than the hypercharge for right-handed u-quark and u-squark. The processes are not proportional to the mass of the exchanged gaugino in the t-channel amplitudes. Thus, the t-channel propagators prefer the lightest exchanged particle and therefore the EW contributions are enhanced compared to the QCD contributions. Moreover, the U(1)_Y are enhanced relative to the SU(2) contribution.

$u\bar{u} \rightarrow \tilde{d}_L\bar{\tilde{d}}_L$ and $d\bar{d} \rightarrow \tilde{u}_L\bar{\tilde{u}}_L$ can proceed in QCD only through s-channel diagrams, but receive EW contributions from t-channel (chargino exchange) diagrams. The interference between these diagrams is again destructive. However, for these reactions this is over-compensated by the squared EW t-channel contribution. The absence of QCD t-channel diagrams makes the pure QCD and interference contributions quite small. On the other hand, the factor $\sqrt{2}$ in each chargino coupling relative to the SU(2) neutralino coupling enhances the pure EW t-channel contribution. For the case at hand, the pure QCD, pure EW and interference contributions are of roughly equal absolute size; nevertheless, because of the strong cancellation between the pure electroweak and interference contributions, the total effect of the EW contributions only amounts to a few percent. The total cross sections for these processes therefore remain very small.

The relatively mild suppression of the $\tilde{u}_L\bar{\tilde{d}}_L$ final state, which is also accessible via SU(2) interactions, can be explained from the observation that here no QCD s-channel diagram contributes. This reduces the number of interference terms, but does not change the pure QCD contribution much, since here s-channel diagrams are subdominant.

No interference contribution

The last 10 processes of Table 4.2 have no contributions from interference between QCD and EW diagrams. The first 8 reactions proceed through a t-channel diagram and the last 2 through a s-channel diagram. Since one of the final state squarks is always a SU(2) singlet squark, only U(1)_Y interactions can contribute. Thus the positive EW contributions are very small.

Apart from the last 2 reactions, the cross sections are quite large. E. g., the reaction $ud \rightarrow \tilde{u}_R \tilde{d}_R$ yields the largest cross section. The reason is that this reaction has 2 initial valence quarks and produced squarks are in S-wave and therefore the cross sections are only suppressed by one β factor.

The smallness of the EW hypercharge contribution

After having discussed Table 4.2, the smallness of the EW contribution to the total cross section due to hypercharge interaction can be understood. The hypercharge contributions in the first group lead to a small positive enhancement of the relatively large cross sections. The cross sections in the second group are much smaller, but there are large destructive interference. In total, the $U(1)_Y$ contributions remain positive. The reactions in the third group yield very small positive contributions due to hypercharge interactions and further reduces the importance of the hypercharge contributions.

Gaugino mass dependence

In discussing the different electroweak contributions, it turns out that the most important EW contributions are from the interference between QCD t-channel and EW u-channel and vice versa. The largest EW contributions are from production of 2 SU(2) doublet squarks, but it requires a helicity flip and therefore the matrix element is proportional to the mass of the exchanged gaugino. Thus the electroweak contributions are more dominant for increasing ratio between gaugino and squark masses. In mSUGRA, the squark masses are proportional to $m_{1/2}$, if $m_0 \leq m_{1/2}$. Thus, the ratio between the squark and gaugino masses become independent of $m_{1/2}$ in this case. In this limit, the relative importance of the EW contributions becomes insensitive to $m_{1/2}$ for fixed squark mass.

So far, all mSUGRA scenarios assume the gaugino mass unification at the unification scale. Thus the electroweak gauginos are much lighter than the gluino. The dominant EW contributions are proportional to a product of a gluino and an electroweak gaugino mass. Thus, the EW contributions are sensitive to the ratio of the electroweak gaugino mass and the gluino mass. In Fig. 4.8, the SU(2) gaugino mass M_2 is varied at the weak scale, where all other parameter are kept constant. Here, and in the subsequent figures, the production of 2 SU(2) doublet (anti-) squarks is only taken into account. The electroweak contributions become maximal for $M_2 = m_{\tilde{q}}$, since the interference term is proportional

$$\frac{M_2}{|\hat{t} - M_2^2|}, \quad (4.38)$$

and is maximal for $M_2 = m_{\tilde{q}}$. In Fig. 4.8, one can see, that in a scenario, where the squark and electroweak gaugino mass are the same and for very large squark masses, the EW contributions can enhance the cross section by about 50%. In SPS 2, the contributions are somewhat smaller, since the squark and the gluino mass are smaller, so that the interference term is suppressed. In SPS 1a, the EW contributions yield an enhancement of about 20%. In this scenario, the squark masses are very light. Here, the processes of the second group significantly contribute

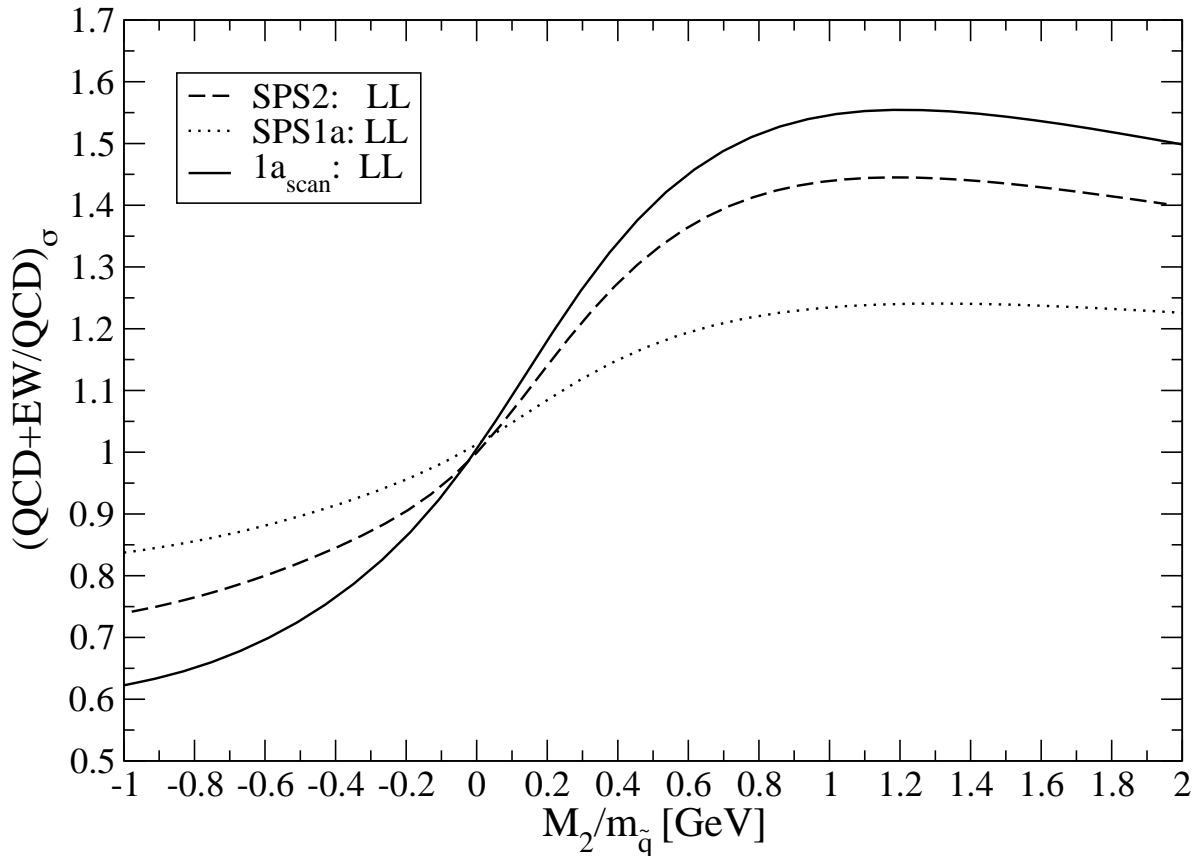


Figure 4.8: The ratio of QCD+EW to pure QCD predictions for the production of two $SU(2)$ doublet (anti-)squarks at the LHC as a function of the ratio of the $SU(2)$ gaugino mass parameter M_2 and the squark mass. The solid and dotted curves are both based on scenario SPS 1a of Table 1, but for the solid curve all soft breaking masses have been scaled up to achieve a squark mass of 2 TeV. The dashed curve is for scenario SPS 2. In all cases M_2 has been varied directly at the weak scale using SPheno [149], leaving all other weak-scale soft breaking parameters unchanged.

as will be shown below. The interference term is destructive and does not require a helicity flip. Thus, the EW contributions decrease with increasing electroweak gaugino mass. Thus in SPS1a, the curve reaches its maximum for larger values of M_2 .

In anomaly-mediated supersymmetry breaking [153], the products of electroweak and QCD

gaugino masses are negative. If one changes the sign of the parameter M_2 and keeps the sign of the gluino mass, the sign of the t–u interference terms, which require a helicity flip, are changed. In Fig. 4.8, one can see that a large and negative M_2 can reduce the QCD contributions. The relative size of the EW contributions is slightly smaller than that for positive M_2 . This is partly because the sign of the $U(1)_Y$ gaugino mass was not changed, keeping the corresponding contribution positive (but very small). Moreover, the cross sections for the (subdominant) processes in the second group remain essentially unchanged when the sign of M_2 is flipped; recall that in group 3, processes do not contribute here.

Altogether, the total cross section for the production of 2 SU(2) (anti-)squarks can change by up to a factor 2.5 as M_2 is varied between $-m_{\tilde{q}}$ and $m_{\tilde{q}}$, provided the squarks are quite heavy and the mass of the squarks and gluino is roughly the same.

$p_{T,\tilde{q}}$ distribution

In mSUGRA, the electroweak gauginos are about 3 and 7 times lighter than the gluino, so that the EW contributions are most prominent for small transverse momenta as it is shown in Fig. 4.9. It shows the ratio of the tree-level differential cross section with and without EW contributions. The Fig. 4.9 can be understood by the following considerations. For the sake of simplicity, it is assumed that the masses of the squarks are degenerate. Then the momenta of both outgoing sparticles with mass $m_{\tilde{q}}$ in the center of mass system (CMS) is given by,

$$p_{\text{CM}}^2 = \frac{1}{4}[s - (2m_{\tilde{q}})^2]. \quad (4.39)$$

With $p_T = p_{\text{CM}} \sin \theta$, where θ is the cms scattering angle, the partonic cms energy and the squark transverse momenta can be written as

$$\hat{s} = \frac{4p_T^2}{\sin^2 \theta} + 4m_{\tilde{q}}^2. \quad (4.40)$$

The parton flux is largest for smallest \hat{s} . Eq. (4.40) is minimal for $\sin^2 \theta = 1$, provided p_T is sizable.

The denominator of the t–channel can be written as

$$\hat{t} - M_{\tilde{V}}^2 = m_{\tilde{q}}^2 - \frac{\hat{s}}{2}(1 - \beta \cos \theta) - M_{\tilde{V}}^2, \quad (4.41)$$

where $M_{\tilde{V}}$ is the mass of the exchanged gaugino. The u–channel propagator is obtained by replacing $\cos \theta$ with $-\cos \theta$ and replacing the Mandelstam variable $\hat{t} \rightarrow \hat{u}$. Both propagator prefer large $\beta|\cos \theta|$, so that the expression in the brackets in Eq. (4.41) is close to zero. But the t– and u–channel propagators prefer different signs of $\cos \theta$. The dominant EW contributions are from the interference terms between t– and u–channel diagrams, whose cross sections are proportional to a single power of the threshold factor β . Since the parton density functions fall off very quickly, the most important electroweak contributions prefer small values of β even for

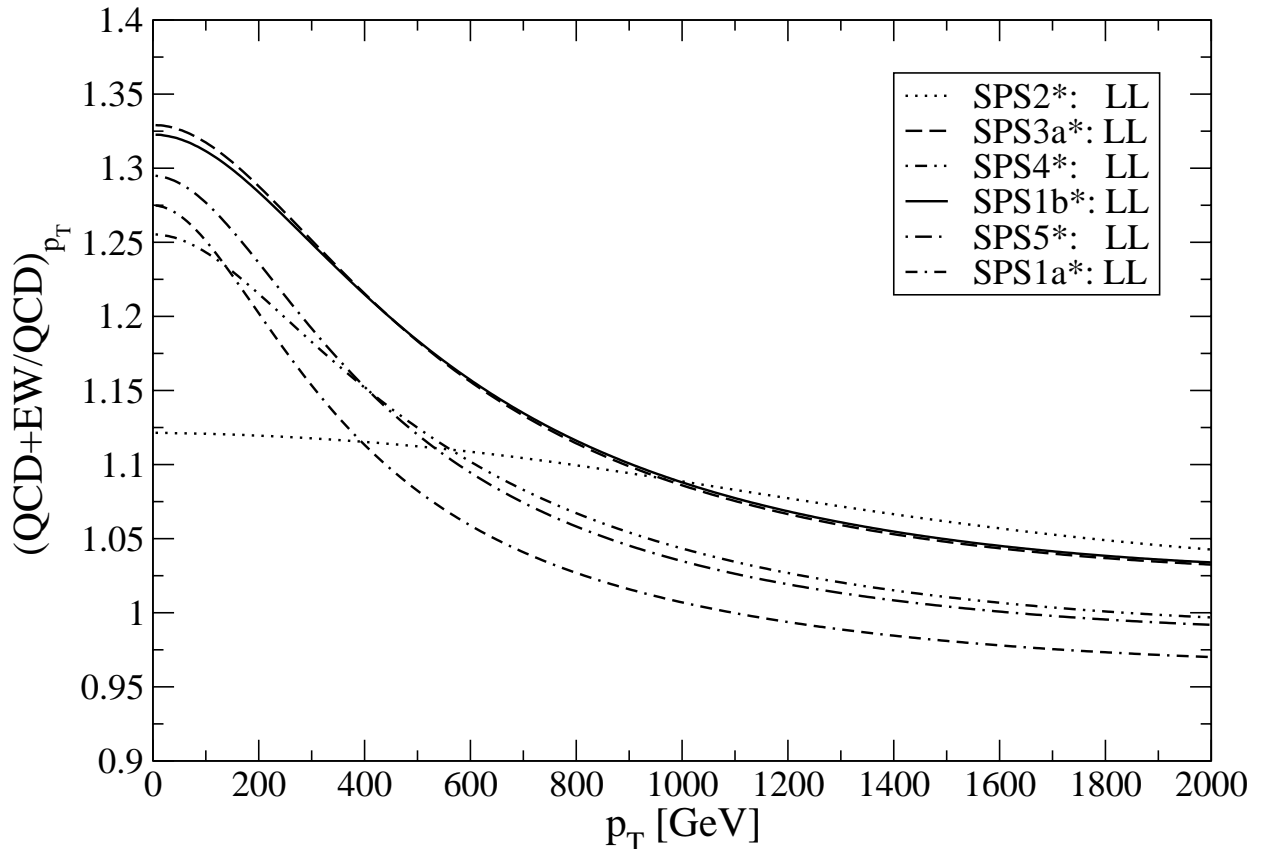


Figure 4.9: The ratio of QCD+EW to pure QCD predictions for the production of two $SU(2)$ doublet (anti-)squarks at the LHC as a function of the squark transverse momentum. The same mSUGRA scenarios are used as in Table 4.1.

small p_T . As an approximation, terms proportional to $\beta|\cos\theta|$ can be ignored. The ratio of EW and QCD t - and u -channel propagators is given by,

$$\frac{\text{EW}}{\text{QCD}} = \frac{\hat{s}/2 - m_{\tilde{q}}^2 + M_{\tilde{g}}^2}{\hat{s}/2 - m_{\tilde{q}}^2 + M_{\tilde{W}}^2} \approx \frac{2p_T^2 + m_{\tilde{q}}^2 + M_{\tilde{g}}^2}{2p_T^2 + m_{\tilde{q}}^2 + M_{\tilde{W}}^2}, \quad (4.42)$$

where $M_{\tilde{W}}$ is the mass of the chargino or neutralino and $M_{\tilde{g}}$ denotes the mass of the gluino. For many mSUGRA scenarios in Table 4.1, the gluino and squark masses are of the same order and much larger than the electroweak gauginos. Thus for small p_T , the interference term is

enhanced by a factor of 2. In SPS 2, the squark masses are much larger than the gluino mass and thus the enhancement vanishes.

The propagator enhancement of the EW contributions disappears for $2p_T \gg m_{\tilde{q}}^2$. At large p_T , the processes of the first group are not dominant. The production of 2 SU(2) doublet squarks in the final state requires a helicity flip, so that the amplitude is proportional to the mass of the exchanged gaugino. For large p_T , the product of 2 gaugino masses in the cross section must be divided by p_T^2 relative to processes without helicity flip due to dimensional considerations. The only processes, which do not require a helicity flip for the production of 2 SU(2) doublet squarks, are found in the second group. However, one initial parton is always an anti-quark and the flux of anti-quarks falls much faster for increasing \hat{s} . The interference between QCD and EW diagrams is negative, so that for large p_T , the cross section should be suppressed by the EW contributions. But it is not clear, which suppressing factor is more dominant for large p_T . Either the factor p_T^{-2} or the quickly falling parton density functions can be more important. For heavier squarks, the suppressing due to parton density functions are more important as can be seen in Eq. (4.40). This observation can be seen in Fig. 4.9, where the largest EW contributions are given in scenarios with the heaviest squarks. On the other hand, in SPS 1a, where the squarks have the smallest mass of all the mSUGRA scenarios in Table 4.2, the cross sections is suppressed by 3% for large p_T due to the EW contributions. Thus numerically, it is shown that the processes of the second group give a sizable contribution, but do not really dominate.

Squark mass dependence

The EW contributions become more important with increasing squark mass scale. This can be seen in Table 4.1. The processes of the second group are suppressed by β^3 . In addition, one of the initial state is an anti-quark. Increasing the squark mass, β is reduced and therefore the processes in the second group are suppressed. Heavier squark masses means, that larger values of Bjorken- x are necessary and thus the flux of the anti-quarks is reduced. Processes of the first group have a cross section proportional to β . Processes contributing large positive EW contributions have 2 valence quarks as initial states. For heavier squarks, i. e. for larger Bjorken- x , the flux of quarks do not drop as quickly as for the anti-quarks. Thus increasing the squark mass scale, the relative importance of processes of the second group are decreased or in other word, the relative importance of the processes of the first group is enhanced. Hence, the electroweak contribution are enhanced.

In Fig. 4.10, the ratio of the cross section for 2 SU(2) doublet squarks between the QCD and EW contribution and the pure QCD contribution is shown. The ratio is given as a function of the average squark mass. Generating the curves, the ratios of the dimensionful mSUGRA parameters, namely, m_0 , A_0 and $m_{1/2}$ are kept fixed. This corresponds to the benchmark slopes of Ref. [152]. In SPS 1a, where the gaugino masses are relatively large, the EW contribution can increase the cross section by more than 30% for $m_{\tilde{q}} = 2$ TeV. Heavier squarks cannot be detected at the LHC. A scenario, where $m_0 = -A_0 = 4.5m_{1/2}$, is also shown in Fig. 4.10. The EW contribution reach up to 13% for $m_{\tilde{q}} = 2$ TeV. This curves include a scenario, which is very similar to SPS 2. However, the corresponding slope [152] does not allow small squark masses.

The maximal relative size of the EW contributions in Fig. 4.10 exceeds that of the most favorable single process in Table 4.2. Thus the result of Fig. 4.10 cannot be entirely due to the change of the relative weights of the various processes in Table 4.2. The EW contributions get more important for increasing squark mass scale. This can be understood by looking closer at the t - and u -channel propagators. If the threshold factor β is very large (for small squark masses), the t - and u -channel propagators of the pure QCD contributions favor large values of $\cos\theta$ relative to the interference term of the pure QCD predictions. The interference terms prefer different signs of $\cos\theta$. Increasing the overall squark mass scale increases the relative importance of the interference terms compared to the squared t - and u -channel contributions. Since the QCD interference term is destructive, the importance of the EW contributions is enhanced.

4.6 Experimental signals

It is important to separate the $SU(2)$ doublet squarks from the $SU(2)$ singlet squarks in the signal, since the largest EW contributions can be found in the production of 2 $SU(2)$ doublet squarks. If at least one $SU(2)$ singlet state is produced, the EW contributions are greatly suppressed.

For the case $m_{\tilde{g}} \geq m_{\tilde{q}} > |M_2|, |M_1|$, the decay of a $SU(2)$ doublet squark is very different compared to the decay for the $SU(2)$ singlet squark. The $SU(2)$ singlet squarks mainly decay into the neutralino with the largest bino component [154]. In mSUGRA, the lightest neutralino has the largest bino component. The $SU(2)$ doublet squarks mainly decay into gauginos, which have large $SU(2)$ gaugino components. In mSUGRA, these are the $\tilde{\chi}_2^0$ and $\tilde{\chi}_1^\pm$. Since the $SU(2)$ singlet squarks decay into the lightest neutralino and a quark, the $SU(2)$ doublet squarks can be experimentally enhanced by requiring the presence of energetic, isolated charged leptons in addition to ≥ 2 jets and missing transverse momentum [155].

If $m_{\tilde{g}} < m_{\tilde{q}}$, the situation is more complicated. Most squarks will now decay into a gluino and a quark. But still a significant number of $SU(2)$ doublet squarks can decay into charginos and neutralinos.

In models with explicit R-parity violation, the $SU(2)$ doublet squarks can have very different decay channels compared to the $SU(2)$ singlet squarks [156].

4.7 Summary and conclusions

In this work electroweak (EW) contributions to the production of 2 squarks or anti-squarks are analyzed at the LHC. Explicit expressions are provided for the squared matrix elements for all processes with (anti-)quarks in the initial state, allowing for different squark masses in the final state. Not surprisingly, corrections due to $SU(2)$ interactions are more important than those from $U(1)_Y$ interactions. In both cases the dominant effect is from the interference of electroweak and QCD interactions. The sign of the interference between EW t - and QCD u -channel diagrams (or vice versa) is positive (negative) for equal (opposite) signs of the

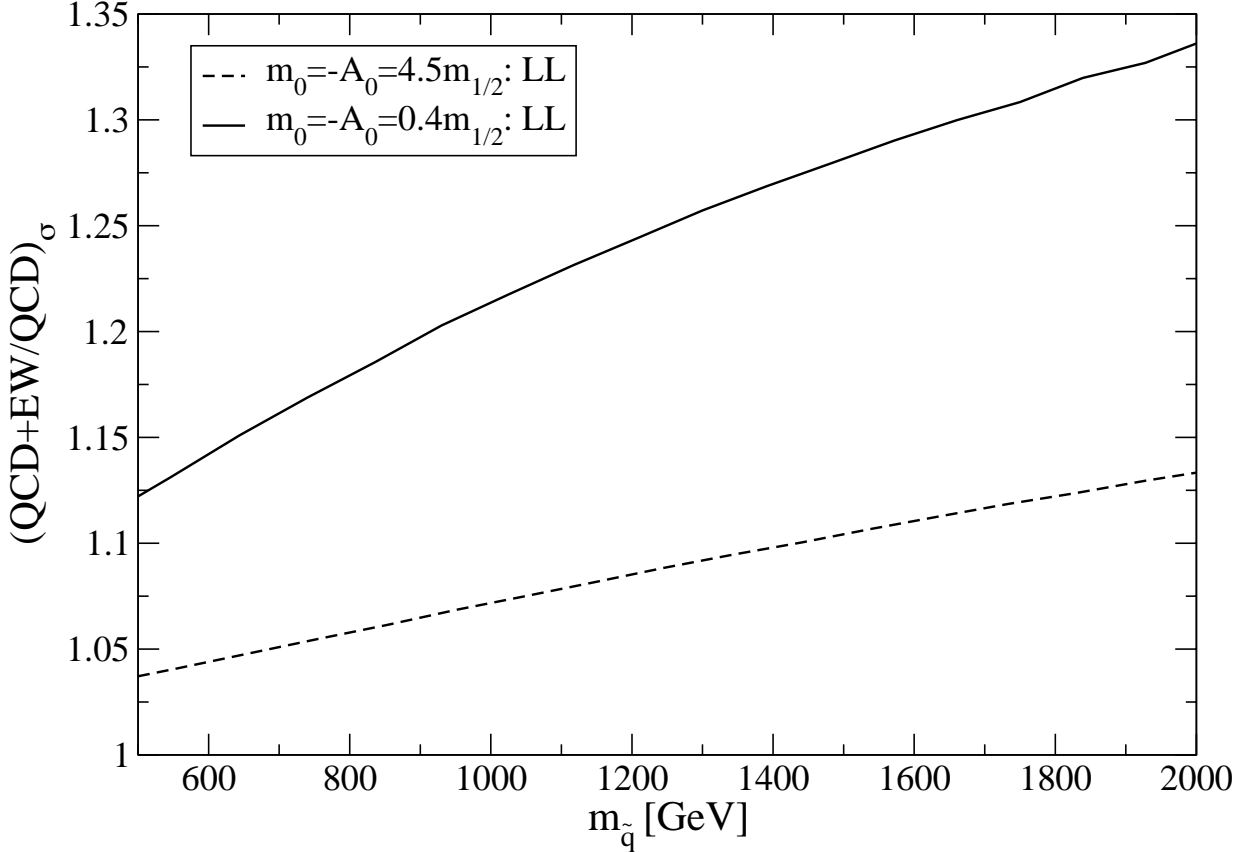


Figure 4.10: The ratio of QCD+EW to pure QCD predictions for the production of two $SU(2)$ doublet (anti-)squarks at the LHC as a function of the squark mass. The upper (lower) curve is for $m_0 = 0.4m_{1/2}$ ($m_0 = 4.5m_{1/2}$), with the overall scale of these soft breaking parameters being varied.

electroweak and QCD gaugino mass parameters. Interference between EW t - and QCD s -channel diagrams (or vice versa) is usually negative, and independent of the sign of the gaugino mass parameters.

The physical significance of the results is threefold:

- The EW contributions can change the total cross section significantly. Focusing on the production of two $SU(2)$ doublet (L -type) squarks, the contributions with interference between t - and u -channel diagrams are dominant. For squark masses near the discovery

reach of the LHC, EW effects can reduce or enhance the total cross section by more than a factor 1.5, if the absolute value of the $SU(2)$ gaugino soft breaking mass is near $m_{\tilde{g}}$; even in scenarios with gaugino mass unification the EW contribution can still change the cross section for the production of 2 $SU(2)$ doublet squarks by more than a factor 1.3. Recall that $SU(2)$ doublet squarks often lead to different final states than singlet squarks do, allowing to distinguish these modes experimentally.

- The EW contributions might give a new, independent handle on the gaugino mass parameters. In particular, they are sensitive to relative *signs* between gaugino mass parameters, which might be difficult to determine using kinematical distributions only. For example, in anomaly-mediated supersymmetry breaking [153] the products of electroweak and QCD gaugino masses are negative. In order to realize this potential, both the experimental and the theoretical uncertainties should be reduced to the 10% level. This is certainly challenging, but should eventually be possible if squarks are not too heavy.
- The EW contributions allow production of 2 squarks without color connection between the squarks. In contrast, at least in leading order QCD diagrams for squark production, there is color flow between the 2 squarks. The absence of such a flow could in principle give rise to a rapidity gap, i.e. a rapidity region into which no QCD radiation is emitted; such radiation would then only occur in the region between the squark and the quark from which it was produced (and from which it inherited its color). This is completely analogous to the gap predicted for ordinary (non-supersymmetric) two-jet events produced at hadron colliders via electroweak interactions [148].

Chapter 5

Summary

Supersymmetry (SUSY) stabilizes the hierarchy between the electroweak scale and the scale of grand unified theories (GUT) or the Planck scale. The simplest supersymmetric extension of the SM, the minimal supersymmetric SM (MSSM) solves several phenomenological problems, e. g. the gauge couplings unify and the lightest supersymmetric particle (LSP) is a dark matter candidate. In this thesis, Jarlskog invariants, squark pair production at the LHC and massive neutrinos are discussed in the framework of the MSSM and its extensions.

The SM contains one flavor-dependent CP-violating phase in the quark Yukawa sector. It can be expressed as a basis-independent CP-odd object, known as the Jarlskog invariant. CP violation is possible if and only if the Jarlskog invariant is non-zero. The leptonic sector is much more complicated. Assuming, that the light neutrino masses are generated via the seesaw mechanism, the effective neutrino mass matrix is a Majorana type. This results in 3 additional CP phases and more complicated CP-odd invariants. In this thesis, the generalization of the Jarlskog invariant to supersymmetric models with right-handed neutrinos has been constructed. The results are that CP violation in supersymmetric models is controlled by CP-odd invariants of the conventional Jarlskog-type (“ J -invariants”) as well as those involving antisymmetric products of 3 Hermitian matrices (“ K -invariants”), which cannot be expressed in terms of the former. The presence of right-handed neutrinos brings in new features, in particular, Majorana-type CP phases in supersymmetric as well as soft terms. It has been shown that the corresponding CP-odd invariants are built out of Hermitian objects involving a product of 2 or 4 flavor matrices as opposed to 2 in the Dirac case. This complicates the analysis, on one hand, but allows for interesting features, on the other hand. For example, CP violation is possible even if the neutrinos are all degenerate. A main result is that there are 39 physical CP phases and corresponding CP-odd invariants which control CP violation in the lepton sector of the MSSM with right-handed neutrinos. Below the seesaw scale, the low energy theory is described by 18 CP phases which can again be linked to 18 independent CP invariants. Basis-independent conditions for CP conservation in the non-degenerate case have been formulated.

The inclusion of *renormalizable* lepton-number violating terms to the MSSM superpotential, namely the baryon triality model (B_3), perturbatively generates neutrino masses. The neutrinos mix with the Higgsino components of the neutralinos, resulting in 1 massive neutrino at tree-level. The other 2 neutrinos obtain masses through radiative corrections from the tri-linear terms in the superpotential. However, 36 new parameters are added to the MSSM superpotential. A simple ansatz for the B_3 Yukawa couplings has been presented in this work, relating them directly to the corresponding Higgs Yukawa couplings via a small set of parameters. This reduces the free B_3 parameters from 36 to 6. The precise values of the parameters, that give the correct neutrino masses, have been numerically determined. A distinguishing feature of B_3 neutrino models is that they require couplings, which are directly observable at collider experiments. The resulting collider signals for the case of a stau LSP have been discussed. Depending on the fit values, a wide range for the possible branching ratios of the stau-LSP has been presented.

With the start of the large hadron collider imminent, it is necessary to precisely know the squark pair cross section, which is one of the largest SUSY cross section. In this thesis, tree-level electroweak (EW) contributions have been calculated in the MSSM. Diagrams with the exchange of neutralinos and charginos are included. In both cases, the dominant contribution is from the interference between electroweak and QCD interactions. The sign of the interference between EW t - and QCD u -channel diagrams (or vice versa) is positive (negative) for equal (opposite) signs of the electroweak and QCD gaugino mass parameters. Interference between EW t - and QCD s -channel diagrams (or vice versa) is usually negative, and independent of the sign of the gaugino mass parameters. Corrections due to $SU(2)$ interaction are more important than those from $U(1)_Y$ interactions. In specific regions of parameter space, this can change the $SU(2)$ doublet squark pair production cross section from -40% to $+55\%$.

Appendix A

Independent CP–odd invariants

The matrices of the first column of Table 2.1 are labelled by X_i , second – Y_i , and third – Z_i , where i refers to the row number. Then the 39 independent invariants can be chosen as

$$\text{Tr}[X_1, X_2]^3, \tag{A.1}$$

$$\text{Tr}[X_1, X_2]X_3, \tag{A.2}$$

$$\text{Tr}[X_1^2, X_2]X_3, \tag{A.3}$$

$$\text{Tr}[X_1, X_2^2]X_3, \tag{A.4}$$

$$\text{Tr}[X_1, X_2]X_4, \tag{A.5}$$

$$\text{Tr}[X_1^2, X_2]X_4, \tag{A.6}$$

$$\text{Tr}[X_1, X_2^2]X_4, \tag{A.7}$$

$$\text{Tr}[X_1, X_2]X_5, \tag{A.8}$$

$$\text{Tr}[X_1^2, X_2]X_5, \tag{A.9}$$

$$\text{Tr}[X_1, X_2^2]X_5, \tag{A.10}$$

$$\text{Tr}[X_1, X_2]X_6, \tag{A.11}$$

$$\text{Tr}[X_1^2, X_2]X_6, \tag{A.12}$$

$$\text{Tr}[X_1, X_2^2]X_6, \tag{A.13}$$

$$\text{Tr}[X_1, X_2]X_7, \tag{A.14}$$

$$\text{Tr}[X_1^2, X_2]X_7, \tag{A.15}$$

$$\text{Tr}[X_1, X_2^2]X_7. \tag{A.16}$$

$$\text{Tr}[Y_1, Y_3]Y_2, \tag{A.17}$$

$$\text{Tr}[Y_1^2, Y_3]Y_2, \tag{A.18}$$

$$\text{Tr}[Y_1, Y_3^2]Y_2, \tag{A.19}$$

$$\text{Tr}[Y_1, Y_3]Y_4, \tag{A.20}$$

$$\text{Tr}[Y_1^2, Y_3]Y_4, \tag{A.21}$$

$$\text{Tr}[Y_1, Y_3^2]Y_4. \tag{A.22}$$

$$\text{Tr}[Z_1, Z_3]Z_2, \tag{A.23}$$

$$\text{Tr}[Z_1^2, Z_3]Z_2, \tag{A.24}$$

$$\text{Tr}[Z_1, Z_3^2]Z_2, \tag{A.25}$$

$$\text{Tr}[Z_1, Z_3]Z_4, \tag{A.26}$$

$$\text{Tr}[Z_1^2, Z_3]Z_4, \tag{A.27}$$

$$\text{Tr}[Z_1, Z_3^2]Z_4, \tag{A.28}$$

$$\text{Tr}[Z_1, Z_3]Z_5, \tag{A.29}$$

$$\text{Tr}[Z_1^2, Z_3]Z_5, \tag{A.30}$$

$$\text{Tr}[Z_1, Z_3^2]Z_5, \tag{A.31}$$

$$\text{Tr}[Z_1, Z_3]Z_6, \tag{A.32}$$

$$\text{Tr}[Z_1^2, Z_3]Z_6, \tag{A.33}$$

$$\text{Tr}[Z_1, Z_3]Z_7, \tag{A.34}$$

$$\text{Tr}[Z_1^2, Z_3]Z_7, \tag{A.35}$$

$$\text{Tr}[Z_1, Z_3^2]Z_7, \tag{A.36}$$

$$\text{Tr}[Z_1, Z_3]Z_8, \tag{A.37}$$

$$\text{Tr}[Z_1^2, Z_3]Z_8, \tag{A.38}$$

$$\text{Tr}[Z_1, Z_3^2]Z_8. \tag{A.39}$$

Similarly, labelling entries of the first column of Table 2.2 by A_i and those of the second column by B_i , the following 18 independent invariants are:

$$\text{Tr}[A_1, A_6]^3, \tag{A.40}$$

$$\text{Tr}[A_5, A_1]A_6, \tag{A.41}$$

$$\text{Tr}[A_5^2, A_1]A_6, \tag{A.42}$$

$$\text{Tr}[A_5, A_1]A_2, \tag{A.43}$$

$$\text{Tr}[A_5^2, A_1]A_2, \tag{A.44}$$

$$\text{Tr}[A_5, A_1^2]A_2, \tag{A.45}$$

$$\text{Tr}[A_5, A_1]A_3, \tag{A.46}$$

$$\text{Tr}[A_5^2, A_1]A_3, \tag{A.47}$$

$$\text{Tr}[A_5, A_1^2]A_3, \tag{A.48}$$

$$\text{Tr}[A_5, A_1]A_4, \tag{A.49}$$

$$\text{Tr}[A_5^2, A_1]A_4, \tag{A.50}$$

$$\text{Tr}[A_5, A_1^2]A_4, \tag{A.51}$$

$$\text{Tr}[B_1, B_3]B_2, \tag{A.52}$$

$$\text{Tr}[B_1^2, B_3]B_2, \tag{A.53}$$

$$\text{Tr}[B_1, B_3^2]B_2, \tag{A.54}$$

$$\text{Tr}[B_1, B_3]B_4, \tag{A.55}$$

$$\text{Tr}[B_1^2, B_3]B_4, \tag{A.56}$$

$$\text{Tr}[B_1, B_3^2]B_4. \tag{A.57}$$

Appendix B

Couplings

In this Appendix explicit expressions are given for all the couplings appearing in Sec. 4.2, using the notation of [150]. Only couplings of squarks are listed. The corresponding couplings of anti-squarks can be obtained using relations (4.12) and (4.16).

B.0.1 Neutralino and Gluino Couplings

Since gluino and neutralino exchange always occur together, they are labelled with the subscript l , with $l \in \{1, 2, 3, 4\}$ denoting the l -th neutralino mass eigenstate and $l = 5$ denoting the gluino. The relevant left- and right-handed quark-squark-gaugino couplings are given, generically denoted by a and b , respectively. The relevant **neutralino couplings** are:

$$\begin{aligned}
 a_{\tilde{\chi}_l^0}(\tilde{d}_{i\alpha}) &= -\delta_{1\alpha}\sqrt{2}g\left(\frac{1}{2}N_{l2}^* - \frac{1}{6}\tan\theta_W N_{l1}^*\right), \\
 b_{\tilde{\chi}_l^0}(\tilde{d}_{i\alpha}) &= \delta_{2\alpha}\frac{\sqrt{2}}{3}g\tan\theta_W N_{l1}, \\
 a_{\tilde{\chi}_l^0}(\tilde{u}_{i\alpha}) &= \delta_{1\alpha}\sqrt{2}g\left(\frac{1}{2}N_{l2}^* + \frac{1}{6}\tan\theta_W N_{l1}^*\right), \\
 b_{\tilde{\chi}_l^0}(\tilde{u}_{i\alpha}) &= -\delta_{2\alpha}\frac{2\sqrt{2}}{3}g\tan\theta_W N_{l1}.
 \end{aligned} \tag{B.1}$$

Here $\alpha = 1$ (2) stands for an L - (R -)type squark, and N_{l1} and N_{l2} stand for the $U(1)_Y$ (bino) and $SU(2)$ (neutral wino) components of $\tilde{\chi}_l^0$, respectively. Quark mass effects are neglected, and hence also Yukawa contributions to the neutralino couplings. Finally, g is the $SU(2)$ gauge coupling, and θ_W is the weak mixing angle.

The corresponding **gluino couplings** are:

$$\begin{aligned}
 a_{\tilde{g}}(\tilde{d}_{i\alpha}) &= -\delta_{1\alpha}g_s\sqrt{2}, \\
 b_{\tilde{g}}(\tilde{d}_{i\alpha}) &= \delta_{2\alpha}g_s\sqrt{2}, \\
 a_{\tilde{g}}(\tilde{u}_{i\alpha}) &= -\delta_{1\alpha}g_s\sqrt{2}, \\
 b_{\tilde{g}}(\tilde{u}_{i\alpha}) &= \delta_{2\alpha}g_s\sqrt{2},
 \end{aligned} \tag{B.2}$$

where g_s is the $SU(3)$ gauge coupling.

B.0.2 Chargino Couplings

For a given process, charginos cannot be exchanged in diagrams of the same topology as neutralinos and gluinos. Here the subscript l labeling the exchanged particle therefore only runs from 1 to 2, corresponding to the two chargino mass eigenstates in the MSSM. Their relevant couplings are:

$$\begin{aligned}
a_{\chi_l^+}(\tilde{d}_{i\alpha}) &= -gU_{l1}\delta_{1\alpha}, \\
b_{\chi_l^+}(\tilde{d}_{i\alpha}) &= 0, \\
a_{\chi_l^+}(\tilde{u}_{i\alpha}) &= -gV_{l1}\delta_{1\alpha}, \\
b_{\chi_l^+}(\tilde{u}_{i\alpha}) &= 0.
\end{aligned}
\tag{B.3}$$

The vanishing of the right-handed, b -type couplings is again due to our neglect of Yukawa couplings.

B.0.3 Gauge Boson Couplings

Here (s -channel) diagrams with photon, Z boson and gluon exchange always occur together. Therefore these particles are labelled with subscript l , $l = 1, 2, 3$ standing for the γ , Z boson and gluon, respectively. e and f represent the left- and right-handed gauge boson-quark-anti-quark couplings,

$$\begin{aligned}
e_\gamma(d_i, \bar{d}_i) &= f_\gamma(d_i, \bar{d}_i) = \frac{1}{3}g \sin \theta_W, \\
e_\gamma(u_i, \bar{u}_i) &= f_\gamma(u_i, \bar{u}_i) = -\frac{2}{3}g \sin \theta_W, \\
e_Z(d_i, \bar{d}_i) &= \frac{g}{\cos \theta_W} \frac{1}{2} \left(1 - \frac{2}{3} \sin^2 \theta_W \right), \\
f_Z(d_i, \bar{d}_i) &= -\frac{g}{\cos \theta_W} \frac{1}{3} \sin^2 \theta_W, \\
e_Z(u_i, \bar{u}_i) &= -\frac{g}{\cos \theta_W} \frac{1}{2} \left(1 - \frac{4}{3} \sin^2 \theta_W \right), \\
f_Z(u_i, \bar{u}_i) &= \frac{g}{\cos \theta_W} \frac{2}{3} \sin^2 \theta_W, \\
e_g(d_i, \bar{d}_i) &= f_g(d_i, \bar{d}_i) = e_g(u_i, \bar{u}_i) = f_g(u_i, \bar{u}_i) = -g_s.
\end{aligned}
\tag{B.4}$$

Their couplings to a squark and an anti-squark, generically denoted by c , are:

$$\begin{aligned}
c_\gamma(\tilde{d}_{i\alpha}, \bar{\tilde{d}}_{i\alpha}) &= \frac{1}{3}g \sin \theta_W, \\
c_\gamma(\tilde{u}_{i\alpha}, \bar{\tilde{u}}_{i\alpha}) &= -\frac{2}{3} \sin \theta_W, \\
c_Z(\tilde{d}_{i\alpha}, \bar{\tilde{d}}_{i\alpha}) &= \frac{g}{\cos \theta_W} \frac{1}{2} \left(\delta_{1\alpha} - \frac{2}{3} \sin^2 \theta_W \right), \\
c_Z(\tilde{u}_{i\alpha}, \bar{\tilde{u}}_{i\alpha}) &= \frac{g}{\cos \theta_W} \frac{1}{2} \left(-\delta_{1\alpha} + \frac{4}{3} \sin^2 \theta_W \right), \\
c_g(\tilde{d}_{i\alpha}, \bar{\tilde{d}}_{i\alpha}) &= c_g(\tilde{u}_{i\alpha}, \bar{\tilde{u}}_{i\alpha}) = -g_s.
\end{aligned} \tag{B.5}$$

Note that in the absence of $L - R$ mixing, the couplings listed in Eq.(B.5) are nonzero only if both the squark and the anti-squark are $SU(2)$ doublets ($\alpha = 1$), or both are singlets ($\alpha = 2$).

Finally, in some cases there are s -channel diagrams in which a W -boson is exchanged. Its couplings to the initial state are given by

$$\begin{aligned}
e_W(d_i, \bar{u}_i) &= e_W(u_i, \bar{d}_i) = -\frac{g}{\sqrt{2}}, \\
f_W(d_i, \bar{u}_i) &= f_W(u_i, \bar{d}_i) = 0,
\end{aligned} \tag{B.6}$$

and the relevant final state couplings are

$$c_W(\tilde{d}_{i\alpha}, \bar{\tilde{u}}_{i\alpha}) = c_W(\tilde{u}_{i\alpha}, \bar{\tilde{d}}_{i\alpha}) = -\frac{g}{\sqrt{2}} \delta_{1\alpha}. \tag{B.7}$$

Bibliography

- [1] T. P. Cheng and L. F. Li, *Oxford, Uk: Clarendon (1984) 536 P. (Oxford Science Publications)*
- [2] L. M. Krauss and F. Wilczek, *Phys. Rev. Lett.* **62** (1989) 1221.
- [3] S. Weinberg, *Phys. Lett. B* **82** (1979) 387.
- [4] L. Susskind, *Phys. Rev. D* **20** (1979) 2619.
- [5] R. K. Kaul and P. Majumdar, *Nucl. Phys. B* **199** (1982) 36.
- [6] Y. Hayato *et al.* [Super-Kamiokande Collaboration], *Phys. Rev. Lett.* **83** (1999) 1529 [arXiv:hep-ex/9904020].
- [7] W.-M. Yao et al. (Particle Data Group), *J. Phys. G* **33**, 1 (2006) and 2007 partial update for the 2008 edition
- [8] H. E. Haber, *Nucl. Phys. Proc. Suppl.* **62** (1998) 469 [arXiv:hep-ph/9709450].
- [9] G. Jungman, M. Kamionkowski and K. Griest, *Phys. Rept.* **267** (1996) 195 [arXiv:hep-ph/9506380].
- [10] D. Bailin and A. Love, “Supersymmetric Gauge Field Theory And String Theory,”
- [11] P. C. West, “Introduction To Supersymmetry And Supergravity,”
- [12] H. Kalka and G. Soff, “Supersymmetry. (In German),”
- [13] P. P. Srivastava, “Supersymmetry, Superfields And Supergravity: An Introduction,”
- [14] L. H. Ryder, “Quantum Field Theory,”
- [15] H. P. Nilles, “Supersymmetry, Supergravity And Particle Physics,” *Phys. Rept.* **110**, 1 (1984).
- [16] M. F. Sohnius, “Introducing Supersymmetry,” *Phys. Rept.* **128**, 39 (1985).
- [17] M. Drees, “An introduction to supersymmetry,” arXiv:hep-ph/9611409.

- [18] S. P. Martin, “A supersymmetry primer,” arXiv:hep-ph/9709356.
- [19] M. Drees, R. Godbole and P. Roy, *Hackensack, USA: World Scientific (2004) 555 p*
- [20] I. J. R. Aitchison,
- [21] D. V. Volkov and V. P. Akulov, Phys. Lett. B **46** (1973) 109.
- [22] J. Wess and B. Zumino, Nucl. Phys. B **70** (1974) 39.
- [23] S. Ferrara, J. Wess and B. Zumino, Phys. Lett. B **51** (1974) 239.
- [24] A. Salam and J. A. Strathdee, Nucl. Phys. B **76** (1974) 477.
- [25] J. Wess and B. Zumino, Nucl. Phys. B **78** (1974) 1.
- [26] A. Salam and J. A. Strathdee, Phys. Rev. D **11** (1975) 1521.
- [27] L. O’Raifeartaigh, Nucl. Phys. B **96** (1975) 331.
- [28] P. Fayet and J. Iliopoulos, Phys. Lett. B **51** (1974) 461.
- [29] L. Girardello and M. T. Grisaru, Nucl. Phys. B **194** (1982) 65.
- [30] H. E. Haber and G. L. Kane, Phys. Rept. **117** (1985) 75.
- [31] H. K. Dreiner, arXiv:hep-ph/9707435.
- [32] H. E. Haber, arXiv:hep-ph/9306207.
- [33] G. R. Farrar and P. Fayet, Phys. Lett. B **76** (1978) 575.
- [34] A.H. Chamseddine, R. Arnowitt and P. Nath, Phys. Rev. Lett. **49** (1982) 970; R. Barbieri, S. Ferrara and C.A Savoy, Phys. Lett. B **119** (1982) 343; L. Hall, J. Lykken and S. Weinberg, Phys. Rev. D **27** (1983) 2359.
- [35] V. D. Barger, M. S. Berger and P. Ohmann, Phys. Rev. D **49** (1994) 4908 [arXiv:hep-ph/9311269].
- [36] S. Weinberg, Phys. Rev. D **26** (1982) 287.
- [37] W. Rarita and J. S. Schwinger, Phys. Rev. **60** (1941) 61.
- [38] E. Cremmer, B. Julia, J. Scherk, S. Ferrara, L. Girardello and P. van Nieuwenhuizen, Nucl. Phys. B **147** (1979) 105.
- [39] A. Santamaria, “Masses, Mixings, Yukawa Couplings And Their Symmetries,” Phys. Lett. B **305** (1993) 90
- [40] M. Kobayashi and T. Maskawa, Prog. Theor. Phys. **49** (1973) 652.

- [41] C. Jarlskog, Phys. Rev. Lett. **55**, 1039 (1985); Z. Phys. C **29**, 491 (1985); Phys. Rev. D **35**, 1685 (1987).
- [42] J. Bernabeu, G. C. Branco and M. Gronau, Phys. Lett. B **169**, 243 (1986).
- [43] M. Gronau, A. Kfir and R. Loewy, Phys. Rev. Lett. **56**, 1538 (1986).
- [44] P. Minkowski, Phys. Lett. B **67**, 421 (1977).
- [45] T. Yanagida, *In Proceedings of the Workshop on the Baryon Number of the Universe and Unified Theories, Tsukuba, Japan, 13-14 Feb 1979*.
- [46] M. Gell-Mann, P. Ramond and R. Slansky, “Complex Spinors And Unified Theories,” *In Supergravity, P. van Nieuwenhuizen and D.Z. Freedman (eds.), North Holland Publ. Co., 1979*.
- [47] R. N. Mohapatra and G. Senjanovic, Phys. Rev. Lett. **44**, 912 (1980).
- [48] H. K. Dreiner, J. S. Kim, O. Lebedev and M. Thormeier, Phys. Rev. D **76** (2007) 015006 [arXiv:hep-ph/0703074].
- [49] G. C. Branco, L. Lavoura and M. N. Rebelo, Phys. Lett. B **180**, 264 (1986).
- [50] L. Lavoura and J. P. Silva, Phys. Rev. D **50** (1994) 4619 [arXiv:hep-ph/9404276].
- [51] G. C. Branco and M. N. Rebelo, New J. Phys. **7**, 86 (2005) [arXiv:hep-ph/0411196].
- [52] F. J. Botella and L. L. Chau, Phys. Lett. B **168**, 97 (1986).
- [53] G. C. Branco and V. A. Kostelecky, Phys. Rev. D **39**, 2075 (1989).
- [54] F. J. Botella and J. P. Silva, Phys. Rev. D **51**, 3870 (1995) [arXiv:hep-ph/9411288].
- [55] O. Lebedev, Phys. Rev. D **67**, 015013 (2003) [arXiv:hep-ph/0209023].
- [56] F. J. Botella, M. Nebot and O. Vives, JHEP **0601**, 106 (2006) [arXiv:hep-ph/0407349].
- [57] F. del Aguila and M. Zralek, Nucl. Phys. B **447**, 211 (1995) [arXiv:hep-ph/9504228].
- [58] B. Pontecorvo, Sov. Phys. JETP **7** (1958) 172 [Zh. Eksp. Teor. Fiz. **34** (1957) 247].
- [59] Z. Maki, M. Nakagawa and S. Sakata, Prog. Theor. Phys. **28** (1962) 870.
- [60] B. Pontecorvo, Sov. Phys. JETP **26** (1968) 984 [Zh. Eksp. Teor. Fiz. **53** (1967) 1717].
- [61] G. C. Branco, M. N. Rebelo and J. I. Silva-Marcos, Phys. Rev. Lett. **82** (1999) 683 [arXiv:hep-ph/9810328].
- [62] P. Dita, J. Phys. A: Math. Gen. **36** (2003) 2781).

- [63] C. Jarlskog, J. Math. Phys. **47** (2006) 013507 [arXiv:math-ph/0510034].
- [64] H. K. Dreiner, C. Luhn and M. Thormeier, Phys. Rev. D **73** (2006) 075007 [arXiv:hep-ph/0512163].
- [65] Y. Grossman and H. E. Haber, Phys. Rev. Lett. **78** (1997) 3438 [arXiv:hep-ph/9702421].
- [66] S. Davidson and R. Kitano, JHEP **0403** (2004) 020 [arXiv:hep-ph/0312007].
- [67] C. Jarlskog, Phys. Lett. B **609** (2005) 323 [arXiv:hep-ph/0412288].
- [68] S. Abel and O. Lebedev, JHEP **0601**, 133 (2006) [arXiv:hep-ph/0508135]; D. A. Demir *et al.*, Nucl. Phys. B **680**, 339 (2004) [arXiv:hep-ph/0311314].
- [69] F. Gabbiani, E. Gabrielli, A. Masiero and L. Silvestrini, Nucl. Phys. B **477** (1996) 321 [arXiv:hep-ph/9604387].
- [70] S. Abel, S. Khalil and O. Lebedev, Phys. Rev. Lett. **89**, 121601 (2002) [arXiv:hep-ph/0112260].
- [71] Jong Soo Kim Diploma thesis, A Simple R-Parity Violating Model For Neutrino Masses
- [72] H. K. Dreiner, J. Soo Kim and M. Thormeier, arXiv:0711.4315 [hep-ph].
- [73] B. T. Cleveland *et al.*, Astrophys. J. **496** (1998) 505; Y. Fukuda *et al.* Phys. Rev. Lett. **82** (1999) 2644 [arXiv: hep-ex/9812014]. Y. Fukuda *et al.* Phys. Rev. Lett. **81** (1998) 1158 [Erratum-ibid. **81** (1998) 4279] [arXiv: hep-ex/9805021]; W. Hampel *et al.* Phys. Lett. B **447** (1999) 127; J. N. Abdurashitov *et al.* Phys. Rev. C **60** (1999) 055801 [arXiv: astro-ph/9907113]; Q. R. Ahmad *et al.* Phys. Rev. Lett. **89** (2002) 011301 [arXiv: nucl-ex/0204008]; B. Aharmim *et al.* Phys. Rev. C **72** (2005) 055502 [arXiv:nucl-ex/0502021]; M. Apollonio *et al.* Eur. Phys. J. C **27** (2003) 331 [arXiv:hep-ex/0301017].
- [74] L. Wolfenstein, Phys. Rev. D **17** (1978) 2369; S. P. Mikheev and A. Y. Smirnov, Sov. J. Nucl. Phys. **42** (1985) 913 [Yad. Fiz. **42** (1985) 1441].
- [75] M. M. Guzzo, A. Masiero and S. T. Petcov, Phys. Lett. B **260** (1991) 154; E. Roulet, Phys. Rev. D **44** (1991) 935; V. D. Barger, R. J. N. Phillips and K. Whisnant, Phys. Rev. D **44** (1991) 1629; H. K. Dreiner and G. Moreau, Phys. Rev. D **67** (2003) 055005 [arXiv:hep-ph/0211354]; R. Adhikari, A. Sil and A. Raychaudhuri, Eur. Phys. J. C **25** (2002) 125 [arXiv:hep-ph/0105119].
- [76] D. G. Michael *et al.* Phys. Rev. Lett. **97** (2006) 191801 [arXiv:hep-ex/0607088].
- [77] See the talk by C. Walter at *The XXXIII International Conference on High Energy Physics, Moscow*, Russian Federation, July 26 - August 2, 2006.
- [78] M. C. Gonzalez-Garcia, arXiv:hep-ph/0410030.

- [79] M. C. Gonzalez-Garcia and M. Maltoni, arXiv: 0704.1800 [hep-ph].
- [80] P. Minkowski, Phys. Lett. B **67** (1977) 421; T. Yanagida, proc. of the Workshop: *Baryon Number of the Universe and Unified Theories, Tsukuba, Japan, 1979*; M. Gell-Mann, P. Ramond, R. Slansky, in the proc. of the *Supergravity Stony Brook Workshop*, ed. by P. van Nieuwenhuizen & D.Z. Freedman (North Holland Publ. Co.), 1979; R. N. Mohapatra, G. Senjanovic, Phys. Rev. Lett. **44** (1980) 912.
- [81] For reviews see: H. P. Nilles, Phys. Rept. **110** (1984); H. Haber, G. Kane, Phys. Rept. **117** (1985) 75; S. P. Martin, arXiv:hep-ph/9709356; M. Drees, R. Godbole, P. Roy, *Hackensack, USA: World Scientific (2004) 555 p*
- [82] L. J. Hall, M. Suzuki, Nucl. Phys. B **231** (1984) 419.
- [83] B. C. Allanach, A. Dedes and H. K. Dreiner, Phys. Rev. D **69** (2004) 115002 [Erratum-ibid. D **72** (2005) 079902] [arXiv:hep-ph/0309196].
- [84] H. K. Dreiner, C. Luhn, H. Murayama and M. Thormeier, arXiv:0708.0989 [hep-ph].
- [85] L. Ibañez and G. G. Ross, Nucl. Phys. B **368**, 3 (1992).
- [86] R. Barbier *et al.*, arXiv:hep-ph/0406039; G. Bhattacharyya, arXiv:hep-ph/9709395.
- [87] M. Hirsch, M.A. Diaz, W. Porod, J.C. Romao, J.W.F. Valle, Phys. Rev. D **62** (2000) 113008 [Erratum-ibid. D **65** (2002) 119901] [arXiv:hep-ph/0004115].
- [88] M.A. Diaz, M. Hirsch, W. Porod, J. Romao, J. Valle, Phys. Rev. D **68** (2003) 013009 [arXiv:hep-ph/0302021].
- [89] Y. Grossman and H. E. Haber, Phys. Rev. D **59**, 093008 (1999) [arXiv:hep-ph/9810536].
- [90] S. Davidson, M. Losada, Phys. Rev. D **65** (2002) 075025 [arXiv: hep-ph/0010325]; S. Davidson, M. Losada, JHEP **0005** (2000) 021 [arXiv: hep-ph/ 0005080].
- [91] R. Hempfling, Nucl. Phys. B **478** (1996) 3 [arXiv:hep-ph/9511288].
- [92] F. Borzumati, Y. Grossman, E. Nardi and Y. Nir, Phys. Lett. B **384** (1996) 123 [arXiv:hep-ph/9606251];
- [93] E. Nardi, Phys. Rev. D **55** (1997) 5772 [arXiv:hep-ph/9610540].
- [94] B. de Carlos and P. L. White, Phys. Rev. D **54** (1996) 3427 [arXiv:hep-ph/9602381].
- [95] V. D. Barger, M. S. Berger, R. J. Phillips and T. Woehrmann, Phys. Rev. D **53** (1996) 6407 [arXiv: hep-ph/9511473]; B. C. Allanach, A. Dedes and H. K. Dreiner, Phys. Rev. D **60** (1999) 056002 [arXiv:hep-ph/9902251]; H. K. Dreiner and H. Pois, arXiv:hep-ph/9511444.

- [96] A. H. Chamseddine, R. Arnowitt and P. Nath, Phys. Rev. Lett. **49** (1982) 970. S. K. Soni and H. A. Weldon, Phys. Lett. B **126** (1983) 215; L. J. Hall, J. D. Lykken and S. Weinberg, Phys. Rev. D **27** (1983) 2359.
- [97] C. Froggatt and H. B. Nielsen, Nucl. Phys. B **146**, 277 (1979).
- [98] H. K. Dreiner and M. Thormeier, Phys. Rev. D **69** (2004) 053002 [arXiv:hep-ph/0305270]. In this reference, we have summarized all existing Froggatt-Nielsen models which yield predictions for the proton hexality violating couplings.
- [99] See for example: H. K. Dreiner, C. Luhn, H. Murayama and M. Thormeier, Nucl. Phys. B **774** (2007) 127 [arXiv:hep-ph/0610026]. This paper summarizes all the Froggatt-Nielsen models to-that-date, which predict low-energy neutrino masses via baryon-triality couplings.
- [100] J. M. Mira, E. Nardi, D.A. Restrepo and J.W.F. Valle, Phys. Lett. B **492**, 81 (2000) [arXiv:hep-ph/0007266].
- [101] See for example: O. C. W. Kong, Mod. Phys. Lett. A **14** (1999) 903 [arXiv:hep-ph/9808304]; G. K. Leontaris, et al. Nucl. Phys. B **436** (1995) 461 [arXiv:hep-ph/9409369].
- [102] M. Drees, S. Pakvasa, X. Tata and T. ter Veldhuis, Phys. Rev. D **57** (1998) 5335 [arXiv:hep-ph/9712392].
- [103] E. J. Chun, S. K. Kang, C. W. Kim and U. W. Lee, Nucl. Phys. B **544** (1999) 89 [arXiv:hep-ph/9807327].
- [104] S. Y. Choi, E. J. Chun, S. K. Kang and J. S. Lee, Phys. Rev. D **60** (1999) 075002 [arXiv:hep-ph/9903465].
- [105] D. E. Kaplan and A. E. Nelson, JHEP **0001** (2000) 033 [arXiv:hep-ph/9901254].
- [106] A. Abada, S. Davidson and M. Losada, Phys. Rev. D **65** (2002) 075010 [arXiv:hep-ph/0111332].
- [107] B. Mukhopadhyaya, S. Roy and F. Vissani, Phys. Lett. B **443** (1998) 191 [arXiv:hep-ph/9808265].
- [108] A. Datta, B. Mukhopadhyaya and F. Vissani, Phys. Lett. B **492** (2000) 324 [arXiv:hep-ph/9910296].
- [109] W. Porod, M. Hirsch, J. Romao and J. Valle, Phys. Rev. D **63** (2001) 115004 [arXiv:hep-ph/0011248].
- [110] A. Datta, R. Gandhi, B. Mukhopadhyaya and P. Mehta, Phys. Rev. D **64** (2001) 015011 [arXiv:hep-ph/0011375].

- [111] E. J. Chun, D. W. Jung, S. K. Kang and J. D. Park, Phys. Rev. D **66** (2002) 073003 [arXiv:hep-ph/0206030].
- [112] V. D. Barger, T. Han, S. Hesselbach and D. Marfatia, Phys. Lett. B **538** (2002) 346 [arXiv:hep-ph/0108261].
- [113] M. Hirsch, W. Porod, J. C. Romao and J. Valle, Phys. Rev. D **66** (2002) 095006 [arXiv:hep-ph/0207334].
- [114] M. Hirsch, T. Kernreiter and W. Porod, JHEP **0301** (2003) 034 [arXiv:hep-ph/0211446].
- [115] M. B. Magro, F. de Campos, O. J. P. Eboli, W. Porod, D. Restrepo and J. W. F. Valle, JHEP **0309** (2003) 071 [arXiv:hep-ph/0304232].
- [116] M. Hirsch and W. Porod, Phys. Rev. D **68** (2003) 115007 [arXiv:hep-ph/0307364].
- [117] F. de Campos, O. J. P. Eboli, M. B. Magro, W. Porod, D. Restrepo and J. W. F. Valle, Phys. Rev. D **71** (2005) 075001 [arXiv:hep-ph/0501153].
- [118] S. P. Das, A. Datta and M. Guchait, Phys. Rev. D **70** (2004) 015009 [arXiv:hep-ph/0309168].
- [119] D. W. Jung, S. K. Kang, J. D. Park and E. J. Chun, JHEP **0408** (2004) 017 [arXiv:hep-ph/0407106].
- [120] A. Datta, J. Saha, A. Kundu and A. Samanta, Phys. Rev. D **72** (2005) 055007 [arXiv:hep-ph/0507311].
- [121] S. P. Das, A. Datta and S. Poddar, Phys. Rev. D **73** (2006) 075014 [arXiv:hep-ph/0509171].
- [122] A. Datta and S. Poddar, Phys. Rev. D **75** (2007) 075013 [arXiv:hep-ph/0611074].
- [123] S. Rakshit, G. Bhattacharyya and A. Raychaudhuri, Phys. Rev. D **59** (1999) 091701 [arXiv:hep-ph/9811500].
- [124] A. Abada and M. Losada, Nucl. Phys. B **585** (2000) 45 [arXiv:hep-ph/9908352].
- [125] A. Abada and M. Losada, Phys. Lett. B **492** (2000) 310 [arXiv:hep-ph/0007041].
- [126] A. Abada, G. Bhattacharyya and M. Losada, Phys. Rev. D **66** (2002) 071701 [arXiv:hep-ph/0208009].
- [127] See for example: J. Butterworth and H. Dreiner, Nucl. Phys. B **397** (1993) 3 [arXiv:hep-ph/9211204]; J. Erler, J. L. Feng and N. Polonsky, Phys. Rev. Lett. **78** (1997) 3063 [arXiv:hep-ph/9612397]; H. Dreiner, P. Richardson and M. H. Seymour, Phys. Rev. D **63** (2001) 055008 [arXiv:hep-ph/0007228]; H. Dreiner, S. Grab, M. Kramer and M. K. Trenkel, Phys. Rev. D **75** (2007) 035003 [arXiv:hep-ph/0611195].

- [128] B. C. Allanach, M. A. Bernhardt, H. K. Dreiner, C. H. Kom and P. Richardson, Phys. Rev. D **75** (2007) 035002 [arXiv:hep-ph/0609263].
- [129] S. Davidson, D. C. Bailey and B. A. Campbell, Z. Phys. C **61** (1994) 613 [arXiv:hep-ph/9309310].
- [130] A. Y. Smirnov and F. Vissani, Phys. Lett. B **380** (1996) 317 [arXiv:hep-ph/9601387].
- [131] B. C. Allanach, A. Dedes and H. K. Dreiner, Phys. Rev. D **60** (1999) 075014 [arXiv:hep-ph/9906209].
- [132] H. K. Dreiner, M. Kramer and B. O’Leary, Phys. Rev. D **75** (2007) 114016 [arXiv:hep-ph/0612278]; H. K. Dreiner, G. Polesello and M. Thormeier, Phys. Rev. D **65** (2002) 115006 [arXiv:hep-ph/0112228].
- [133] K. Agashe and M. Graesser, Phys. Rev. D **54** (1996) 4445 [arXiv:hep-ph/9510439].
- [134] W. M. Yao *et al.* [Particle Data Group], J. Phys. G **33** (2006) 1.
- [135] Y. Grossman and S. Rakshit, Phys. Rev. D **69** (2004) 093002 [arXiv:hep-ph/0311310].
- [136] This rotation was first discussed in [82]. The most general case with complex parameters is given in [98].
- [137] See Fig. 9.2 and Eq. (9.17) in: R. N. Mohapatra and P. B. Pal, World Sci. Lect. Notes Phys. **60** (1998) 1 [World Sci. Lect. Notes Phys. **72** (2004) 1]. Note that there is a typo in the equation and the functions K should be replaced by K^2 . (R.N. Mohapatra, *privat communication*).
- [138] A. Osipowicz *et al.* [KATRIN Collaboration], arXiv: hep-ex/0109033.
- [139] V. D. Barger, G. F. Giudice and T. Han, Phys. Rev. D **40** (1989) 2987.
- [140] H. Dreiner, Jong-Soo Kim, M. Thormeier, *Colldier Signals of a Simple B_3 Model for Neutrino Masses*. In preparation.
- [141] H. K. Dreiner, P. Richardson and M. H. Seymour, JHEP **0004** (2000) 008 [arXiv:hep-ph/9912407].
- [142] J. F. Gunion and H. E. Haber, Nucl. Phys. B **272** (1986) 1 [Erratum-ibid. B **402** (1993) 567].
- [143] See for example: H. Baer, C. Kao and X. Tata, Phys. Rev. D **51** (1995) 2180 [arXiv:hep-ph/9410283]; B. C. Allanach *et al.*, JHEP **0103** (2001) 048 [arXiv:hep-ph/0102173].
- [144] ATLAS collab., *Detector and physics performance technical design report*, Vol. 2, Ch. 20, CERN-LHCC-99-15; CMS Collab., S. Abdullin *et al.*, J. Phys. **G28**, 469 (2002), hep-ph/9806366.

- [145] P.R. Harrison and C.H. Llewellyn Smith, Nucl. Phys. **B213**, 223 (1983); Erratum ibid. **B223**, 542 (1983); S. Dawson, E. Eichten and C. Quigg, Phys. Rev. **D31**, 1581 (1985); H. Baer and X. Tata, Phys. Lett. **B160**, 159 (1985).
- [146] W. Beenakker, R. Hopker, M. Spira and P.M. Zerwas, Phys. Rev. Lett. **74**, 2905 (1995), hep-ph/9412272, and Nucl. Phys. **B492**, 51 (1997), hep-ph/9610490.
- [147] CTEQ Collab., H.L. Lai et al., Eur. Phys. J. **C12**, 375 (2000), hep-ph/9903282.
- [148] H. Chehime, M.B. Gay Ducati, A. Duff, F. Halzen, A.A. Natale, T. Stelzer and D. Zeppenfeld, Phys. Lett. **B286**, 397 (1992).
- [149] W. Porod, Comput. Phys. Commun. **153**, 275 (2003), hep-ph/0301101.
- [150] J.F. Gunion and H.E. Haber, Nucl. Phys. **B272**, 1 (1986), Erratum-ibid. **B402**, 567 (1993).
- [151] B.C. Allanach, Comput. Phys. Commun. **143**, 305 (2002), hep-ph/0104145.
- [152] B.C. Allanach et al., presented at *APS / DPF / DPB Summer Study on the Future of Particle Physics (Snowmass 2001)*, Snowmass, Colorado, 30 Jun - 21 Jul 2001, hep-ph/0202233.
- [153] G.F. Giudice, M.A. Luty, H. Murayama and R. Rattazzi, JHEP **9812**, 027 (1998), hep-ph/9810442; L. Randall and R. Sundrum, Nucl. Phys. **B557**, 79 (1999), hep-th/9810155.
- [154] H. Baer, V.D. Barger, D. Karatas and X. Tata, Phys. Rev. **D36**, 96 (1987).
- [155] M.M. Nojiri and M. Takeuchi, Phys. Rev. **D76**, 015009 (2007), hep-ph/0701190.
- [156] B.C. Allanach, M.A. Bernhardt, H.K. Dreiner, C.H. Kom and P. Richardson, Phys. Rev. **D75**, 035002 (2007), hep-ph/0609263.
- [157] H. K. Dreiner and G. G. Ross, Nucl. Phys. B **365** (1991) 597.
- [158] L. E. Ibanez and G. G. Ross, Phys. Lett. B **260** (1991) 291.
- [159] S. Bornhauser, M. Drees, H. K. Dreiner and J. S. Kim, Phys. Rev. D **76** (2007) 095020 [arXiv:0709.2544 [hep-ph]].